

## **INFORMATION TO USERS**

This manuscript has been reproduced from the microfilm master. UMI films the text directly from the original or copy submitted. Thus, some thesis and dissertation copies are in typewriter face, while others may be from any type of computer printer.

**The quality of this reproduction is dependent upon the quality of the copy submitted.** Broken or indistinct print, colored or poor quality illustrations and photographs, print bleedthrough, substandard margins, and improper alignment can adversely affect reproduction.

In the unlikely event that the author did not send UMI a complete manuscript and there are missing pages, these will be noted. Also, if unauthorized copyright material had to be removed, a note will indicate the deletion.

Oversize materials (e.g., maps, drawings, charts) are reproduced by sectioning the original, beginning at the upper left-hand corner and continuing from left to right in equal sections with small overlaps.

Photographs included in the original manuscript have been reproduced xerographically in this copy. Higher quality 6" x 9" black and white photographic prints are available for any photographs or illustrations appearing in this copy for an additional charge. Contact UMI directly to order.

ProQuest Information and Learning  
300 North Zeeb Road, Ann Arbor, MI 48106-1346 USA  
800-521-0600

**UMI<sup>®</sup>**



**University of Alberta**

**Thin film / liquid crystal composite optical  
materials and devices**

by

**Jeremy Chiu-Hung Sit**



**A thesis submitted to the Faculty of Graduate Studies and Research in partial fulfillment  
of the requirements for the degree of Doctor of Philosophy**

**Department of Electrical and Computer Engineering**

**Edmonton, Alberta, Canada**

**Spring 2002**



**National Library  
of Canada**

**Acquisitions and  
Bibliographic Services**

**395 Wellington Street  
Ottawa ON K1A 0N4  
Canada**

**Bibliothèque nationale  
du Canada**

**Acquisitions et  
services bibliographiques**

**395, rue Wellington  
Ottawa ON K1A 0N4  
Canada**

*Your file Votre référence*

*Our file Notre référence*

**The author has granted a non-exclusive licence allowing the National Library of Canada to reproduce, loan, distribute or sell copies of this thesis in microform, paper or electronic formats.**

**The author retains ownership of the copyright in this thesis. Neither the thesis nor substantial extracts from it may be printed or otherwise reproduced without the author's permission.**

**L'auteur a accordé une licence non exclusive permettant à la Bibliothèque nationale du Canada de reproduire, prêter, distribuer ou vendre des copies de cette thèse sous la forme de microfiche/film, de reproduction sur papier ou sur format électronique.**

**L'auteur conserve la propriété du droit d'auteur qui protège cette thèse. Ni la thèse ni des extraits substantiels de celle-ci ne doivent être imprimés ou autrement reproduits sans son autorisation.**

0-612-68625-6

**Canada**

**University of Alberta**

**Library Release Form**

**Name of Author:** Jeremy Chiu-Hung Sit

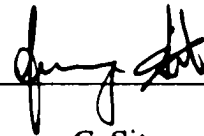
**Title of Thesis:** Thin film / liquid crystal composite optical materials and devices

**Degree:** Doctor of Philosophy

**Year this Degree Granted:** 2002

Permission is hereby granted to the University of Alberta Library to reproduce single copies of this thesis and to lend or sell such copies for private, scholarly, or scientific research purposes only.

The author reserves all other publication and other rights in association with the copyright in the thesis, and herein before provided, neither the thesis nor any substantial portion thereof may be printed or otherwise reproduced in any material form whatever without the author's written permission.



---

Jeremy C. Sit  
7 Blue Quill Crescent NW  
Edmonton, Alberta  
T6J 6C3 Canada

31 January 2002

**University of Alberta**

**Faculty of Graduate Studies and Research**

The undersigned certify that they have read, and recommended to the Faculty of Graduate Studies and Research for acceptance, a thesis entitled "Thin film / liquid crystal composite optical materials and devices" submitted by Jeremy Chiu-Hung Sit in partial fulfillment of the requirements for the degree of Doctor of Philosophy.



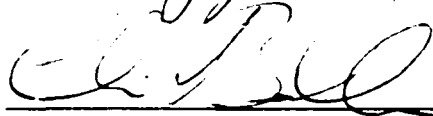
Dr. M. J. Brett



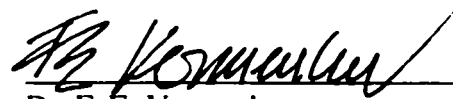
Dr. N. G. Durdle



Dr. A. Elezzabi



Dr. C. Backhouse



Dr. F. E. Vermeulen



Dr. A. Meldrum



Dr. J. Young

January 30, 2002

**To my parents**

## **Abstract**

Using a specialised thin film deposition process called glancing angle deposition (GLAD), one may fabricate porous thin films consisting of isolated columns with highly controllable microstructure. An extensive range of column shapes can be produced by using carefully managed substrate motion during the deposition process. Certain types of GLAD films, such as those possessing helical (or chiral) microstructure, have previously been shown to exhibit unique optical properties including rotation of the plane of polarisation of transmitted light and circular dichroism. The optical response of these GLAD films has been compared to that observed in liquid crystals (LC). When the pores of GLAD films are filled with liquid crystalline materials, the LC molecules take on an orientation governed by the presence and shape of the GLAD film structure, resulting in a new type of composite optical material exhibiting enhanced optical properties compared to those of the film alone. Further, because of their electro-optic characteristics, the LC component in GLAD-LC composite films may be switched by an electric field, yielding switchable devices based on GLAD-LC hybrid materials. This thesis presents an overview of glancing angle deposition and how it leads to the development of GLAD-liquid crystal composite optical materials and devices. Optics based on GLAD-LC composites show potential for improved optical switch and flat panel display technology.



## **Acknowledgements**

**I thank my parents for their love, guidance, and support. There are not enough words to express my debt to them.**

**To my supervisor extraordinaire, Professor Michael Brett, I am grateful for an environment where I am free to pursue research to its fullest and for the opportunities to learn and explore and for the confidence placed in me.**

**To Dr Dirk Broer of Philips Research Laboratories, I thank you for our continued and fruitful collaboration, for being a gracious host, and affording me the opportunity to experience Philips' Natuurkundig Laboratorium and all of the fascinating Netherlands. Hartelijk bedankt, Dick!**

**George Braybrook, SEM wizard, your pictures are simply amazing.**

**Among several researchers at Philips Research Laboratories in Eindhoven, I am particularly grateful to Christianne de Witz for her assistance with LC cell fabrication.**

**To my fellow graduate students and colleagues in the MicroFab, I am thankful for the friendships, games of foosball, and occasional spontaneous "safety meeting".**

**Generous financial support from Micralyne Inc. and the Natural Sciences and Engineering Research Council of Canada is much appreciated.**

# Table of contents

---

<b>Chapter 1: Introduction</b> .....	<b>1</b>
1.1 About this thesis .....	1
1.1.1 Project motivation and goals of this thesis .....	1
1.1.2 Scope of this thesis .....	3
1.2 Thin films .....	3
1.2.1 Introduction .....	3
1.2.2 Deposition methods .....	5
1.3 Glancing angle deposition .....	6
1.3.1 Oblique angle deposition .....	6
1.3.2 GLAD: Taking oblique deposition to the extreme .....	8
1.3.3 Column angle in obliquely deposited films .....	9
1.3.4 Growth geometry .....	11
1.3.5 Computer control .....	13
1.3.6 Basic forms .....	15
1.3.7 Applications of GLAD .....	18
<b>Chapter 2: GLAD toolbox</b> .....	<b>19</b>
2.1 Sputter deposition techniques for GLAD .....	19
2.1.1 Introduction .....	19
2.1.2 Experimental .....	20
2.1.3 Results .....	21
2.2 Techniques for advanced microstructural control .....	24
2.2.1 Introduction .....	24
2.2.2 Column angle control: paused growth versus spinning growth .....	26
2.2.3 Column cross-section shape control .....	32
<b>Chapter 3: The optics bench — optics of GLAD films</b> .....	<b>37</b>
3.1 Light and polarisation .....	37

3.1.1 Linear and circular polarisation . . . . .	38
3.2 Anisotropy and chirality . . . . .	40
3.3 Chiral optical response . . . . .	44
3.3.1 Optical activity. . . . .	45
3.3.2 Circular dichroism . . . . .	47
3.3.3 Bragg reflection . . . . .	48
3.3.4 Overall response . . . . .	48
3.4 Measurements of GLAD films . . . . .	49
3.4.1 Experimental setup . . . . .	50
3.4.2 Results . . . . .	53
3.4.3 Discussion . . . . .	55
3.5 Liquid crystals. . . . .	58
3.5.1 Introduction . . . . .	58
3.5.2 Properties . . . . .	61
3.5.3 Alignment techniques . . . . .	62
3.5.4 Application in displays . . . . .	64
3.5.5 Reflective displays and chiral LCs . . . . .	66
3.6 Discussion . . . . .	67
<b>Chapter 4: Liquid crystal hybrid optics . . . . .</b>	<b>69</b>
4.1 Introduction. . . . .	69
4.2 Experimental setup . . . . .	71
4.2.1 Film deposition . . . . .	71
4.2.2 LC cell fabrication . . . . .	74
4.2.3 Cell filling . . . . .	75
4.2.4 Inspection. . . . .	77
4.2.5 Surface treatment of substrates . . . . .	77
4.2.6 Optical measurements . . . . .	79
4.3 Results – Enhancement of optical properties . . . . .	79
4.3.1 Effect of addition of an isotropic index matching fluid. . . . .	79
4.3.2 Effect of addition of LC . . . . .	80

4.3.3 Effect of film handedness .....	83
4.3.4 Effect of film pitch .....	84
4.3.5 Optical rotatory dispersion measurements .....	86
4.3.6 Effects of GLAD film structure .....	89
4.4 Electro-optical switching .....	91
4.4.1 Switching characteristic .....	93
4.4.2 Switching speed .....	94
4.5 Discussion .....	96
4.5.1 Summary of results .....	96
4.5.2 Evaluation of GLAD/LC technology .....	97
<b>Chapter 5: Summary and conclusions .....</b>	<b>99</b>
5.1 Summary of this thesis .....	99
5.2 Future experiments .....	101
5.2.1 GLAD films .....	101
5.2.2 Surface treatments .....	103
5.2.3 Cell fabrication .....	103
5.2.4 LC experiments .....	104
5.2.5 Display ideas .....	104
5.3 Related projects .....	106
5.3.1 Simulation of film deposition .....	106
5.3.2 Periodically seeded substrates .....	106
5.3.3 Photonic band gap crystals .....	108
5.3.4 Inverse optics .....	108
5.4 Closing remarks .....	109
<b>Appendix A: Glancing angle deposition microstructural formulae .....</b>	<b>111</b>
A.1 Tilted columnar film .....	111
A.2 Zig-zag microstructure .....	111
A.3 Helical microstructure variants .....	112
A.3.1 Standard helical microstructure .....	112

A.3.2 Special case: pillar microstructure .....	112
A.3.3 Stepped (polygonal) helical microstructure .....	112
A.3.4 Graded pitch helical .....	113
A.4 Twisted ribbon chiral .....	114
<b>References .....</b>	<b>115</b>

## List of tables

---

Table 1-1: Examples of applications of thin films . . . . .	4
Table 2-1: Comparison of normal and oblique deposition . . . . .	26
Table 2-2: Comparison of paused and spinning growth in GLAD. . . . .	27
Table 3-1: Simple comparison of effects on circular polarisations in a chiral film . . . . .	45
Table 3-2: Theoretical maximum optical rotation for several optical materials. . . . .	47
Table 3-3: Light efficiency of several key TN-LCD elements. . . . .	66
Table 3-4: Comparison of conventional thin film, GLAD thin film, and LC optics . . . . .	67
Table 4-1: Optical GLAD film sample space parameters. . . . .	72
Table 4-2: A selection of GLAD optical thin film samples used . . . . .	73
Table 4-3: Properties of liquid crystals used . . . . .	76
Table 4-4: Peak LCP/RCP transmission difference wavelength for SiO <sub>2</sub> films. . . . .	85
Table 4-5: Maximum rotation versus number of turns . . . . .	87
Table 4-6: Maximum rotation per $\mu\text{m}$ before and after adding LC . . . . .	89
Table 4-7: Comparison of LC, GLAD, and hybrid GLAD/LC technologies . . . . .	97

## List of figures

---

Figure 1-1: Traditional thin film deposition . . . . .	5
Figure 1-2: Oblique angle deposition . . . . .	7
Figure 1-3: Shadowing mechanism in obliquely deposited thin films . . . . .	8
Figure 1-4: The most basic form of a glancing angle deposition thin film . . . . .	9
Figure 1-5: Definition of flux incidence and column angles . . . . .	10
Figure 1-6: Substrate geometry for glancing angle deposition . . . . .	12
Figure 1-7: GLAD system schematic . . . . .	13
Figure 1-8: Block diagram of GLAD control system . . . . .	14
Figure 1-9: Screenshots of GLAD control system software . . . . .	15
Figure 1-10: Examples of four basic GLAD film morphologies . . . . .	16
Figure 1-11: Definition of helical pitch . . . . .	17
Figure 2-1: SEM images of sputter-deposited GLAD films . . . . .	22
Figure 2-2: Effects of deposition angle $\alpha$ on film structure in oblique deposition . . . . .	25
Figure 2-3: Control of porosity and column angle in standard GLAD . . . . .	25
Figure 2-4: Controlling column angle and porosity independently . . . . .	28
Figure 2-5: Control of porosity and column angle in advanced GLAD techniques . . . . .	29
Figure 2-6: Geometry of helical microstructure . . . . .	30
Figure 2-7: Control of column cross-section shape in GLAD . . . . .	33
Figure 2-8: Twisted ribbon chiral microstructure . . . . .	35
Figure 2-9: GLAD film with twisted ribbon chiral microstructure . . . . .	36
Figure 3-1: Resolution of linear polarised light into LCP and RCP . . . . .	40
Figure 3-2: Left- and right-handed chiral structures . . . . .	42
Figure 3-3: Examples of LH and RH chiral GLAD films . . . . .	43
Figure 3-4: LCP/RCP transmission measurements . . . . .	51
Figure 3-5: Optical rotatory dispersion measurements . . . . .	52
Figure 3-6: SEM of a LH helical GLAD film . . . . .	53
Figure 3-7: LCP/RCP transmission measurements . . . . .	54
Figure 3-8: SEM of a helical film used in optical rotation measurements . . . . .	55

Figure 3-9: Chiral optical measurements for RH helical GLAD film .....	56
Figure 3-10: Liquid crystal mesophases .....	59
Figure 3-11: Nematic and smectic liquid crystal phases .....	59
Figure 3-12: Chiral nematic liquid crystal phase .....	61
Figure 3-13: Structure of a typical rod-like LC molecule .....	62
Figure 3-14: Anisotropic properties in LCs .....	63
Figure 3-15: Twisted nematic liquid crystal display cell .....	65
Figure 4-1: Films with fixed pitch/handedness and variable number of turns .....	74
Figure 4-2: LC switching cell fabrication .....	76
Figure 4-3: LCP/RCP transmission measurements for a SiO <sub>2</sub> helical film .....	80
Figure 4-4: Effect of addition of LC .....	81
Figure 4-5: LCP/RCP transmission measurements for a MgF <sub>2</sub> helical film .....	83
Figure 4-6: Enantiomeric pair of GLAD thin films .....	84
Figure 4-7: Effects of handedness .....	84
Figure 4-8: Effect of helical pitch .....	85
Figure 4-9: Rotatory dispersion .....	86
Figure 4-10: Maximum optical rotation for films before and after adding LC .....	88
Figure 4-11: SEM of a square spiral helical GLAD film .....	90
Figure 4-12: LCP/RCP transmission measurements for square helical film .....	91
Figure 4-13: Electro-optic switching of LC component in GLAD/LC devices .....	92
Figure 4-14: Measurement of electro-optic switching in a GLAD/LC cell .....	93
Figure 4-15: Transmission spectra for a GLAD/LC cell versus driving voltage .....	95
Figure 4-16: Luminance versus cell driving voltage .....	95
Figure 5-1: Chiral dopants C15 and CB15 .....	105
Figure 5-2: Helical GLAD film with 3D-FILMS simulation .....	107



## List of symbols and abbreviations

---

$E$	Electric field.
$\hat{\mathbf{n}}$	Nematic director unit vector.
$p$	Pitch. The thickness of each complete rotation in a vertically periodic film morphology. For optical GLAD films, pitch controls the spectral characteristics.
$\%T$	Percent transmission (for optical measurements).
$T$	Temperature.
$T_m$	Melting point (of a film material).
$\hat{\mathbf{x}}, \hat{\mathbf{y}}, \hat{\mathbf{z}}$	Unit vectors along $x, y, z$ directions.
$z$	Film thickness.
$dz/dt$	Deposition rate defined as time derivative of the film thickness.
$\alpha$	Flux incidence angle, measured from the substrate normal. $\alpha = 0^\circ$ represents conventional, normal-incidence thin film deposition while $\alpha = 85^\circ$ would be a typical value deposition angle used with GLAD.
$\beta$	Column angle, measured from the substrate normal as with $\alpha$ .
$\varphi$	Azimuthal (rotational) position of substrate, measured as rotation about an axis normal to the surface of the substrate.
$d\varphi/dt$	Substrate rotation rate defined as time derivative of $\varphi$ .
CCW	Counterclockwise.
CD	Circular dichroism.
CW	Clockwise.
CLC	Chiral liquid crystal <i>or</i> cholesteric liquid crystal.
GDLC	Gel-dispersed liquid crystals.

<b>GLAD</b>	<b>Glancing angle deposition.</b>
<b>ITO</b>	<b>Indium-tin oxide, a transparent conductor.</b>
<b>LC</b>	<b>Liquid crystal <i>or</i> liquid crystalline.</b>
<b>LCP</b>	<b>Left-handed circular polarisation (contrast RCP).</b>
<b>LH</b>	<b>Left-handed (contrast RH).</b>
<b>MEMS</b>	<b>Micro-electro-mechanical systems.</b>
<b>ORD</b>	<b>Optical rotatory dispersion (i.e. rotation versus wavelength).</b>
<b>PBG</b>	<b>Photonic band gap.</b>
<b>PDLC</b>	<b>Polymer-dispersed liquid crystals.</b>
<b>PVD</b>	<b>Physical vapour deposition.</b>
<b>RCP</b>	<b>Right-handed circular polarisation (contrast LCP).</b>
<b>RGB</b>	<b>Red-green-blue, the primary colours needed for full-colour displays.</b>
<b>RH</b>	<b>Right-handed (contrast LH).</b>
<b>SEM</b>	<b>Scanning electron microscope <i>or</i> scanning electron micrograph.</b>

## 1.1 About this thesis

### 1.1.1 Project motivation and goals of this thesis

In a world where portable devices such as notebook computers, mobile telephones, and hand-held organizers are becoming increasingly common, the technological importance of information displays is readily apparent. Certainly in these kinds of portable devices the display is one of the most important parts. What makes a good display? On the one hand there are of course optical performance factors such as high brightness and contrast, good colour range, and fast switching response. With portable devices, however, power consumption is also a critical characteristic to consider. It is well known that in laptop computers, the liquid crystal displays (LCDs) currently used<sup>1</sup> are the biggest drain on electrical power in the system, consuming more power than even the hard disk drive or microprocessor.

One of the challenges in the field of display technology is of course to improve performance. In battery powered devices, battery life is a main factor in the device's usefulness and thus improved performance at the expense of increased power consumption (hence decreased battery life) would be in general unacceptable. Improvement in the technology should instead come in the form of improved performance for the same power consumption or perhaps in the form of the same performance but with decreased power consumption. Ideally, one would like to have advances in display technology which could bring improved optical performance and lower power consumption simultaneously. Developments in display technologies might include schemes to reduce switching voltages and eliminate the need for absorptive polarisers and/or backlight systems.

---

1. More specifically, it is the backlight system used in LCDs that is the main consumer of energy. Furthermore, the use of absorptive polarisers means that even in the case of ideal polarisers, 50% of the backlight is wasted.

In all areas of display technology, the key to improved performance is to achieve control over the optical properties. For the ubiquitous liquid crystal display, which currently dominates the vast flat-panel display market for portable devices (especially notebook computers), control over the optical properties is achieved by controlling the orientation and positional ordering of the liquid crystals (LC). What this thesis presents is the possibility of enhanced optical properties in LC devices through improved control over the LC ordering.

This thesis describes work leading to the fabrication and characterisation of a new type of composite optical material based on porous thin films of inorganic optical materials embedded with liquid crystalline (LC) materials. Using a recently developed technique called glancing angle deposition (GLAD) [1, 2, 3], porous thin films can be grown with custom-engineered columnar morphology. Guided by theoretical studies of structurally chiral media, initial studies of porous GLAD films with helical chiral microstructure grown from optical materials revealed properties similar to those seen in certain classes of LC materials. This comparison gave rise to the inevitable question: what is the result of combining GLAD films with LCs?

As shown in subsequent sections of this thesis, embedding LCs into the void regions in porous GLAD films with chiral (handed) microstructure was found to enhance the optical properties significantly. Furthermore, the structure of the film was found to influence the orientation of the LCs embedded into the films, and thus there is a mechanism for control of the LC ordering. This new hybrid GLAD/LC material not only exhibits the promise of enhanced optical performance, but also allows for the potential of a switchable device because of the presence of the LC.

Optical measurements of GLAD/LC hybrid films reveal that the presence and structure of the film is the primary governor of the spectral response. This relationship is investigated to gain an improved understanding of how the LC molecular orientation is controlled by the GLAD film. Because of the electro-optic properties of LCs, the switching behaviour in GLAD/LC composites is also studied, leading to future developments in tunable or switchable LC devices. The development of GLAD/LC composite optical materials augments the

liquid crystal technology toolbox and may possibly lead in the future to displays that exhibit enhanced properties coupled with reduced power requirements.

### **1.1.2 Scope of this thesis**

The remainder of this chapter could be aptly titled “The Evolution of GLAD” and takes the reader through a brief introductory tour of the glancing angle deposition thin film fabrication technique. The discussion begins with fundamental thin film growth mechanisms and how GLAD exploits highly oblique angle deposition in combination with substrate motion to achieve control over the columnar structure in porous films.

Chapter 2 describes some of the relevant tools which expand the range of capabilities of the GLAD technique. The author’s work on the development of sputter deposition and advanced substrate motion control techniques for GLAD is presented.

Chapter 3 moves into a discussion of GLAD optics in detail, describing the unique optical properties observed in chiral GLAD films and some of the theory behind the results.

Chapter 4 describes the central work of this thesis: the combination of GLAD films with liquid crystalline materials to produce a novel hybrid optical material. The enhancement of optical properties resulting from the addition of LCs to GLAD films is described.

Finally, Chapter 5 presents the main conclusions of this work and describes the current state of this project, potential applications, and proposed future experiments.

## **1.2 Thin films**

### **1.2.1 Introduction**

Thin films have a wide variety of applications in the modern world. They can be found on everything from drill bits to automobile parts and jet turbine blades to food packaging. Thin films of boron nitride make an attractive and convincing substitute for a polished brass finish on doorknobs, but will not tarnish like real brass does through prolonged exposure to

the harsh outdoor environment. Optical coatings on window glass provide substantial improvement in insulation value to keep heat out in summer while helping to slow heat loss during winter. Coatings of zirconium oxide serve as thermal barrier films to protect the metal blades in jet engine turbines from the intense heat of fuel combustion. In microelectronic devices, electrical interconnect layers are formed from metal films. Some common examples of applications of thin films are described below in Table 1-1.

**Table 1-1: Examples of applications of thin films**

<b>Application</b>	<b>Examples</b>
protective coatings	wear resistant coatings on tools such as drill bits, thermal barriers coatings on jet turbine blades
optical films	solar coatings on window glass, anti-reflection coatings on lenses
magnetic films	magnetic storage media such as tapes and disks
food packaging	thin metal films deposited on plastic food packaging helps increase shelf-life of product
sensors	chemical, mechanical sensors
microelectronics	electrical interconnects, gate oxides, inter-level dielectric, passivation layers
micro- and nano-electro-mechanical systems (MEMS, NEMS)	electrodes, mechanical actuators, and other components of such devices

As their name suggests thin films are basically coatings of material over a substrate of some sort. Depending on application, "thin" can refer to any range of thickness from a few nanometres ( $10^{-9}$  m) up to almost a millimetre, though in this thesis, the films discussed generally fall into the range of 0.5 to 5.0  $\mu\text{m}$  in thickness.

The common thread which runs through all applications of thin films is the need to tailor certain properties of the film (be it hardness, index of refraction, or magnetic properties for example) to the application. It is well known that the properties of thin films are influenced by the structure of the film and that, in turn, the structure is influenced by the deposition

process. Thus, careful control of the deposition process leads to control over the properties of the film.

### 1.2.2 Deposition methods

One of the most common classes of thin film deposition processes is physical vapour deposition (PVD) wherein a vapour of the thin film material produced by physical means is made to condense on the substrate to be coated. Two of the most popular and important PVD processes are evaporation [4] and physical sputtering [5]. In evaporation, vapour flux is produced by thermal means, for example by resistive heating of a "boat" or filament containing the source material (thermal evaporation) or alternately by using an electron beam to heat the source material in a crucible (e-beam evaporation) [6, 7]. Sputter deposition most commonly involves igniting a plasma discharge of a working gas (usually Ar) and accelerating the gaseous ions into a target of the film material to dislodge atoms of the target to create the vapour flux.

As most thin film applications require durable, hard coatings, the deposition methods used generally have been optimized to produce films with such characteristics. To this end, PVD is generally performed such that the incident vapour flux arrives normal to the substrate, resulting in a film with a dense microstructure (Fig. 1-1). This arrangement has the further advantage of maximizing deposition efficiency (high rate and optimized source utilization), an important consideration in production environments.

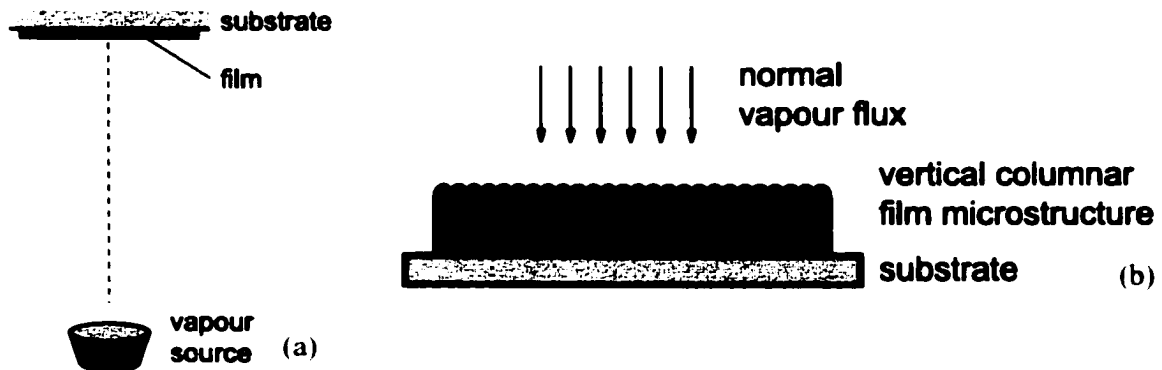


Figure 1-1: Traditional thin film deposition  
 (a) The geometry of this setup is such that the vapour flux arrives normal to the substrate, creating (b) a dense microstructure.

Four basic mechanisms influence the microstructure in PVD thin films: shadowing, surface diffusion, bulk diffusion, and desorption [8]. The latter three are often grouped together as a characteristic diffusion and sublimation process. Shadowing arises because of geometry and the line-of-sight impingement of arriving deposition flux [9, 10]. Diffusion, on the other hand, is a thermal process and depends on temperature of the substrate relative to the melting point of the material ( $T/T_m$  ratio). Under appropriate deposition conditions, one or more of the basic mechanisms may become the dominant influence on the film microstructure. Structure zone models such as those proposed by Movchan and Demchishin [11] for thick evaporated films and by Thornton [12] for sputtered metal films describe the effect on film structure by factors such as substrate temperature and gas pressure. These models divide thin film microstructure into zones of basic morphologies based on deposition conditions. For example, at high temperatures, the diffusion processes become dominant and recrystallization and grain growth are seen in films grown under such conditions. More recent work has proposed revised structure zone models (for example Refs. 13, 14) which go further in describing the link between growth conditions and film morphology.

### **1.3 Glancing angle deposition**

#### **1.3.1 Oblique angle deposition**

The situation becomes far more interesting when the substrate is oriented not normal to the vapour source, but rather at an angle so that deposition flux arrives at an oblique incidence angle  $\alpha$ , measured relative to the substrate normal (Fig. 1-2(a)). Under these conditions, the two dominant growth mechanisms are shadowing and adatom diffusion. Geometric shadowing would tend to create voids in the film structure, whereas diffusion processes would be expected to fill in the voids. The two mechanisms thus produce competing effects. Under appropriate deposition conditions, one or the other may be dominant on the film microstructure [15, 16].

Consider now a set of experiments involving oblique deposition onto unheated substrates where the angle of incidence  $\alpha$  is varied, but all other conditions held constant. As diffusion is a thermal process, it is assumed that it would be roughly constant throughout this set of



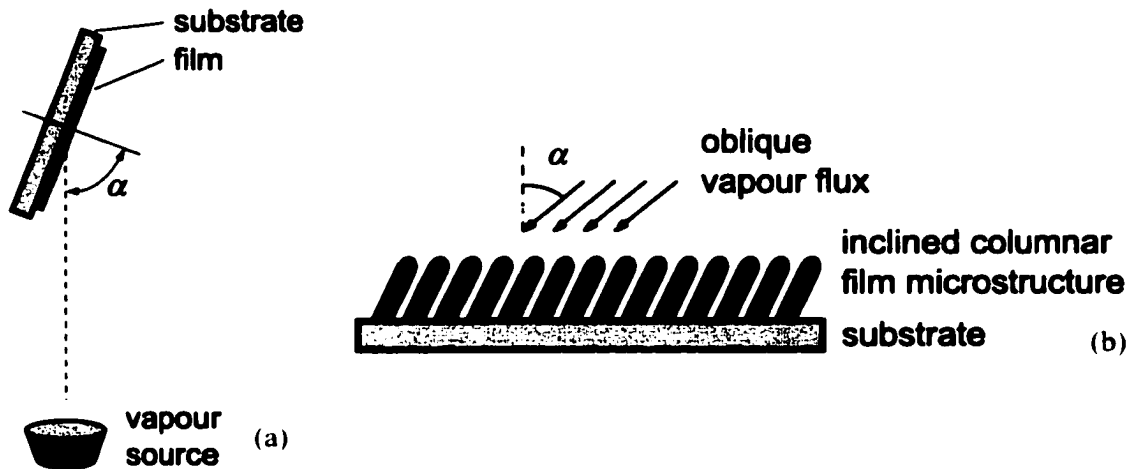


Figure 1-2: Oblique angle deposition  
 (a) source-substrate geometry (b) the resultant film has a semi-porous microstructure consisting of columns tilted toward the source of the obliquely incident vapour flux.

experiments<sup>2</sup>. Shadowing, however, is influenced purely by geometry and will increase with increasing deposition angle  $\alpha$ . Thus, as the angle of deposition becomes increasingly oblique, shadowing becomes the dominant growth mechanism.

Assuming a clean, flat substrate as a starting point, the first stage of film growth has incoming vapour flux condensing to form nuclei which in turn coalesce to form larger clusters. In standard thin film deposition, this process continues until eventually a solid layer of film is formed. With oblique deposition at sufficiently large flux incidence angles, however, nuclei on the surface will cast long shadows behind themselves (with respect to the direction of incoming flux), creating regions in which new flux cannot arrive. A schematic illustrating initial shadowing conditions is shown in Fig. 1-3 below. Under these growth conditions, nucleation is a stochastic process where growing nuclei produce regions shadowed from incoming deposition flux in which further growth is inhibited. By the same token, high points in the film such as the tops of growing nuclei and columns will exhibit preferred growth. As growth continues in this regime, material tends to accumulate more on one side of the growing columns, resulting in an inclined columnar microstructure. Because the dif-

2. When tilting the substrate holder to vary  $\alpha$ , there will of course be unavoidable but subtle changes in substrate heating effects due to the change in geometry (i.e. angle subtended by substrate holder).

fusion process is limited, the void regions created by the shadowing will never become filled in, so as the film grows, void regions will be left in the film.

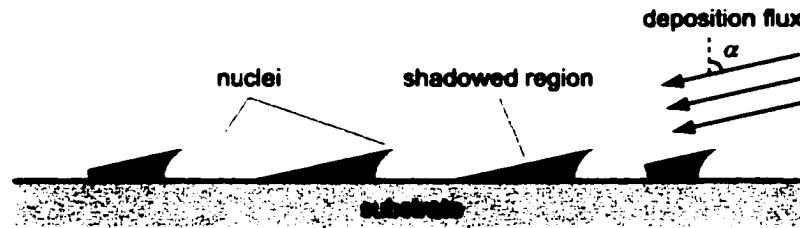


Figure 1-3: Shadowing mechanism in obliquely deposited thin films  
Flux arrives at oblique angle  $\alpha$  to the substrate and forming nuclei begin to cast shadows in the regions behind themselves, preventing further vapour flux from reaching those areas. With increasing  $\alpha$ , shadowing is accentuated and the shadowed regions become large.

### 1.3.2 GLAD: Taking oblique deposition to the extreme

While oblique deposition itself is not a new idea, the technique of glancing angle deposition (GLAD) [1-3, 17], which involves taking oblique angle deposition to the extreme, is a newer development. Previous studies [12, 15, 16] have investigated the effects of varying deposition angle from  $\alpha = 0^\circ$  to approximately  $70^\circ$ , but going beyond this regime was not given much consideration. GLAD was first developed when investigating the effects of oblique deposition on film porosity by looking at the effects of highly oblique incidence PVD. In the regime of highly oblique deposition,  $\alpha > 70^\circ$ , it was found that the shadowing mechanism is greatly enhanced, resulting in a highly porous structure [18]. Fig. 1-4 below shows a scanning electron micrograph (SEM) of an example of a thin film fabricated using the GLAD technique in this, its most basic form.

Because the shadowing mechanism is accentuated in the GLAD regime, there is an enhanced competition amongst the growing columns. Not unlike a forest, where a tree that grows larger and higher than its neighbours becomes dominant and receives more sunlight, the columns which grow sufficiently large will become dominant and continue to grow as they continue to receive deposition flux. Meanwhile, neighbouring columns which fall into the shadow of larger columns will not receive further deposition flux and thus will “die out” and cease to grow. Nucleation, competition, and growth are revisited further in discussions

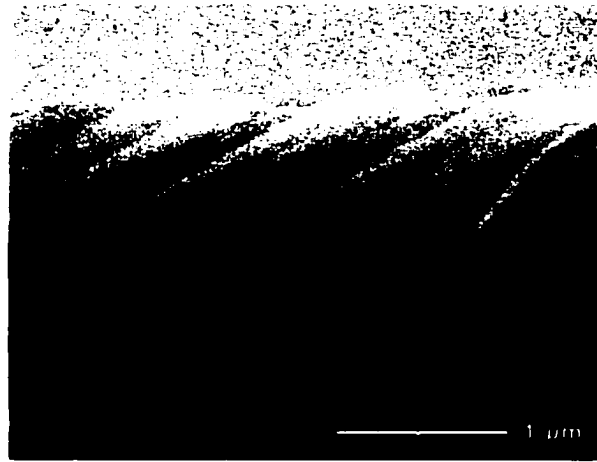


Figure 1-4: The most basic form of a glancing angle deposition thin film. The porous film consists of columns inclined in a direction toward, but not parallel to, the incoming vapour flux.

---

presented in Chapter 2.

Flux angles used with the GLAD technique are typically in the regime of  $75^\circ$  or higher. GLAD thin films can be broadly classified as “dense” for  $75^\circ < \alpha < 80^\circ$ , “porous” for  $80^\circ < \alpha < 85^\circ$ , or “super-porous” for  $\alpha > 85^\circ$ . Lower flux incidence angles result in more efficient deposition, but the films produced may not have a very open structure. Higher flux incidence angles give a more porous, open structure, but also lead to an increasing falloff in effective deposition rate (growth rate of the GLAD film versus a “normal” film deposited at  $\alpha = 0^\circ$ ). For most materials and applications, the range of flux angles between  $80^\circ$  and  $85^\circ$  strikes a suitable compromise between the required porosity and a reasonable growth rate. Typically, in this regime of flux incidence angles, the effective deposition rate for a GLAD film falls in the range of one-half to one-third that of a normally deposited film, positioned at the same distance from the source.

### 1.3.3 Column angle in obliquely deposited films

With flux arriving from a non-normal incidence angle  $\alpha$ , and assuming sufficiently limited adatom diffusion, the resultant film grows with columnar microstructure inclined<sup>3</sup> at an an-

---

3. As with flux incidence angle  $\alpha$ , the column angle is measured relative to the substrate normal, so that  $0^\circ$  represents columns growing vertically (perpendicular to the substrate).

gle  $\beta$  (Fig. 1-5). For  $\alpha > 0^\circ$ , the relation

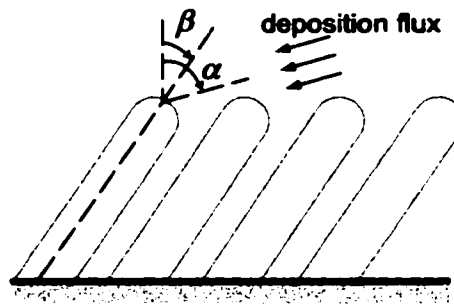


Figure 1-5: Definition of flux incidence and column angles

The flux arrives at an oblique angle  $\alpha$ , while the columns grow inclined toward the direction of incoming flux, at an angle  $\beta$ . Both angles are measured with respect to the substrate normal.

$$0^\circ < \beta < \alpha \quad (1-1)$$

will hold. It is possible to show by counter-example that the column angle cannot be the same as the flux angle. If it is assumed for a moment that  $\beta = \alpha$ , then there would be a direct path between the growing columns all the way down to the substrate for the incoming vapour flux. This would imply that there is no shadowing effect at all and hence the film should be as dense as a normally-deposited film. As obliquely deposited films clearly are more porous and exhibit inclined columnar structure, the shadowing mechanism must therefore play a role and this in turn requires that  $\beta < \alpha$ .

Discussion of the angle of the columnar microstructure begs the question about the relationship between the flux incidence column and the column angle. A series of experiments of preparing films grown with different materials and at several oblique angles would quickly reveal that the relationship between  $\beta$  and  $\alpha$  is a poorly understood one. The complexity of this relationship arises because there are many factors influencing the column angle including: film material, deposition conditions such as substrate and film temperature, source/substrate geometry, angular distribution of the deposition flux, flux energetics, cleanliness of the substrate, and purity of vacuum conditions.

There have been several attempts to quantify the relationship between column angle and deposition angle. One such relationship, given by:

$$\tan \beta = \frac{1}{2} \tan \alpha \quad (1-2)$$

is the empirically-derived “tangent rule” [19]. While this relationship is quite simple, it tends to give poor results for deposition angles in the range  $\alpha > 50^\circ$ . Based on a geometrical analysis of oblique deposition, Tait *et al.* [20] derived a relationship which gives more accurate predictions for large  $\alpha$ :

$$\beta = \alpha - \arcsin\left[\frac{1}{2}(1 - \cos \alpha)\right] \quad (1-3)$$

This relation has been verified by Messier *et al.* [21] who studied a series of films deposited at varying oblique angles. While both the basic tangent rule and the rule put forward by Tait *et al.* may be of utility in that they give some qualitative predictions of column angle as a function of deposition angle, neither takes into account the effect of varied material or deposition conditions such as those listed earlier: both simply give  $\beta$  as a function of  $\alpha$ . Hodgkinson *et al.* [22] used a modified form of the tangent rule with an empirically determined factor replacing the one-half factor in the tangent rule. As the empirical factor was found to depend on the film material, this modified version of the tangent rule can partially take into account the effects of material.

Because of its improved accuracy in the range of deposition angles typically used in GLAD (large  $\alpha$ ), Tait’s rule will be used in discussion throughout with the caveat that its use is for illustrative purposes only.

### 1.3.4 Growth geometry

The key step in the development of GLAD is to recognise that the obliquely tilted columns will always grow in a plane parallel to one defined by the trajectory of the incoming vapour flux and the substrate normal. (For the purposes of discussion, this plane shall be called the deposition plane.) This fact on its own is logical and obvious; however, the next step in the

development of GLAD is not so. What happens when the deposition plane is moved during deposition, for instance by rotating the substrate about an axis normal to its surface? Since the columns always grow in the deposition plane and tilted toward the source of the deposition flux, moving the deposition plane allows the direction of the columnar microstructure to be steered during growth. Thus, GLAD is the combination of extreme oblique incidence deposition with substrate motion [1, 3]. Fig. 1-6 below illustrates the substrate geometry for the GLAD process, defining the deposition plane and azimuthal and polar angles.

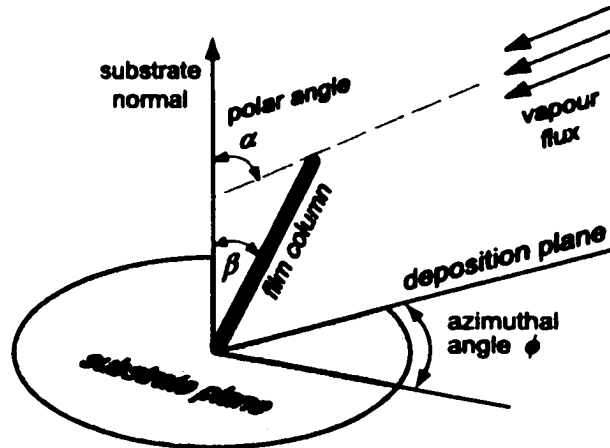


Figure 1-6: Substrate geometry for glancing angle deposition  
Columns always grow in the deposition plane, so moving the deposition plane permits the control of the direction in which the columns grow.

It is important to point out that movement of the deposition plane is motion relative to the substrate. In the current implementation of GLAD, the source is fixed while the substrate holder is moved. It is equally effective to have the source move with the substrate fixed. This could be implemented for example by using a large ring-shaped sputter target and having a moving magnetic field confine the plasma discharge to the location on the ring where sputtering is desired. While such an implementation is likely not practical for research and development work, it may be of more utility for larger scale manufacturing of GLAD films.

A specially designed substrate holder is used to implement the GLAD technique and is shown in Fig. 1-7 below. Two stepper motors are used to control the orientation of the substrate holder relative to the vapour source (evaporation source or sputter gun). The first mo-

tor tilts the substrate holder along an axis parallel to and passing through the surface of the substrate to set the flux incidence angle  $\alpha$ . The second stepper motor rotates the substrate holder about an axis normal to the surface of the substrate to control azimuthal rotation  $\varphi$  of the deposition plane (Fig. 1-6).

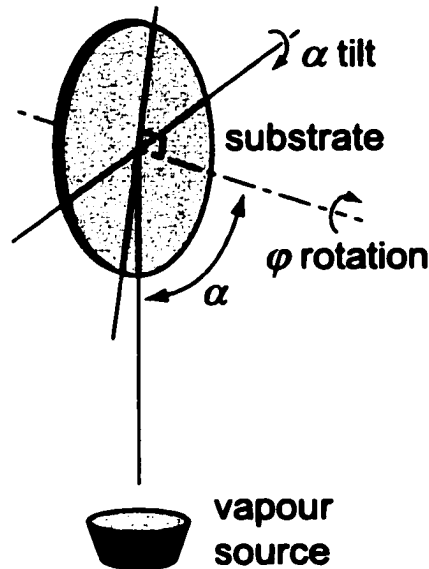


Figure 1-7: GLAD system schematic  
Stepper motors control the tilt (polar) angle  $\alpha$  and rotation (azimuthal) angle  $\varphi$  of the substrate holder.

For most applications, films with approximately uniform porosity throughout are required. Since the flux incidence angle  $\alpha$  is the primary determinant of the porosity in a GLAD film, then for most microstructure types,  $\alpha$  is held constant during the deposition.

### 1.3.5 Computer control

The GLAD process is driven by a feedback control system which consists of a computer running the control software program, an input/output and data acquisition interface card, and an external stepper motor controller. A block diagram of the GLAD control system is shown below in Fig. 1-8. The control system manages the motion of the  $\alpha$  and  $\varphi$  stepper motors with feedback from a quartz crystal oscillator thin film deposition thickness/rate monitor. The motors are moved in accordance with parameterised functions of accumulated thickness:

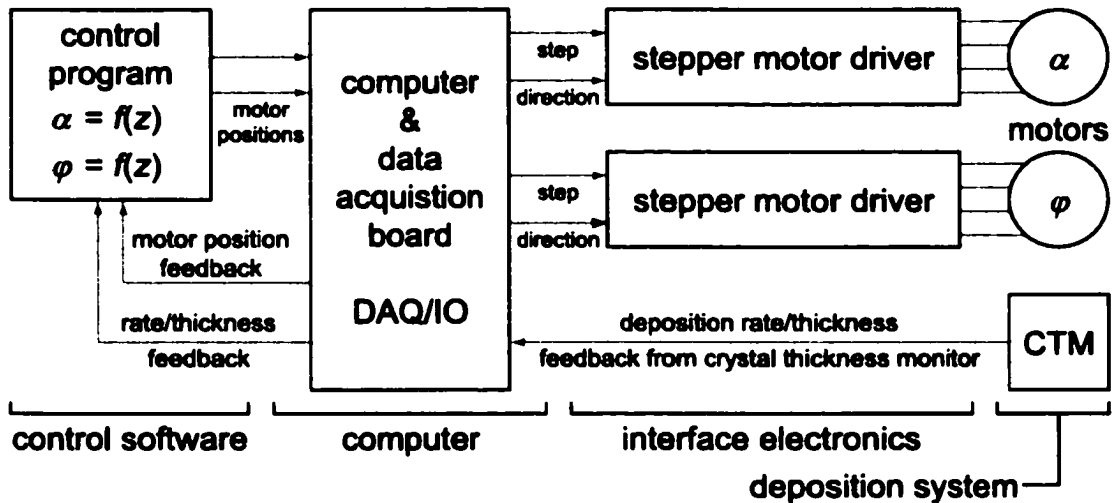


Figure 1-8: Block diagram of GLAD control system

The motors are moved in accordance with parameterised functions of thickness which is fed back by the crystal thickness/rate monitor.

$$\alpha = f(z) \quad \text{and} \quad \varphi = f(z) \quad (1-4)$$

These functions are defined for a set of several microstructure types that can be produced by the system. As the software is extensible, addition of new microstructure types is easily accomplished simply by defining algorithms for the new desired morphology. To set up a deposition, the user specifies the desired structural parameters such as microstructure type and thickness. The algorithms which define the motor positions based on thickness and structural parameters are used to determine the required substrate motion to generate the desired structure.

The control system illustrated in Fig. 1-8 consists of the control system software (see screenshots shown in Fig. 1-9) based on LabVIEW (National Instruments Corp.) running on a personal computer with a PC-LPM-16 multifunction input/output (I/O) data acquisition card (National Instruments) to interface with the external electronics. In-house developed external stepper motor electronics interface the computer with the stepper motors. This stepper motor driver uses direction and step pulse data output from the I/O card to power and actuate the stepper motors through a high-current output stage.



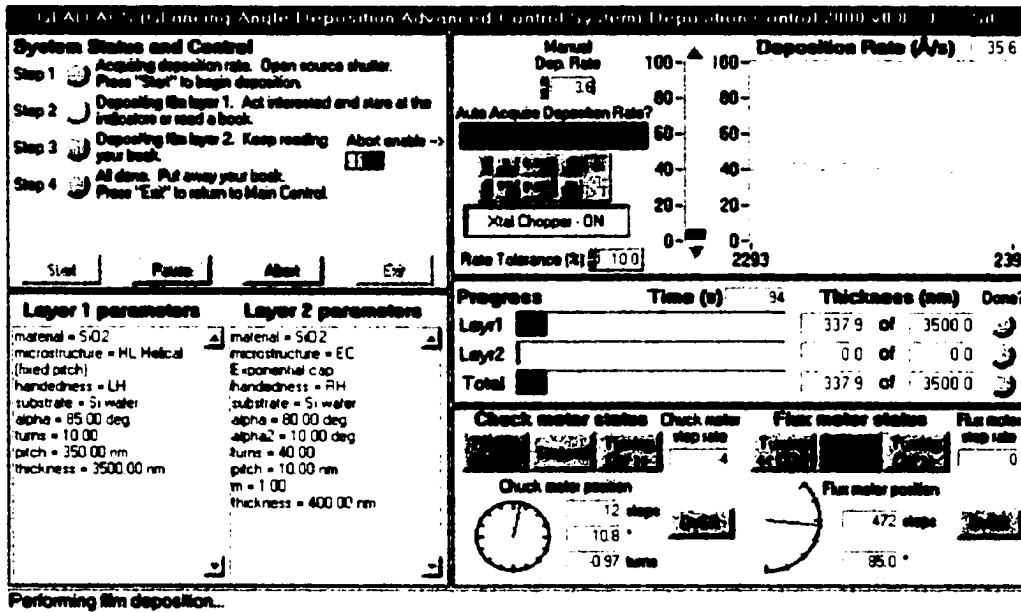
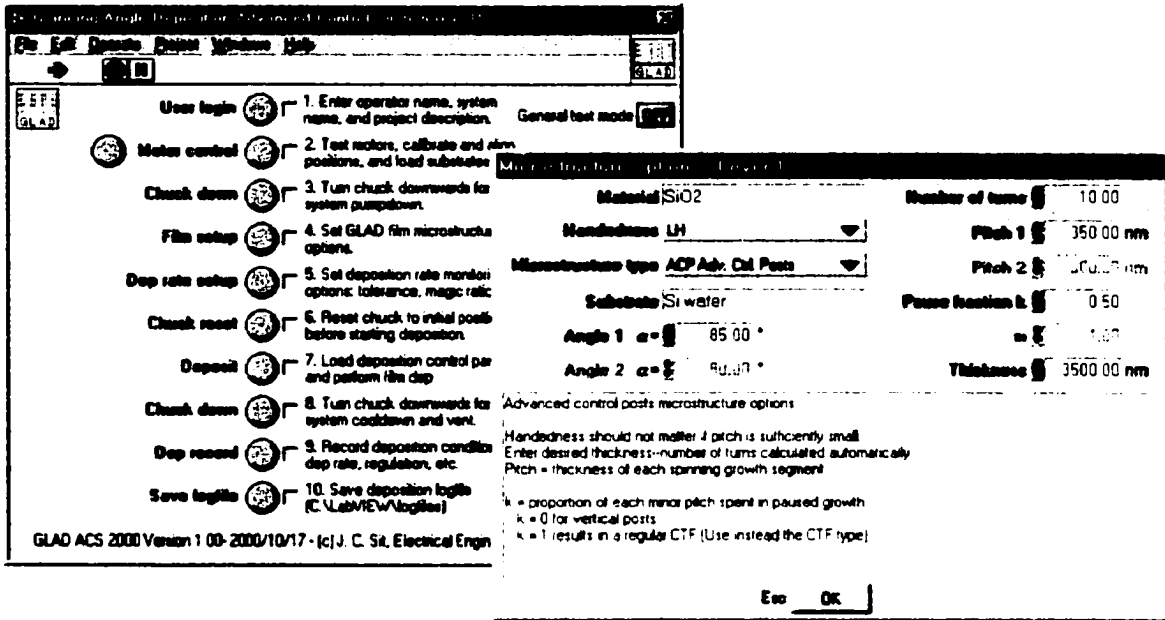


Figure 1-9: Screenshots of GLAD control system software (top to bottom) Main control panel, microstructure parameters dialogue box, deposition monitoring screen.

### 1.3.6 Basic forms

To illustrate the capabilities of GLAD, a set of four fundamental morphologies is discussed here. These four microstructure types, which form the basis of other more complex structures, are:

1. tilted columns
2. zig-zags
3. helices
4. vertical posts

Examples of GLAD films with each of these shapes are shown in Fig. 1-10 below.



Figure 1-10: Examples of four basic GLAD film morphologies  
 (a) tilted columns,  $\text{SiO}_2$  at  $\alpha = 85^\circ$ ; (b) zig-zags,  $\text{MgF}_2$  at  $\alpha = 89^\circ$ ; (c) helices,  $\text{SiO}_2$  at  $\alpha = 85^\circ$ ; (d) vertical posts,  $\text{MgF}_2$  at  $\alpha = 85^\circ$ .

A GLAD film consisting of tilted columns as in Fig. 1-10(a) can be grown simply by holding the substrate stationary at an appropriate flux incidence angle. This type of microstructure is GLAD in its most basic form.

Zig-zag [18, 23] (also called chevron) shaped columns such as those seen in Fig. 1-10(b) are produced by rotating the substrate in  $\phi$  by  $180^\circ$  between each arm of the zig-zag<sup>4</sup>. This type of film illustrates how stepped rotation of the substrate can be used to create columns

composed of discrete segments.

A film consisting of helically-shaped columns, for example that shown in Fig. 1-10(c), can be fabricated by maintaining continuous slow rotation of the substrate ( $d\phi/dt$ ) relative to the deposition rate [24, 25]. The thickness of each turn of the helical columns is called the pitch (Fig. 1-11) and is determined by the ratio of the rotation rate to the deposition rate (each complete rotation of the substrate about the  $\phi$  axis results in a single turn of the helical structure). A faster rotation results in a tighter pitch, while a slower rotation produces a longer pitch. The helical microstructure demonstrates the effect of smooth, continuous substrate rotation.

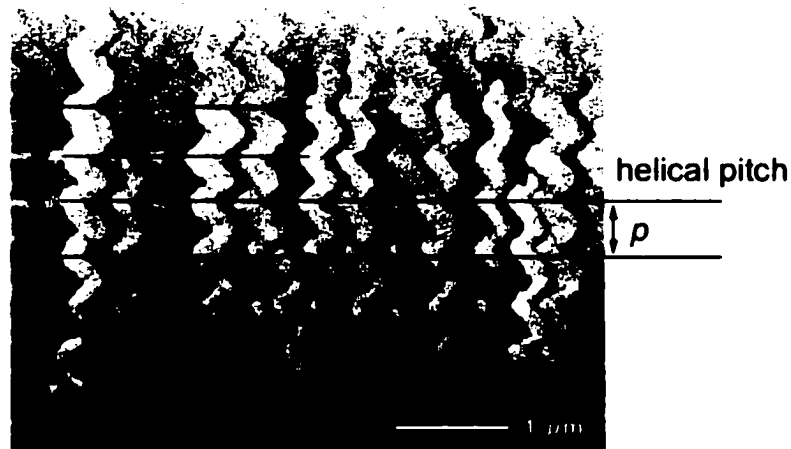


Figure 1-11: Definition of helical pitch

The pitch in a period GLAD film is the thickness of one period or complete turn of the structure.

The fourth microstructure type is a special case of the helical morphology, but deserves to be highlighted as a fundamental type in its own right. If the pitch in a helical film is made very small by choice of a high rotation rate relative to the deposition rate, the helical structure degenerates into a vertical post or pillar structure as seen in Fig. 1-10(d). When the pitch decreases to less than about twice the average column diameter, it is no longer possi-

4. An alternate way to implement (and visualise) zig-zag deposition is to alternately deposit from angles  $+\alpha$  and  $-\alpha$  without  $\phi$  rotation. This action has the same effect of rotating the deposition plane  $180^\circ$  between each arm of the zig-zag.

ble to resolve individual adjacent turns of the helix, and the helical structure is blurred into a vertical pillar. The post microstructure illustrates the ability of GLAD to fabricate vertical columnar thin films [26].

These four basic forms illustrate the fundamental column shapes possible with the GLAD technique. Essentially any structure, including some “exotic” varieties, can be produced by appropriate combination (stacked layers) of these fundamental forms. From the perspective of the stepper motor control, column shape is engineered through judicious permutation of stationary substrate or stepped or continuous substrate rotation.

A brief discussion of the mathematical definitions of these microstructure types and a few others is presented in Appendix A (p. 111). Advanced techniques for engineering the GLAD film morphology which go beyond these four fundamental microstructure types are discussed later. (See “Techniques for advanced microstructural control” on p. 24.)

### **1.3.7 Applications of GLAD**

The unique ability of the glancing angle deposition technique to fabricate thin films with highly controllable, porous microstructure leads to many potential applications. GLAD has been demonstrated with a wide variety of materials and processes, showing the flexibility of the technique. Areas of application for GLAD presently being studied include: mechanical devices [27, 28], optical devices [29, 30], thermal barrier coatings [31], field emission devices [32], magnetics [33], sensors and catalysis [34, 35], and biological devices [36].

## Chapter 2

### GLAD toolbox

---

This chapter describes a few of the techniques developed which expand the capabilities of glancing angle deposition and hence become part of the “GLAD toolbox”. Having a robust and capable set of tools is beneficial as this technology progresses from a purely scientific study, where the approach is “what can we do?”, to the practice of engineering films to develop applications, where the approach is instead “how can we make a film that does *this*?”

The two primary topics described in this chapter are techniques for sputter deposition of GLAD films [37] and for advanced microstructural control [38, 39]. The ability to use sputter deposition opens up a wider range of materials, and hence potential applications, for GLAD. Such materials include those that are difficult or impractical to deposit by evaporation — tungsten for instance.

Using careful control of the substrate motion via advanced control algorithms, the capabilities of the basic GLAD control techniques can be surpassed allowing a partial decoupling of column angle and shape from film porosity, thus permitting more independent control of these structural parameters.

## 2.1 Sputter deposition techniques for GLAD<sup>1</sup>

### 2.1.1 Introduction

As discussed earlier, the growth of obliquely deposited films is influenced primarily by the mechanisms of adatom diffusion and atomic shadowing. In particular, at flux incidence angles in the range  $\alpha > 75^\circ$ , the shadowing mechanism is accentuated and the porosity of the resultant film increases sharply with increasing  $\alpha$  in this range. Since adatom diffusion is not in general dependent on deposition angle (if at all), at highly oblique angles of deposi-

---

1. Part of this work has been previously published in [37] J. C. Sit, D. Vick, K. Robbie, and M. J. Brett, “Thin film microstructure control using glancing angle deposition by sputtering”. *J. Mater. Res.* 14, 1197-1199 (1999). Excerpted with permission.

tion, the shadowing mechanism becomes the dominant factor and is the main governor of the porosity of the film.

Tait *et al.* [20] used geometrical arguments to show that film porosity is a monotonically increasing function of  $\alpha$ . At highly oblique deposition angles such as those used in GLAD ( $\alpha > 75^\circ$ ), the ratio of intercolumn spacing to column diameter becomes a very strong function of  $\alpha$ . Thus, small variations in  $\alpha$  can result in large changes in film density. The resultant film density is therefore expected to be most strongly influenced by that portion of the incoming angular flux distribution which is least oblique and consequently least subject to the shadowing mechanism.

In the initial development of GLAD, thermal or electron beam evaporation was used as the deposition process of choice as it is a relatively easier process to work with, especially in a research environment. Because the operating pressure is low with evaporation (a typical value is 0.1 mTorr = 0.013 Pa or less), one can assume that, for adequate source-to-substrate separation, the vapour flux arriving at the substrate has a very small angular distribution ( $\Delta\alpha$  small) and can generally be considered collimated ( $\Delta\alpha \rightarrow 0$ ).<sup>2</sup>

In contrast to evaporation, sputter deposition generally requires a higher operating pressure due to the presence of the sputtering gas (typically in the range of 5 to 20 mTorr = 0.6 to 2.6 Pa) and also tends to have larger sources (sputter target size). Physical sputtering therefore typically exhibits a wider angular flux distribution than evaporation, in part due to scattering of the sputtered flux by the working gas and in part due to the solid angle subtended by the target as seen at the substrate. It is thus not *a priori* apparent that sputtered GLAD films can be grown.

### 2.1.2 Experimental

There are several methods available for narrowing the flux distribution in sputter PVD. The techniques which are applicable to work with GLAD include: collimated sputtering [40, 41], ionized PVD [42], and low-pressure, long-throw (LPLT) sputtering [43]. Physical

2. The mean free path  $\lambda$  is also of sufficient magnitude such that little scattering of the flux occurs.

collimation of the sputtered flux generally results in too sharp a drop in deposition rate to be of practical use. For this work, LPLT sputtering was used as it was the simplest of the practical choices.

In a low pressure regime, including the 1 to 1.5 mTorr (0.13 to 0.20 Pa) range used in these depositions, the scattered component of the sputtered flux distribution can be reduced such that the solid angle subtended by the angular flux distribution approaches that of the target as seen at the substrate. Increasing the throw (substrate-to-target separation) further narrows the angular distribution by reducing the solid angle subtended by the target.

For the initial series of depositions which led to the first demonstration of sputter-deposited GLAD films, the substrate holder was mounted at a fixed distance from the sputter gun and tilted such that the vapour flux arrives at glancing angle  $\alpha$ . A small stepper motor with 0.9° resolution (200 step/rev motor operated in half-step mode) was used to control the substrate rotation ( $\varphi$ )<sup>3</sup>. For these experiments, a 2 inch (5 cm) diameter circular planar magnetron sputter gun was used with a titanium metal target.

In contrast to evaporation, sputter deposition is usually quite stable, and as such, deposition performed at these conditions and at constant power results in a steady deposition rate. This stability obviates the need for deposition rate feedback control for sputter GLAD depositions, further simplifying the experimental setup. Nominal deposition rates of 0.5 to 1.0 Å/s were realized at the substrate for the depositions described below.

### 2.1.3 Results

A set of films with three types of microstructure was prepared to demonstrate the use of sputter deposition for GLAD. Fig. 2-1(a) shows a Ti GLAD film with “zig-zag” microstructure created by alternately depositing at tilt angles  $\alpha = +84^\circ$  and  $-84^\circ$  without rotation (fixed  $\varphi$ ). The throw distance was 23 cm and the nominal flux angle was measured from the substrate to the centre of the target. Sputtering was performed at 1.0 mTorr (0.13 Pa) with Ar working gas and 350 W constant power regulation.

3. A simplified version of the GLAD substrate holder assembly was used for this set of experiments.

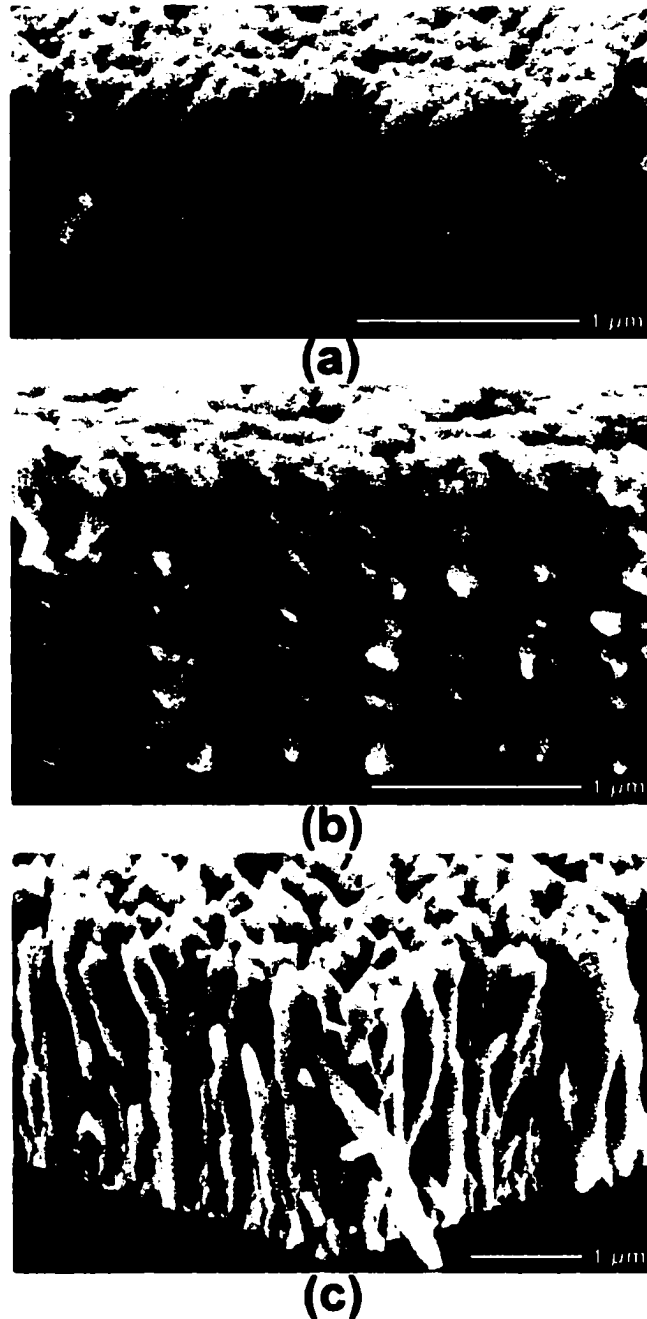


Figure 2-1: SEM images of sputter-deposited GLAD films  
 Three types of microstructure are shown: (a) “zig-zag”, (b) helical (or chiral), and  
 (c) post or “pillar”. All films are Ti.

Using the Monte Carlo sputter flux transport simulator SIMSPUD (SIMulation of SPUtter Distribution) [44], the half-width of the sputter flux distribution for this geometry was found to be  $8^\circ$ . This angular deposition spread is significantly higher than that seen in evaporated GLAD depositions, where the angle subtended by the vapour sources is typically



less than  $2^\circ$ . This larger angular distribution may account for the slightly denser appearance of sputtered GLAD films versus those grown by evaporation. Simulations showed that further reduction of the pressure would not significantly narrow the angular flux distribution as the width of the sputter flux distribution approached that of the solid angle subtended by the target.

With  $\alpha$  held constant and a slow  $\varphi$  rotation (relative to the deposition rate) introduced, helically shaped columns can be produced, as shown in Fig. 2-1(b). This film was deposited at  $\alpha = 80^\circ$  at 14 cm throw distance. The deposition pressure was 1.6 mTorr (0.21 Pa) and the sputter source regulated at 320 W constant power. Using the same substrate geometry, but with a rapid  $\varphi$  rotation results in a film with a porous, vertical post or "pillar" microstructure, as seen in Fig. 2-1(c). This film was deposited at 1.3 mTorr (0.17 Pa) and 350 W power. Visually, the films shown in Fig. 2-1(b) and (c) exhibit similar porosity due to the identical source/substrate geometry during deposition. Deposition of GLAD films by sputtering has also been demonstrated with other materials such as chrome and molybdenum, using similar geometries in other sputter systems.

Using LPLT sputtering to achieve a narrowed angular distribution of the angular flux, glancing angle deposition was successfully adapted to work with sputter deposition, demonstrating a variety of porous tailored microstructures. The ability to use sputter deposition enables simplified process control and an expanded range of thin film materials and applications for the GLAD process.

One of the problems with LPLT sputtering is that low operating pressure also translates into an overall low deposition rate. Since this first demonstration of sputtered GLAD, B. Dick and colleagues have performed more extensive studies with sputter deposition including use of larger targets (3 inch = 7.5 cm diameter) to achieve improved efficiency, lower target-to-substrate separation in combination with collimation, and the effect of periodic seeding layers [45]. In a related vein, other techniques for deposition of GLAD films such as pulsed laser deposition have also been developed [46].

## 2.2 Techniques for advanced microstructural control<sup>4</sup>

### 2.2.1 Introduction

It was established earlier that for deposition with the incident flux arriving at an angle  $\alpha$  from the normal, the resultant film would exhibit an inclined columnar microstructure which grows at an angle  $\beta$ . Based on geometrical arguments, Tait *et al.* [20] formulated a mathematical relationship for  $\beta$  as a function of  $\alpha$ . (See Eqn. 1-3 (p. 11), introduced earlier.) A graph of Tait's rule for column angle is plotted below in Fig. 2-2(a). In the same work, Tait also derived an expression for the ratio of inter-column spacing to column diameter as a function of  $\alpha$ :

$$a = \frac{1}{2}[1 + 1/(\cos \alpha)] \quad (2-1)$$

where  $a$  is the inter-column spacing, measured in column diameters. This ratio of inter-column spacing to column diameter is a measure of the porosity of the film. This equation is plotted in Fig. 2-2(b) below. At low (near normal) deposition angles, the inter-column spacing approaches unity, representing a dense microstructure with little or no gaps between neighbouring columns. In contrast, at higher flux incidence angles ( $\alpha > 80^\circ$ ), the porosity becomes a highly sensitive function of  $\alpha$ , illustrating the remarkable increase in porosity with deposition conditions in the GLAD regime.

It is clear that deposition angle affects both column angle and porosity. These two properties are inextricably linked: changing the one will affect the other (Fig. 2-3). Low deposition angles  $\alpha$  will produce a dense, vertical microstructure, while high deposition angles  $\alpha$  will produce a porous, inclined microstructure. Normal and oblique deposition modes are compared below in Table 2-1.

Given the relationship between flux incidence angle  $\alpha$ , column angle  $\beta$  and porosity, if one wishes to control column angle  $\beta$ , then the only obvious solution is to accomplish this goal

---

4. Part of this work has been previously published in [38] K. Robbie, J. C. Sit, and M. J. Brett, "Advanced techniques for glancing angle deposition", *J. Vac. Sci. Technol. B* 16, 1115-1122 (1998). Used with permission.

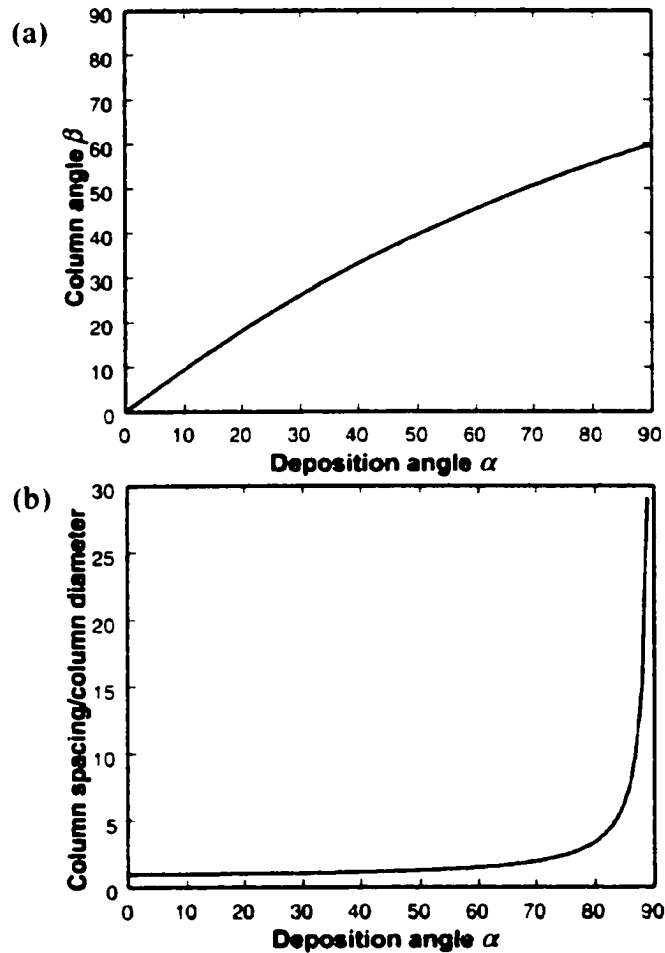


Figure 2-2: Effects of deposition angle  $\alpha$  on film structure in oblique deposition (a) Graph of relationship of Tait's rule for column angle  $\beta$  as a function of  $\alpha$ . (b) Graph of porosity, defined by ratio of inter-column spacing to column diameter, as a function of  $\alpha$  [20].

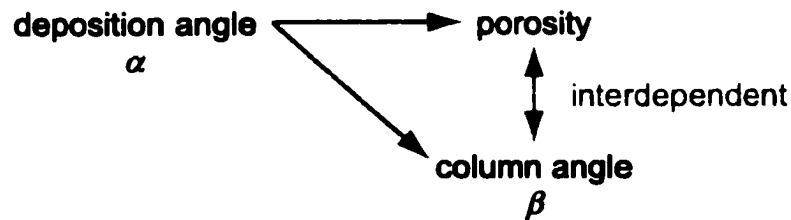


Figure 2-3: Control of porosity and column angle in standard GLAD  
In the standard GLAD technique, the flux incidence angle  $\alpha$  affects both porosity and column angle  $\beta$ . These two properties cannot be controlled independently.

by varying the flux incidence angle  $\alpha$ . Variation of  $\alpha$ , however, necessarily leads to variation of the porosity of the film which may be an undesired property. In optical films, variation in porosity leads to inhomogeneity of the refractive index of the thin film medium and

Table 2-1: Comparison of normal and oblique deposition

Deposition type	Normal	Oblique
Deposition angle ( $\alpha$ )	$\alpha = 0^\circ$	$\alpha$ large, 80 to 85° (typical range)
Substrate motion	stationary	stationary
Column angle ( $\beta$ )	vertical, $\beta = 0^\circ$	inclined, $0^\circ < \beta < \alpha$
Porosity	dense	porous
Microstructure type	dense film	GLAD film, tilted columns

may thus be detrimental to the optical properties one wishes to engineer.

Periodically bent nematic (PBN) materials were proposed by Meyer [47] who also put forth a liquid crystal model for their realization [48]. A thin film realization of a PBN material would be a film composed of smoothly bent, periodic, “C-” or “S-” shaped columns. Messier *et al.* [21], using their sculptured thin film (STF) technique, produced PBN films by varying the deposition angle  $\alpha$  in order to control the column angle  $\beta$ . While these films illustrate an engineered structure with controlled column angle, the STF method cannot escape the side effect of varying porosity, as the variation of the deposition angle results in a periodic variation of the density and hence the index of refraction. The film will thus function as a multilayer (rugate) interference filter. Robbie *et al.* [29] have intentionally exploited periodic variation of density in GLAD films to produce rugate filters.

### 2.2.2 Column angle control: paused growth versus spinning growth

What is needed, then, is a method to separate control over porosity from control over column angle. Looking only at oblique angle deposition onto stationary substrates held at fixed angle  $\alpha$  does not reveal a solution. However, recalling the basic forms of GLAD films discussed earlier (see “Basic forms” on p. 15), the post microstructure (Fig. 1-10(d)) provides a means of achieving a vertical, but porous film structure.

As described earlier, GLAD films possessing post or pillar microstructure are fabricated with rapid rotation of the substrate about an axis normal to the surface of the substrate ( $\varphi$

axis). Rapid rotation causes the plane of deposition (Fig. 1-6 (p. 12)) to rotate about the substrate normal axis quickly and as a result, deposition flux arrives equally from all azimuthal angles, producing a vertical columnar microstructure. In this GLAD microstructure, the deposition angle  $\alpha$  controls porosity of the film as before, but the use of substrate motion enforces column angle  $\beta = 0$ . This allows one to “get away with” a high porosity film but with a vertical column angle, depending on substrate motion.

Table 2-2 below compares growth of GLAD films in two modes: with the substrate held stationary at an oblique angle  $\alpha$  (“paused growth”) and with rapid substrate rotation about the  $\varphi$  axis as described above (“spinning growth”). The key comparison here is that the flux incidence angle  $\alpha$  can be kept constant to maintain uniform porosity, while achieving a microstructure composed of either inclined or vertical columns.

Table 2-2: Comparison of paused and spinning growth in GLAD

Deposition type	Paused growth	Spinning growth
Deposition angle ( $\alpha$ )	80 to 85° (typical range)	80 to 85° (typical range)
Substrate motion	stationary	rapid rotation in $\varphi$ axis
Column angle ( $\beta$ )	inclined, $0^\circ < \beta < \alpha$	vertical, $\beta = 0^\circ$
Porosity	porous	porous
Microstructure type	GLAD film, tilted columns	GLAD film, vertical posts

To achieve true independent control of column angle  $\beta$ , the technique must allow for films with column angles other than that seen in paused growth, where the columns grow at an angle which can be estimated using Tait’s rule (Eqn. 1-3 (p. 11)), or that seen in spinning growth, where the columns grow vertically. The advanced technique for controlling the column angle  $\beta$  is illustrated below in Fig. 2-4.

Letting  $\beta_{\text{Tait}}$  denote the column angle in paused growth mode, the column angle in paused growth (Fig. 2-4(a)) and spinning growth (Fig. 2-4(b)) modes is given by:

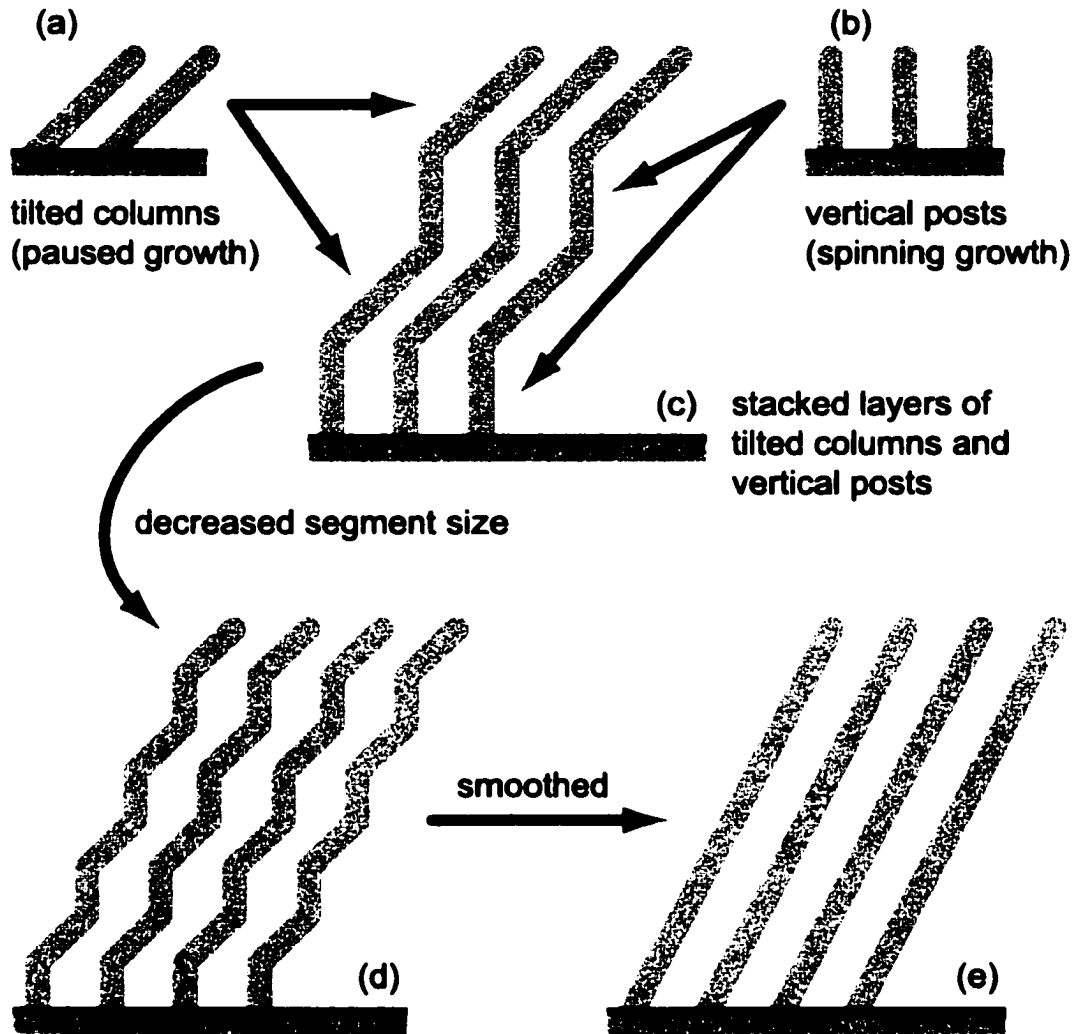


Figure 2-4: Controlling column angle and porosity independently  
 By combining segments of (a) paused growth, which produces tilted columns, and (b) spinning growth, which creates vertical columns, any column angle from 0 to  $\beta_{\text{Tait}}$  can be achieved. See main text for a more detailed description.

$$\beta(\text{paused growth}) = \beta_{\text{Tait}} = \alpha - \arcsin\left[\frac{1}{2}(1 - \cos \alpha)\right]$$

$$\beta(\text{spinning growth}) = 0 \tag{2-2}$$

Earlier, it was mentioned that essentially any column shape can be engineered by stacking layers of the four fundamental GLAD microstructures in the appropriate permutation. The advanced technique for controlling column angle does just this by alternating layers of paused growth and spinning growth (Fig. 2-4(c)). If the thickness of each of the layers is decreased (Fig. 2-4(d)) and made sufficiently small, a smoothed structure with column an-

gle lying between  $0^\circ$  and  $\beta_{\text{Tait}}$  is achieved (Fig. 2-4(e)). At this time, there is currently no known method to achieve column angles of greater than  $\beta_{\text{Tait}}$ .

In the current implementation of the GLAD control system software, the thickness of spinning growth sub-layers is typically chosen to be in the range 10 to 15 nm. The spinning growth sub-layers are deposited alternately with sub-layers of paused growth. By varying the proportions of paused versus spinning growth (that is, the duty cycle), the resulting column angle can be chosen with column angle  $0^\circ < \beta < \beta_{\text{Tait}}$ . More spinning growth produces a more vertical structure, whereas more paused growth yields a more oblique structure.

By alternating paused growth and spinning growth modes with this technique, near independent control of porosity and column angle is achieved. Instead of having  $\alpha$  control both porosity and column angle  $\beta$ , these two properties are controlled separately. The relationship amongst these properties is shown below in Fig. 2-5. Flux incidence angle  $\alpha$  affects porosity as before. Deposition angle is generally held constant throughout the deposition to produce a film with uniform (high) porosity<sup>5</sup>. The major difference with these advanced control techniques is that substrate motion is used to control column angle.

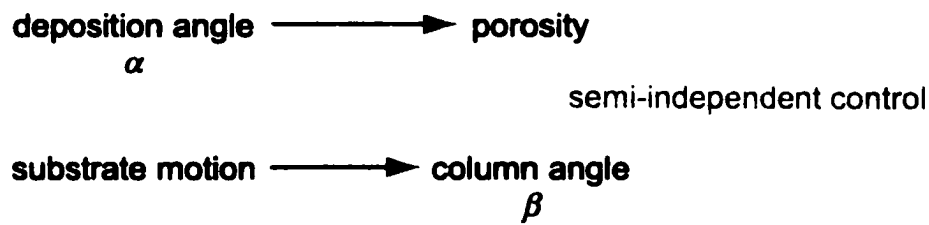


Figure 2-5: Control of porosity and column angle in advanced GLAD techniques. With advanced techniques for GLAD, semi-independent control between porosity and column angle is achievable. Porosity, as before, is controlled by choice of flux incidence angle  $\alpha$ . Substrate motion is used to control column angle  $\beta$ . The influence of deposition angle  $\alpha$  on column angle  $\beta$  is largely eliminated.

This advanced control technique which provides near-independent control of column angle and porosity can be demonstrated with two microstructures described here which cannot be fabricated using standard GLAD control techniques.

---

5. As stated before,  $\alpha$  typically is in the range of  $80$  to  $85^\circ$  for GLAD to produce high porosity films.

With standard GLAD substrate motion control, films possessing helical microstructure are produced by depositing at a constant oblique angle  $\alpha$  while maintaining a steady rotation about the  $\varphi$  axis. With standard control techniques, the column angle  $\beta$  of the helix<sup>6</sup> cannot be chosen independently of deposition angle  $\alpha$  (as in Fig. 2-3). Because  $\beta$  is fixed for a given value of  $\alpha$ , the radius and pitch in a helical film cannot be controlled independently. Consider a single-turn helical film, and to visualise the geometry easily, let the helical column be “unrolled” and laid flat on the page (Fig. 2-6 below).

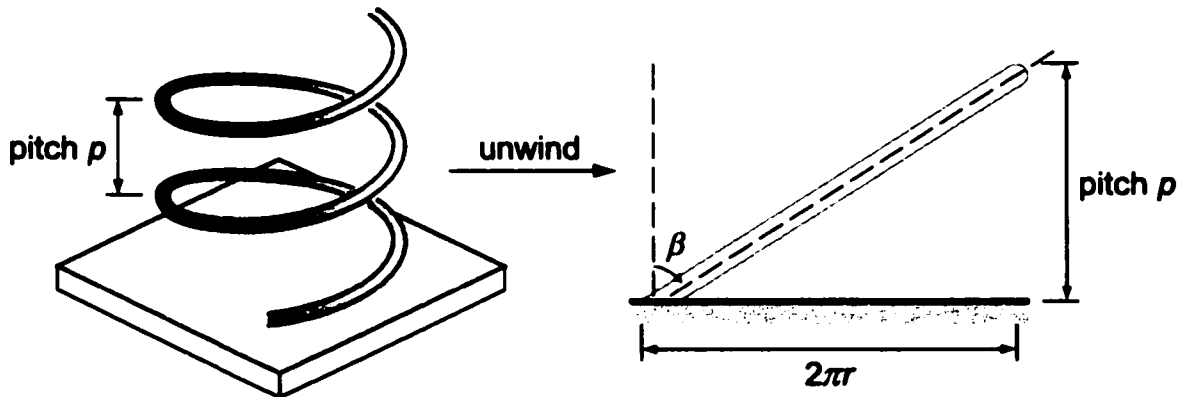


Figure 2-6: Geometry of helical microstructure

If a single turn of a helix is “unrolled”, the geometry of the structure becomes more obvious. The radius and pitch of the structure are linked by the column angle  $\beta$ . With advanced control techniques, the rise angle can be controlled independently, allowing for independent control of pitch and radius.

The unrolled helical column appears to be the same as a column resulting from GLAD deposition onto a stationary substrate (what was earlier described as paused growth). For this single turn helix, the thickness of this film corresponds to the helical pitch  $p$ , while the width of the unrolled column is actually the circumference of the helix  $C = 2\pi r$ , where  $r$  is the radius. Some elementary trigonometry reveals that:

$$C = 2\pi r = p \tan \beta \quad (2-3)$$

Using advanced control techniques, column angle can be controlled independently of flux

- 
6. Recall that column angle  $\beta$  is measured relative to the substrate normal. It is usual to describe the rise angle of the helix, measured as an elevation from the substrate plane. Rise angle would be  $90^\circ - \beta$ .



incidence angle, thus pitch and radius can likewise be controlled independently to some extent. Helical films fabricated from optical materials are of particular interest in optical applications. The ability to control the column angle in helical films permits, for instance, the fabrication of a set of films with equal pitch, but different radii in order to study the effects on optical properties of the helical radius. While control of helical geometry may in this case seem simplistic, theoretical studies by Venugopal and Lakhtakia [49] on chiral or helical structures fabricated with GLAD suggest the electromagnetic properties of chiral media have a strong dependence on the geometry of the structure. Thus a means to improve structural control with GLAD is important when investigating the structure-property relationships.

While the preceding example of advanced control illustrates column angle manipulation, one can take this technique one step further by dynamically varying the column angle during deposition. As described earlier, with the advanced technique, column angle is controlled by varying the proportion of paused growth to spinning growth modes. An example of a structure which illustrates dynamic control of column angle, but with constant porosity, is the periodically bent nematic (PBN) microstructure.

PBN GLAD films with smoothly bent “S”-shaped columns are produced by varying the proportion of paused versus spinning growth dynamically. In portions of the film where the columns grow leaning to the right, the spinning growth sub-layers are made thin and coupled with thicker sub-layers of paused growth with the pause position set such that the flux would be arriving from the right. As the film growth proceeds, the proportion of paused growth is gradually reduced to zero, causing the column direction to evolve from leaning towards the right to vertical. Growth continues by once again increasing the proportion of paused growth relative to the spinning growth, but this time the pause position is set such that flux would be arriving from the left during paused growth sublayers to cause the column direction to evolve from vertical to tilting to the left. From the standpoint of implementing the software program, it is somewhat of a challenge to describe dynamically evolving position and proportion of paused growth versus spinning growth as a mathematical algorithm for the GLAD control software, but is certainly not an impossible task.

In contrast to the PBN films produced by Messier *et al.* with their STF technique, those deposited using advanced substrate motion with the GLAD technique are largely free of density inhomogeneity. These films are expected to produce optical properties similar to the theoretically conceived PBN liquid crystal concept and will be discussed again later in relation to GLAD-liquid crystal composites, the central work of this thesis.

### 2.2.3 Column cross-section shape control

The form of advanced control described in the preceding section involves decoupling control column angle and porosity so that they may be controlled semi-independently. Advanced substrate motion control techniques can be used to implement a second form of advanced microstructural control: the control of column cross-section shape.

Recall the deposition of GLAD post microstructures which were explained as a degenerate helical microstructure with pitch  $p$  small.<sup>7</sup> Ideally it would be desired that  $p \rightarrow 0$ , but practically a value of approximately  $p < 15$  nm (when the pitch becomes comparable to the column thickness) reduces the pitch to an adequately small value such that adjacent turns of the helical structure cannot be discerned. The condition stipulated earlier was that when the pitch was made adequately small, the incoming flux arrives essentially uniformly from all azimuthal angles  $\varphi$ . Fig. 2-7(a) illustrates the case where there is a uniform azimuthal distribution of flux. The columnar cross-section (taken in a plane parallel to the substrate) will be circular in this case, assuming that 1) the rotation rate is constant relative to the deposition rate and 2) the rotation rate is sufficiently fast.

If, on the other hand, non-uniform rotation of the substrate is used, the resulting uneven distribution of flux would be expected to distort or “bias” the column shape. This effect can be exploited using advanced control techniques to allow the column cross-section shape to be tailored as desired. Fig. 2-7(b) illustrates non-uniform distribution of the incoming vapour flux. One possible method of implementing this distribution is to combine “regular”

---

7. The post, or pillar, microstructure type was introduced as one of the four fundamental microstructure types in Chapter 1 (see “Basic forms” on p. 15) and revisited earlier as “spinning growth” for advanced GLAD microstructural control techniques.

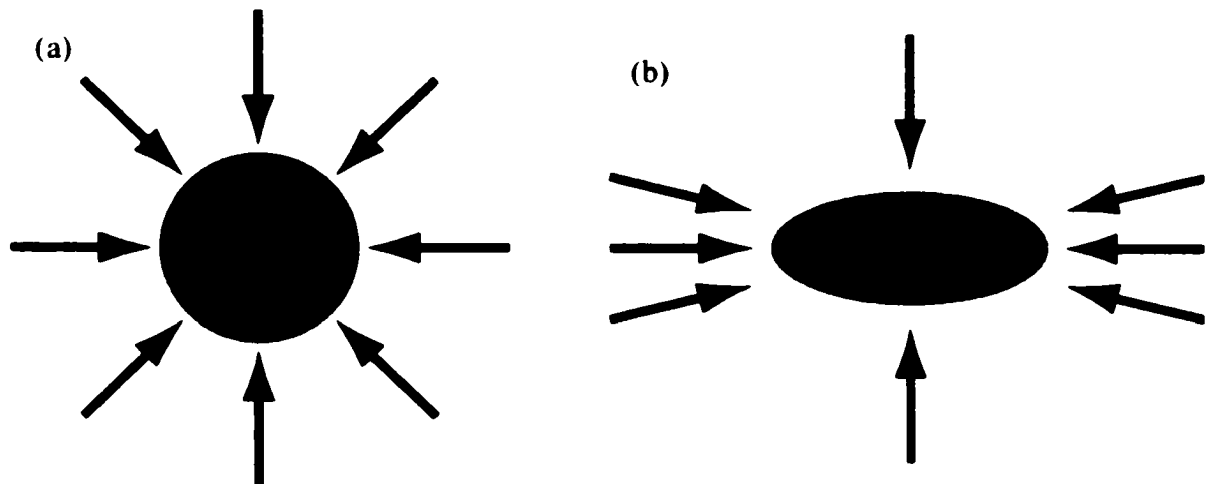


Figure 2-7: Control of column cross-section shape in GLAD  
 Cross-sections are diagrammed in planes parallel to the substrate. (a) With flux arriving evenly from all azimuthal angles, the column grows vertically, with a circular cross-section. (b) With flux arriving non-uniformly, such that flux arrives preferentially along one axis, the column shape can be made elliptical in cross-section.

spinning growth with the addition of paused growth at positions  $\varphi = 0^\circ$  and  $\varphi = 180^\circ$  (the left and right sides in the figure). This causes a larger proportion of flux to arrive from the azimuthal angles corresponding to the pause positions. Another way to visualise this implementation is to consider the paused growth at positions  $\varphi = 0^\circ$  and  $\varphi = 180^\circ$  to be similar to the deposition of a zig-zag microstructure, except with the pitch<sup>8</sup> made very small so that the individual segments of the zig-zag microstructure cannot be resolved. By biasing the flux distribution in this manner, the column cross-section shape can be elongated into an elliptical shape. As with the first form of advanced microstructural control described earlier, one can vary the fraction of paused versus spinning growth modes to control the ellipticity of the column shape. A low proportion of paused growth would give a more uniform distribution of flux and result in a more circular cross-section, while a high proportion of paused growth would give a distribution of flux strongly biased towards the pause positions and result in a more elliptical cross-section. As usual, the flux incidence angle  $\alpha$  is kept in the GLAD regime to attain high porosity in the films.

One subtlety that should be noted is the structural anisotropy in oblique incidence thin films

8. Pitch, as always, is defined as the vertical period or “wavelength” of the film. For the zig-zag or chevron structure, pitch corresponds to the thickness of a “zig” plus a “zag”.

[50]. Thin films fabricated by oblique deposition (onto stationary substrates) are well known to exhibit anisotropy between the film plane parallel to the deposition plane and the film plane perpendicular to the deposition plane. As a film's structure affects its properties, obliquely deposited thin films have been found to possess anisotropic properties including resistivity [51] and thermal conductivity [52]. Anisotropic optical properties, resulting from oblique deposition, have likewise been the subject of extensive research [53, 54, 55].

Thin film specialists following the preceding discussion no doubt would question whether the diagram in Fig. 2-7(b) is correct as shown or if instead the column cross-section elongation should instead be in the perpendicular direction (vertically in the diagram). The ambiguity arises because there are two competing processes which can affect the column cross-section shape. The non-uniform distribution of flux may cause the column cross-section shape to be elongated as shown in Fig. 2-7(b), but the structural anisotropy effects seen in oblique thin film growth [50] would tend to cause the elongation to occur in the perpendicular direction. So long as one or the other effect can be made to dominate, however, the goal of achieving an anisotropic column shape can be achieved, and the orientation of the anisotropy (whether it is parallel to or perpendicular to the deposition plane) is itself immaterial.

One possible structure that can be fabricated using this second form of advanced microstructural control is a "twisted ribbon" chiral structure. This structure, shown below in Fig. 2-8(a), is conceptualized in two steps. First, a vertical columnar film with elliptical cross-section (Fig. 2-7(b)) is grown using the technique described above. Second, a "twist" is introduced into the structure by precessing the pause positions during growth, as shown in Fig. 2-8(b). Suppose, for instance, the initial pause positions are  $\varphi = 0^\circ$  and  $\varphi = 180^\circ$ . Then for subsequent paused growth sublayers, the pause positions move to  $\varphi = 1^\circ$  and  $\varphi = 181^\circ$ , then  $\varphi = 2^\circ$  and  $\varphi = 182^\circ$  and so forth. Each time the pause positions precess by  $180^\circ$ , one half-twist of the structure is completed. Two half-twists correspond to a full  $360^\circ$  rotation and hence the thickness of two half-twists is defined as the pitch ( $p$ ) for this structure. As the direction of the pause position precession can be made clockwise or counter-clockwise, the direction of the twist can be chosen, resulting in two possible versions of the film. The

so called left- (LH) and right-handed (RH) versions are essentially identical except for the direction of the twist, making them mirror images of each other. This concept of chirality will be revisited in Chapter 3 (see “Anisotropy and chirality” on p. 40). Hodkinson *et al.* have also demonstrated this technique of column shape control in a process they call serial bi-deposition [56, 57].

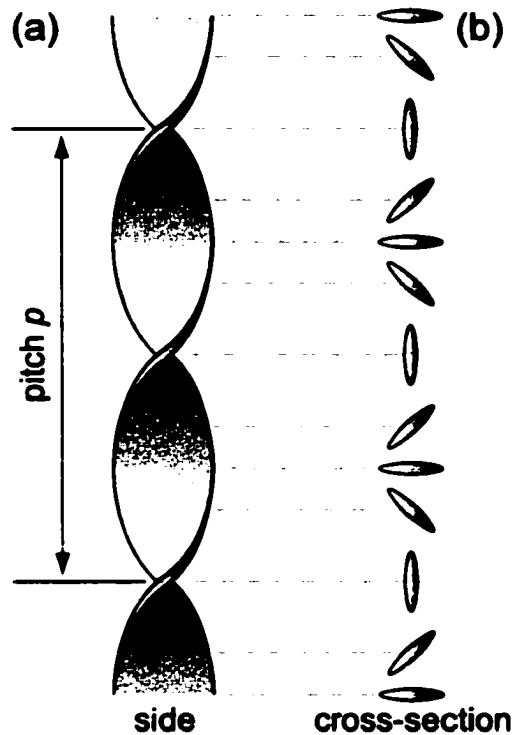


**Figure 2-8: Twisted ribbon chiral microstructure**  
Using advanced substrate motion control, GLAD films possessing an elliptical cross-section are fabricated to create a somewhat flat “ribbon” structure growing vertically. The addition of a twist in the ribbon results in a new type of chiral GLAD structure, whose pitch is equal to the thickness of two half-twists of the structure..

A realisation of the twisted ribbon chiral structure using GLAD is shown below in Fig. 2-9. This film possess a left-handed twisted ribbon chiral structure with 10 turns and pitch of approximately  $p = 830$  nm. The film material used was  $\text{Al}_2\text{O}_3$  and was grown on glass and Si wafer substrates.

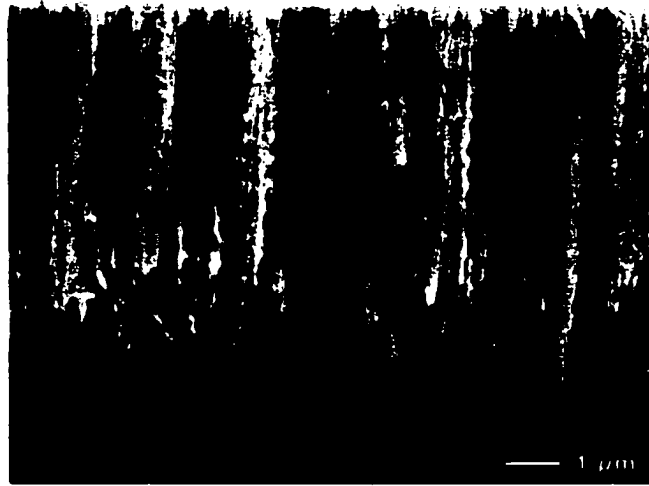


**Figure 2-9: GLAD film with twisted ribbon chiral microstructure**  
The film is composed of  $\text{Al}_2\text{O}_3$  deposited by electron-beam evaporation. As the deposition angle is lower ( $\alpha = 83\text{--}84^\circ$ ), the film has a “denser” appearance than other GLAD films typically used in this work.

---

## Chapter 3

# The optics bench — optics of GLAD films

---

This chapter discusses the chiral optics of GLAD thin films. The first section gives some background about the electromagnetic representation of light, focussing on polarisation states — elliptical, linear, and circular — and how they relate to each other. Polarisation is then related to the geometric concepts of anisotropy and chirality, as the optical response of materials possessing these attributes is sensitive to the state of polarisation of the incident light. Next, a simplified model is used to describe some of the optical phenomena observed in chiral media such as helical GLAD films. Following this introductory section, the optical response of GLAD films (without embedded materials) is presented. This is referred to as the “dry optics” of GLAD films in contrast to the optics of hybrid GLAD/LC materials presented in Chapter 4.

In the second half of this chapter, liquid crystalline materials are introduced with a description of their properties and application in current display technologies. The similarities of the optical response of chiral GLAD media to those of certain types of LCs is presented, culminating in a comparison of GLAD and LC technologies to set the stage for the combination of GLAD films with LC materials to be presented in the next chapter.

### 3.1 Light and polarisation

Light can be treated as a transverse electromagnetic wave [58, 59]. In the most general case the electric field (vector) is represented as  $\mathbf{E}(\mathbf{r}, t)$ . The state of polarisation is determined by tracking the temporal and spatial variance of the endpoint of the electric field vector  $\mathbf{E}$ . For a general disturbance  $\mathbf{E}$ , the endpoint of the electric field vector traces out an ellipse, but this varies in space and time, so the polarisation state is said to be random.

If discussion is restricted (using some simplifying assumptions) to the case of a coherent, harmonic electromagnetic wave travelling along the z-axis in an isotropic, uniform medium, the wave may be represented by the following expression for the electric field:

$$\mathbf{E}(z, t) = \text{Re}[\mathbf{A}e^{j(\omega t - kz)}]$$

with  $\mathbf{A} = \hat{\mathbf{x}}E_x + \hat{\mathbf{y}}E_y$  (3-1)

where  $E$  represents the amplitude,  $\omega$  the frequency, and  $k$  the wavevector.  $\mathbf{A}$  is the complex envelope, with magnitudes  $E_x$  and  $E_y$  in the  $x$  and  $y$  directions, respectively. Looking at how the electric field varies in time and space reveals the state of polarisation of the light.

### 3.1.1 Linear and circular polarisation

The simplest state of polarisation is linearly polarised light (also called plane-polarised), in which the orientation of the electric field remains constant. A wave polarised with respect to the  $x$ -axis follows from Eqn. 3-1:

$$\mathbf{E}_x = \hat{\mathbf{x}}E_x \cos(\omega t - kz) \quad (3-2)$$

By combining two linearly polarised waves which have the same frequency and whose planes of polarisation are orthogonal to each other, a number of more interesting polarisation states can be examined. The two linearly polarised waves can be represented in the most general case as:

$$\begin{aligned} \mathbf{E}_x &= \hat{\mathbf{x}}E_x \cos(\omega t - kz + \delta) \\ \mathbf{E}_y &= \hat{\mathbf{y}}E_y \cos(\omega t - kz) \end{aligned} \quad (3-3)$$

where  $\delta$  represents an arbitrary relative phase difference between the  $x$  and  $y$  waves and propagation of the waves is in the  $z$ -direction. Looking at the time variance of the electric field vector in a plane of observation perpendicular to the direction of propagation at a fixed point  $z$  reveals that, in the general case, the endpoint of the electric field vector  $\mathbf{E}$  traces out an ellipse in a plane perpendicular to the  $z$ -axis (the direction in which the wave is propagating). This state is known as elliptical polarisation.

In the case where the phase difference between the  $x$  and  $y$  components is an integer multiple of  $\pi$  (i.e.  $\delta = m\pi$ , where  $m$  is any integer), the resultant wave given by the vector sum of  $\mathbf{E}_x$  and  $\mathbf{E}_y$  is:



$$\begin{aligned} \mathbf{E} &= (+ \hat{\mathbf{x}} E_x + \hat{\mathbf{y}} E_y) \cos(\omega t - kz) \text{ for } m \text{ even} \\ \mathbf{E} &= (- \hat{\mathbf{x}} E_x + \hat{\mathbf{y}} E_y) \cos(\omega t - kz) \text{ for } m \text{ odd} \end{aligned} \quad (3-4)$$

At the plane of observation, the resultant  $\mathbf{E}$  vector traces out a line. This is of course recognised as linearly polarised light and it is shown that the linear polarisation can be derived as a special case of the elliptical polarisation. The angle of the plane of polarisation depends on the magnitudes of  $E_x$  and  $E_y$ .

Going back to the elliptical polarisation defined in Eqn. 3-3, if the amplitudes of the two component waves are now made equal ( $E_x = E_y = E$ ) and the relative phase shift between  $E_x$  and  $E_y$  components is made  $\delta = \pm \pi/2$  (a  $90^\circ$  or quarter-wave phase shift), then a second special case is generated. For the case of  $\delta = +\pi/2$  (or more generally,  $\delta = +\pi/2 + 2m\pi$ , where  $m$  is any integer<sup>1</sup>), the resultant wave is left-circularly polarised (LCP); for the case of  $\delta = -\pi/2 + 2m\pi$  ( $m$  any integer), the resultant wave is right-circularly polarised (RCP):

$$\begin{aligned} \mathbf{E}_x &= \hat{\mathbf{x}} E \cos(\omega t - kz \pm \pi/2) \\ \mathbf{E}_y &= \hat{\mathbf{y}} E \cos(\omega t - kz) \\ \text{LCP} &= E \cdot [\hat{\mathbf{x}} \cos(\omega t - kz + \pi/2) + \hat{\mathbf{y}} \cos(\omega t - kz)] \\ \text{RCP} &= E \cdot [\hat{\mathbf{x}} \cos(\omega t - kz - \pi/2) + \hat{\mathbf{y}} \cos(\omega t - kz)] \end{aligned} \quad (3-5)$$

For circularly polarised light, at any plane of observation<sup>2</sup> at a fixed location  $z$ , and looking back toward the source, the  $\mathbf{E}$  field vector traces out a circular path of radius  $E$  with angular frequency  $\omega$  and rotates clockwise for RCP and counter-clockwise for LCP. At a fixed time  $t$  (taking a “freeze frame snapshot” of the wave), the tip of the  $\mathbf{E}$  field vector follows a RH helix for RCP or a LH helix for LCP as the observation point is moved in the  $z$ -direction.

Eqn. 3-5 shows that as well as being a special case of elliptically polarised light, circularly polarised light can be expressed as the combination of two plane polarised waves, one polarised with respect to the  $x$  axis and the second polarised with respect to the  $y$  axis but with a phase shift of  $\pm \pi/2$  ( $90^\circ$ ). Alternately one could say that, given the proper conditions,

1. Because of the time-harmonic nature of the wave, one can add any  $2\pi$  multiple to the phase shift.
2. Perpendicular to the  $z$ -axis which is the direction of propagation of the wave.

linear + linear yields circular.

Further, if one were to sum the LCP and RCP waves given in Eqn. 3-5, the  $x$  components cancel out, leaving a wave plane polarised in the  $y$  direction. It can be further shown that the sum of LCP and RCP yields linear polarised light for any arbitrary phase shift between the LCP and RCP components, so long as they are of equal amplitude<sup>3</sup>. Thus, LCP + RCP yields linear polarised light.

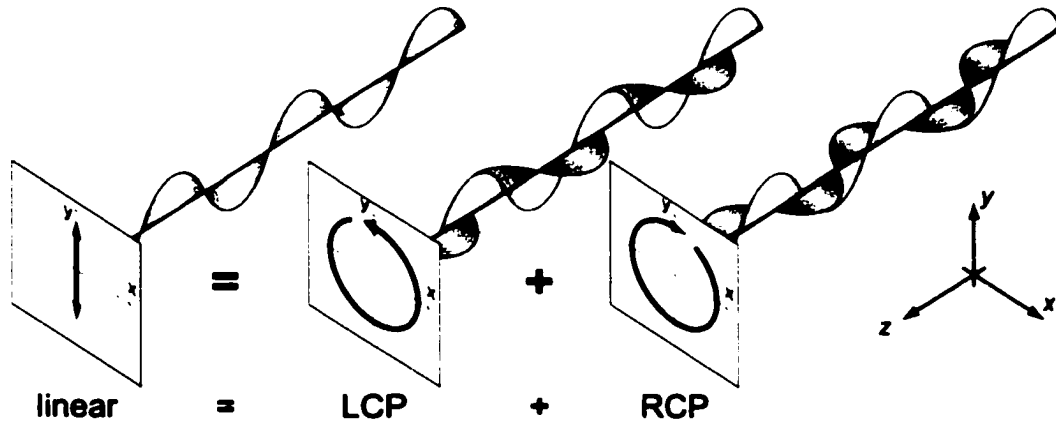


Figure 3-1: Resolution of linear polarised light into LCP and RCP  
Linear polarised light can be resolved into its orthogonal LCP and RCP components. The effect of a medium can then be examined separately for LCP and RCP.

It has thus been shown that two orthogonal linearly polarised components may be brought together to produce circularly polarised light. Likewise, two orthogonal circularly polarised components (i.e. LCP and RCP) may be brought together to yield linearly polarised light. By corollary, one can resolve a circular polarisation into orthogonal linearly polarised components or resolve linear polarisation into orthogonal circularly polarised components. This duality of linear and circular polarisations is important to the optical characterisation of anisotropic and chiral materials.

### 3.2 Anisotropy and chirality

Anisotropy and chirality are geometric concepts both referring to a medium exhibiting dif-



3. If the amplitudes are unequal, the result is elliptically polarised light. The present discussion is restricted to the case of monochromatic waves.

ferent properties depending on “direction”. Anisotropy is the more easily understood of the two concepts. A medium is said to be anisotropic when its properties have different values along different axes. In the context of the present discussion on optics and polarisation, an anisotropic medium has, for instance, different indices of refraction along different axes. The optical response of such a medium thus depends on the direction of polarisation of incident linearly polarised light and is said to be linearly birefringent. Similarly, the response of a chiral medium depends on the handedness of incident circularly polarised light and is thus said to be circularly birefringent.

Chirality is a geometric concept referring to the lack of symmetry of an object [60]. An object is chiral (Fig. 3-2) if it cannot be superimposed by rotation and translation onto its mirror image. An object is achiral (or non-chiral) if it does not fit this condition. All objects are therefore either chiral or achiral, but only three dimensional objects can possess chirality<sup>4</sup>. The most obvious example of chirality are one’s hands. In fact, the word “chiral” derives from the Greek word meaning “hand” and the two possible “versions” or enantiomorphs of chiral objects are appropriately and by definition called left-handed (LH) and right-handed (RH). Other examples of chiral objects include some types of snail shells, the Möbius strip (there are two ways for the half-twist to occur), golf clubs (left and right-handed versions), screws (there are two ways to wind the threads although in practice only RH threads are used), and many types of molecules (generally these are organic substances). Helical GLAD films (Fig. 3-3) also are chiral. The handedness of a helical GLAD film simply depends on whether the substrate holder rotates clockwise or anti-clockwise during deposition.

The examples of chiral objects given above show that chirality can occur at any size scale because it is a strictly geometric notion. Chirality can occur on a macroscopic scale such as with gloves and coil springs. At the opposite end of the spectrum, chirality may be a feature of a substance itself, rather than being the product of the way in which an object is

---

4. The two dimensional “analogue” of a chiral object would be a spiral. However, two dimensional objects cannot be chiral because they can always be “flipped over” and superimposed onto their mirror images. e.g. spiral shapes  and 

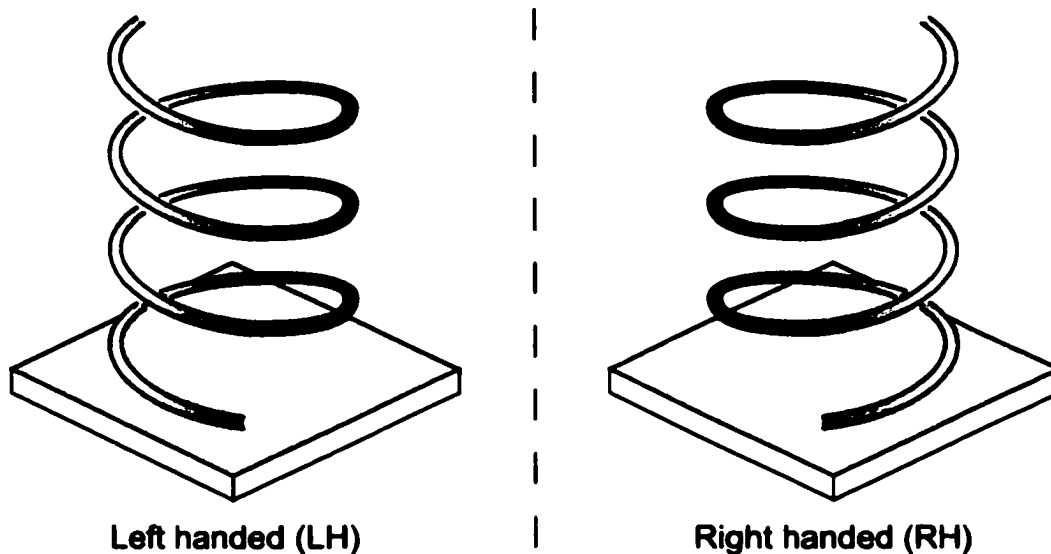


**Figure 3-2: Left- and right-handed chiral structures**  
 The left-handed (LH) and right-handed (RH) helical structures shown here are identical except for the direction of twist. The two structures are mirror images of each other, but cannot be superimposed.

manufactured. Quartz crystals, for instance, occur in both LH and RH versions, depending on the arrangement of the atoms in the crystal structure. In other substances, the molecules themselves are chiral. Examples include sugar, tartaric acid, and turpentine.

In substances which have chiral crystal structure, chiral molecular structure, or possibly both, a phenomenon called optical activity [61] may be observed. Optical activity, the rotation of the plane of polarisation of linearly polarised light, is the most evident manifestation of the unique optical properties which arise because of the chiral nature of these substances. (Optical activity and other optical phenomena are discussed in further detail later in this chapter.) LH and RH enantiomorphs of a chiral medium, which are otherwise identical, exhibit optical activity of equal magnitude but of opposite sense.

In the case of quartz crystals, the optical activity is related to the chiral arrangement of atoms in the crystal structure, although the molecules ( $\text{SiO}_2$ ) themselves are achiral. As a result, quartz exhibits optical activity only in crystalline form. Molten  $\text{SiO}_2$ , and non-crystalline solid forms such as fused silica exhibit no optical activity. In the other case, where

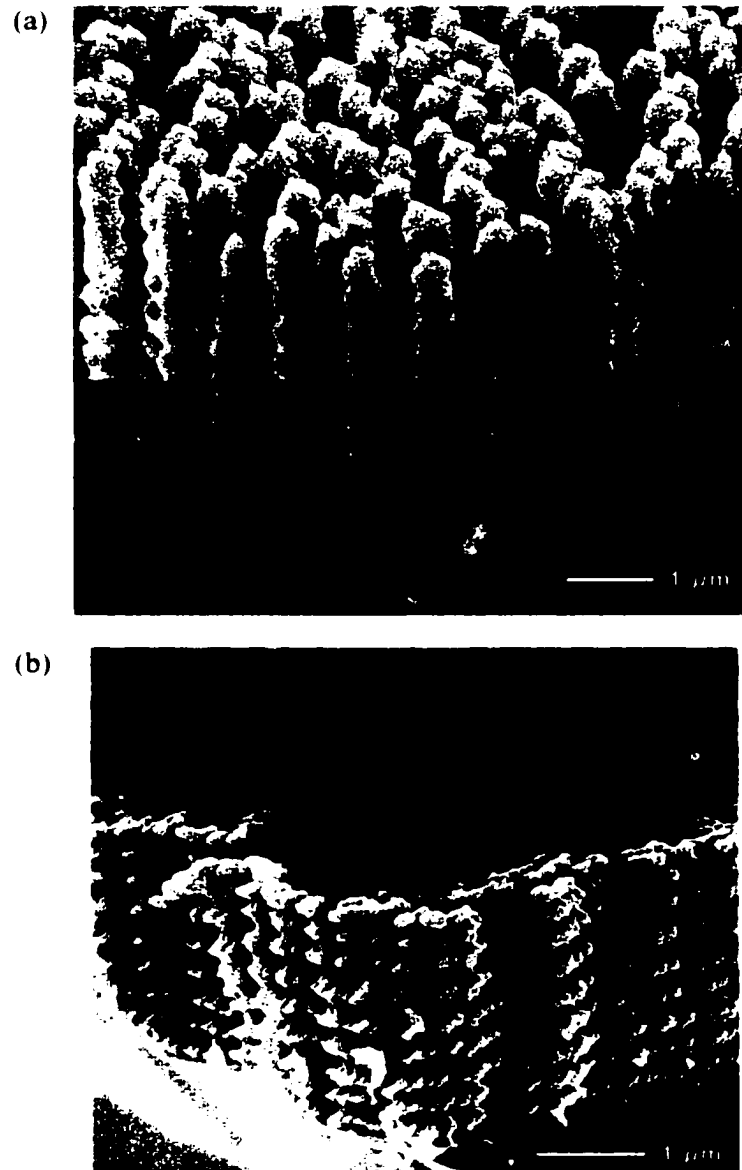


Figure 3-3: Examples of LH and RH chiral GLAD films  
(a) LH helical film,  $\text{SiO}_2$ . (b) RH helical film,  $\text{Al}_2\text{O}_3$ .

optical activity has a molecular basis, optical activity is observed in these substances for both the solid and liquid states as well as when they are in solution. Here, the chirality is by virtue of the structure of the molecule itself and hence the rotatory power is intrinsic to the individual molecules. In some substances, optical activity arises from both the crystal structure and the molecular structure.

Chirality is a particularly important concept in the fields of chemistry and biology, where

examination of the chiral optical effects reveals insights into the structure of molecules and stereochemical problems. Although optical activity was first observed nearly two centuries ago, only in recent decades has the measurement optical activity phenomena become a widespread tool. Extensive study has been undertaken with these chiroptical methods [62].

### 3.3 Chiral optical response

The optical response of a chiral medium such as a helical GLAD film may be analysed and measured in terms of the difference in response to LCP and RCP light. Here, a simplified “layman’s” model will be used to describe the phenomenon. One circular polarisation will match the handedness of the film because the wavefront and chiral GLAD film share the same shape and is therefore named here the coupled polarisation. The other circular polarisation, however, is of opposite handedness to the film so its wavefront and chiral film intersect only at a series of discrete points (once per “turn”) and is thus called the uncoupled polarisation.

Because the wavefront of the coupled circular polarisation matches the shape of the chiral film, it is as if the coupled polarisation travels entirely in within the film medium and hence one may say that the coupled polarisation “sees” the film and only the film (a crude description of perfect coupling). In contrast, because the uncoupled polarisation and chiral film possess different shapes, the uncoupled polarisation travels solely within the void medium and therefore one may say the uncoupled polarisation does not “see” the film at all.

A comparison of the effects of a chiral medium on the coupled and uncoupled circular polarisations is presented in Table 3-1 below. For the simplified model described here, it is initially assumed that there is perfect coupling of the circular polarisation whose handedness matches that of the chiral medium and that there is no coupling whatsoever of the orthogonal circular polarisation<sup>5</sup>. For a porous, chiral GLAD film, then, the coupled polarisation is assumed to be coupled into (that is, travelling completely within) the film which has refractive index  $n_{\text{film}}$ , while the uncoupled polarisation sees only (and hence propagates

---

5. These assumptions are of course incorrect, but they help to illustrate how the chiral optical effects in GLAD films arise. Further discussion is presented later in this chapter.

exclusively through) the medium in the void regions of the film which is assumed to be air. This circular birefringence results in a net phase retardation of the coupled polarisation relative to the uncoupled polarisation, because propagation velocity through a material with higher index is slower.

Table 3-1: Simple comparison of effects on circular polarisations in a chiral film

	coupled polarisation	uncoupled polarisation
Effective index	$n_{\text{film}}$	$n_{\text{void}} = n_{\text{air}} = 1.0$
Phase retardation	retarded	no retardation
Bragg reflection	yes	no
Absorption by film	yes (dichroism)	no

In chiral GLAD films (applicable microstructures include helices or the twisted ribbon introduced in the previous chapter) fabricated from appropriate optical materials, the chiral optic response manifests itself in several forms. First, the films exhibit optical activity, or rotation of the plane of polarisation of linearly polarised light. Second, they may exhibit circular dichroism, or selective absorption of one of the two circular polarisations. Third, the films cause circular Bragg reflection, that is the selective scattering/reflection of the circular polarisation which matches the handedness of the film in the resonance regime when the wavelength of the incident light matches the pitch (periodicity) of the chiral medium. These phenomena are discussed further below.

### 3.3.1 Optical activity

Let linearly polarised light be incident on a LH, chiral GLAD film where:

$$\mathbf{E}_{\text{in}} = 2E \cdot \cos(\omega t - kz) \quad (3-6)$$

Recalling that linearly polarised light can be resolved into RCP and LCP components, the two components may be written as:

$$\text{RCP} = E \cdot [\hat{\mathbf{x}} \cos(\omega t - kz) + \hat{\mathbf{y}} \cos(\omega t - kz + \pi/2)]$$

$$\text{LCP} = E \cdot [\hat{x} \cos(\omega t - knz) + \hat{y} \cos(\omega t - knz - \pi/2)] \quad (3-7)$$

where  $n$  is the index of refraction of the film material. Because the film is LH,  $n_{\text{RCP}} = n_{\text{void}} = 1.0$  while  $n_{\text{LCP}} = n_{\text{film}}$ . Assuming no absorption, scattering, or reflection of the incident wave, the transmitted wave as it exits from the film may be expressed as the following sum of LCP and RCP components which were given in Eqn. 3-7:

$$\mathbf{E}_{\text{out}} = \text{LCP} + \text{RCP} = 2E \cdot \cos(\omega t - \frac{1}{2}k(n+1)z) [\hat{x} \cos(\frac{1}{2}k(n-1)z) - \hat{y} \sin(\frac{1}{2}k(n-1)z)] \quad (3-8)$$

The resultant wave is once again linearly polarised, but now the plane of polarisation has been rotated (represented by the factor in square brackets in Eqn. 3-8) by an angle:

$$\theta = \frac{1}{2}k(n-1)z \quad (3-9)$$

The rotation arises from the phase retardation of the coupled polarisation (LCP in this case) relative to the non-coupled polarisation (RCP). It depends on wavelength, index of refraction of the film material, and thickness of the film. Substituting in  $k = 2\pi/\lambda_0$  and  $z = L$  (thickness of the film), yields the following:

$$\theta = \pi(n-1)L/\lambda_0$$

$$\frac{\theta}{L} = \frac{\pi(n-1)}{\lambda_0} \quad (3-10)$$

which is an expression of the theoretical maximum rotation per unit thickness of the film<sup>6</sup> in this idealised case of perfect coupling for the one circular polarisation and zero coupling for the other. The  $\theta/L$  value for several optical materials commonly used with GLAD is calculated below in Table 3-2 and is given over a range of wavelengths. It can be seen that rotation decreases with wavelength and increases with index of the film material. Because of the wavelength dependence of rotation, the measurement of this optical phenomenon versus wavelength is more accurately called optical rotatory dispersion (ORD). It will be seen later that actual measured rotation in chiral GLAD films is on the order of two orders

---

6. Units rad/m which are easily converted to  $^{\circ}/\mu\text{m}$ .



of magnitude smaller than the theoretical maximum values calculated here.

Table 3-2: Theoretical maximum optical rotation for several optical materials

Wavelength, $\lambda_0$ [nm]	Optical rotation per unit length, $\theta/L$ [ $^\circ/\mu\text{m}$ ]		
	MgF <sub>2</sub> ( $n = 1.38$ )	SiO <sub>2</sub> ( $n = 1.47$ )	Al <sub>2</sub> O <sub>3</sub> ( $n = 1.66$ )
300	228.0	282.0	396.0
400	171.0	211.5	297.0
500	136.8	169.2	237.6
600	114.0	141.0	198.0
700	97.7	120.9	169.7
800	85.5	105.8	148.5

The expressions in Eqn. 3-10 can be generalised for the case of circular birefringence wherein the chiral medium is assumed to have two refractive indices,  $n_{\text{RCP}}$  and  $n_{\text{LCP}}$ :

$$\theta = \pi(n_{\text{LCP}} - n_{\text{RCP}})L/\lambda_0$$

$$\frac{\theta}{L} = \frac{\pi(n_{\text{LCP}} - n_{\text{RCP}})}{\lambda_0} \quad (3-11)$$

The angle  $\theta$  through which the plane of polarisation is rotated by a chiral medium is taken as positive for a clockwise rotation when looking back at the source. Clockwise rotation occurs when  $n_{\text{LCP}} > n_{\text{RCP}}$  and is called dextrorotatory; counterclockwise rotation occurs when  $n_{\text{LCP}} < n_{\text{RCP}}$  and is called levorotatory.

### 3.3.2 Circular dichroism

Thus far, it was assumed for the sake of convenience that that no absorption occurs. Of course this is untrue in general due to a second chiral optical phenomenon, circular dichroism (CD), the selective absorption of one of the two circular polarisations. A chiral medium will preferentially absorb the coupled polarisation compared to the uncoupled polarisation. Using the simplified model discussed earlier, this phenomenon is explained by

saying that the coupled polarisation is absorbed because it interacts with the structure (they are of similar “shape”); the uncoupled polarisation, in contrast, does not interact to any appreciable degree with the chiral structure (as they are of different “shapes”) and thus is not subject to absorption by the chiral medium. For linear polarised light incident on a LH medium, one would find that the transmission of LCP is lower than that of RCP; the opposite would occur in a RH medium. A chiral medium made of a highly absorbing material could function as a dichroic circular polariser as the coupled polarisation would be absorbed by the lossy medium, while the uncoupled polarisation could pass through unperturbed.

Taken together, CD and ORD are important characterisation tools to biologists and chemists as they provide insight into the structure of the materials being examined.

### 3.3.3 Bragg reflection

The third manifestation of chiral optical properties is circular Bragg reflection (analogous to Bragg reflection from a multi-layer coating). When the wavelength of light matches the pitch of the film,  $p$ , scaled by the effective refractive index of the film, the coupled polarisation will be selectively scattered/reflected by the chiral medium. The resonance condition is defined by:

$$\lambda_R = n_{\text{effective}} p \quad (3-12)$$

In the ideal case, the coupled polarisation would be 100% reflected at resonance, meaning that only the uncoupled polarisation would be transmitted through the film. From the point of view of optical activity, this would correspond to infinite rotation at resonance.

### 3.3.4 Overall response

Unfortunately, all three chiral optical effects described above occur together. Optical activity, circular dichroism, and circular Bragg reflection all play a part in the overall optical response of a chiral medium. It is difficult, if not impossible, to deconvolute the chiral optical measurements into constituent components due to ORD, CD, and circular Bragg reflection. Because of circular dichroism and circular Bragg reflection, at a wavelength range

near resonance, the transmission of the coupled polarisation will be lower than that of the uncoupled polarisation. But how much of this is due to CD effects and how much is due to Bragg effects? It is difficult to say. However, because the intensity of the two circular polarisations in the transmitted light is unequal, this results in an elliptical polarisation state, rather than a linear polarisation state as assumed previously. Chiral optical measurements on GLAD films are therefore a matter of interpretation given the interdependent nature of the chiral optical phenonema discussed here.

### 3.4 Measurements of GLAD films

While the fundamentals of chiral optical activity were discovered in the mid-nineteenth century, initial work focussed on so-called natural optical activity, that is when this phenomenon occurs naturally in a substance. Much of the work done related to the field of chemistry. Lindman, in the 1920s, experimented with wire spirals and microwave propagation [63, 64]. His experiments were significant in that they represented some of the earliest reported work on “optical activity” (i.e. electromagnetic activity) of an artificial chiral medium. Much later, Tinoco *et al.* [65, 66] also reported measurements supporting the earlier findings by Lindman. They looked at electromagnetic activity of microwaves incident on copper wire helices in a box.

While the copper wire helices used in the experiments described here [63-66] have a pitch on the order of  $\sim 1$  cm and thus display electromagnetic activity in the microwave regime, a thin film realisation of a chiral medium with pitch on the order of hundreds of nanometres would exhibit electromagnetic activity in the optical regime, and may be of particular interest if optical activity can be achieved in the visible wavelength range. Optical activity and circular Bragg reflection similar to cholesteric liquid crystals (CLCs, described later in this chapter), was observed as early as 1959 by Young and Kowal [67] who deposited films at oblique angles (but at lower deposition angles,  $\alpha < 70^\circ$ ) onto rotating substrates and demonstrated optical activity in these films. Unfortunately, at the time of their experiment, the scanning electron microscope was not yet available (the SEM was not in commercial production until the mid 1960s) and thus the structure of their films is not known. Following theoretical work by Azzam [68] and Lakhtakia and Weiglhofer [69-72] which revived in-

terest in the field, Robbie *et. al.* fabricated the first porous helical thin films using GLAD [24] and subsequently reported spectroscopic measurements of optical activity [73, 74, 75]. The unique chiral optic response of chiral GLAD films arises from the structural chirality and the index difference between the film material and the void material (air). Optical measurements have also been reported on thin films fabricated by oblique incidence deposition by other researchers [76, 77]. There exists also an extensive body of work on modelling of the interaction of electromagnetic waves in chiral media (see for example, Refs. 78, 79, 80).

### 3.4.1 Experimental setup

In this section, some of the measurements of the chiral optical response in GLAD films are presented. The two main types of chiral optical measurements that have been used to characterise the chiral optical response in GLAD films are measurements of the transmission of LCP/RCP and of rotation.

Spectroscopic transmission measurements of LCP and RCP are performed with a spectrophotometer set up as shown in Fig. 3-4. The beam path consists of light source, depolariser, linear polariser oriented with transmission axis oriented at  $0^\circ$ , quarter-wave retarder oriented at  $\pm 45^\circ$  relative to the polariser, GLAD film sample, depolariser, and detector. The majority of the spectroscopic measurements were performed using a Perkin-Elmer Lambda 900 spectrophotometer which has the general purpose optical bench option allowing for flexible setups. The depolarisers are not strictly necessary to the measurements, but generally provide “cleaner” measurements. The depolariser before the detector was not used for most measurements, while the depolariser after the light source was left in place for nearly all measurements.<sup>7</sup> The linear polariser and quarter-wave plate together generate circularly polarised light. When the quarter-wave plate fast axis is oriented at  $+45^\circ$  relative to the polariser transmission axis, RCP is produced; with the quarter-wave plate fast axis oriented at  $-45^\circ$  relative to the polariser transmission axis, LCP is produced. A Glan-Taylor

---

7. A further reason to use the depolariser after the light source is that it ensures that the intensity of the light beam after the linear polariser is independent of the orientation of the polariser transmission axis. If the light source is partially polarised, the intensity will vary as the linear polariser is rotated.

polariser was used as it works across a broad wavelength range and polarises by refraction rather than by absorption. An achromatic quarter-wave plate was used. Percent transmission (%T) scans over the wavelength range of interest are taken twice, once for RCP and once for LCP. The difference spectra can then be calculated.

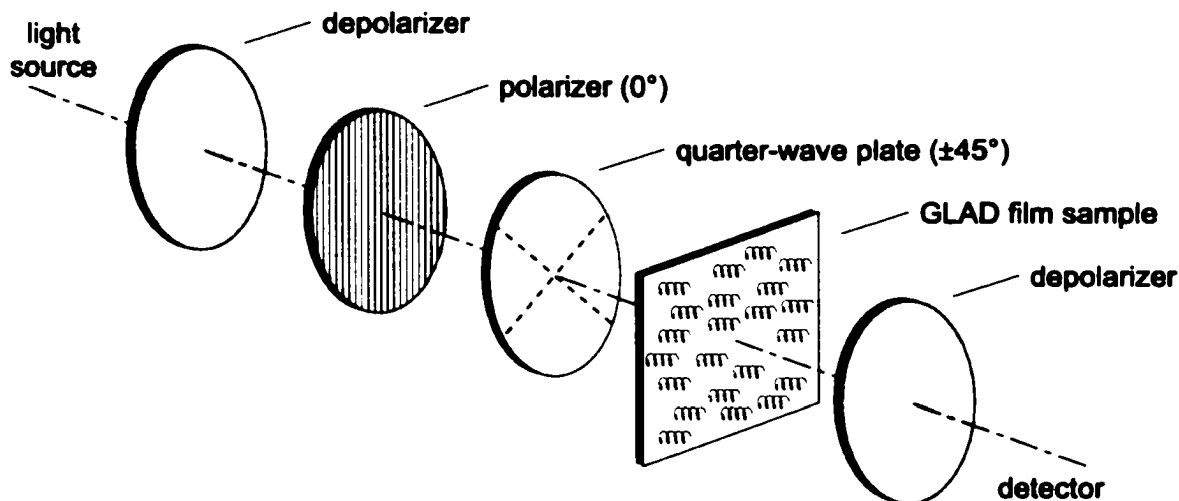


**Figure 3-4: LCP/RCP transmission measurements**  
The linear polariser and quarter-wave retarder together produce left- or right-circularly polarised light.

Measurement of polarisation rotation uses the same instrument but with a somewhat more involved scan procedure. For ORD measurements, the beam path consists of light source, depolariser, first linear polariser, GLAD film sample, second linear polariser (analyser), and detector. The apparatus is shown in Fig. 3-5 below. The usual convention for ORD measurements is to have the first polariser fixed (at  $0^\circ$ ) and to use a rotating analyser (second polariser). For this instrument however, a stepper motor polariser drive rotates the first polariser and the second polariser is held fixed.

Rotation is measured using the extinction (minimum transmission) technique which is based on the fact that crossed polarisers exhibit minimum transmission (ideally zero). If an optically active medium is then introduced between the polarisers, light passing through the one polariser is rotated slightly by the medium. The plane of polarisation of the light is therefore not perpendicular to the transmission axis of the second polariser, allowing some

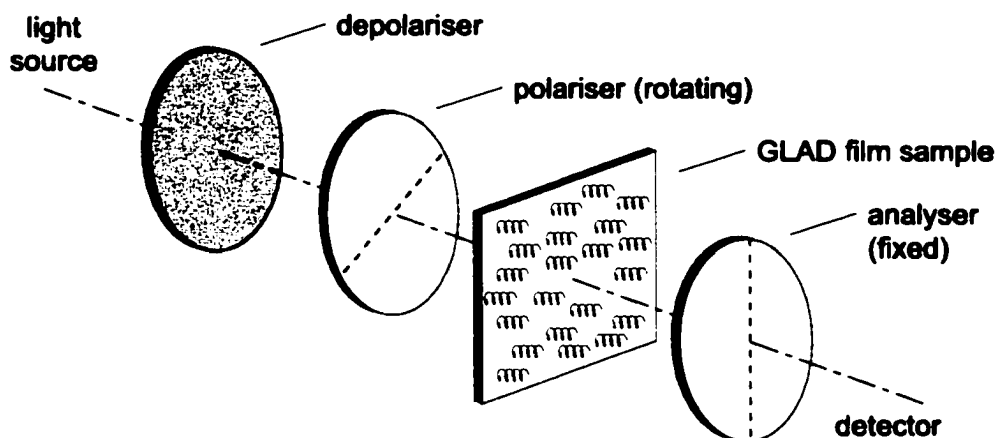


Figure 3-5: Optical rotatory dispersion measurements  
A stepper motor polariser drive, built into the spectrophotometer is used to help automate the measurements.

light to escape. One of the polarisers is then rotated until minimum transmission is found. Physical rotation of the polariser therefore compensates for the optical rotation introduced by the medium. The direction and angle of polariser rotation indicates the sign and magnitude of optical rotation of the medium<sup>8</sup>.

At the present time, rotation measurements are accomplished by taking %*T* scans for each angle of the polariser. Unfortunately this procedure yields an unwieldy amount of data (a three-dimensional array) which must be subsequently analysed to determine the angle of polariser which gives the minimum transmission at each wavelength (the data is distilled to obtain the two-dimensional data of angle of polariser for minimum transmission versus wavelength). There are several aspects of the current procedure which can be improved. First, because a %*T* scan must be completed for each angle of polariser considered, the process is very time consuming. Second, there must be a compromise between the range of angles considered and the angular resolution. Going from 0.50° to 0.25° intervals doubles the number of scans required if the range of angles scanned is not changed. New software is currently being developed to optimize ORD measurements and will address these

8. As usual with optical measurements, one must be mindful of sign conventions. For rotation measurements, sign of the optical rotation depends on which polariser is rotated, in what direction (clockwise or counterclockwise), and whether one is looking back at the light source (usual convention) or towards the detector.

issues. Most importantly it will “hunt” for the polariser angle which gives minimum transmission rather than scanning the entire spectrum multiple times. This new algorithm promises to significantly reduce scanning times and boost angular resolution.

### 3.4.2 Results

To illustrate the chiral optical response of GLAD films, measurements of LCP/RCP transmission and polarisation rotation are presented here. The simplest measurements to perform are transmission measurements for LCP and RCP. These were done for a left-handed helical GLAD film composed of  $\text{SiO}_2$  shown below in Fig. 3-6. This film was deposited at an angle of about  $\alpha = 85^\circ$  and has 8.4 turns and pitch  $p = 410$  nm.

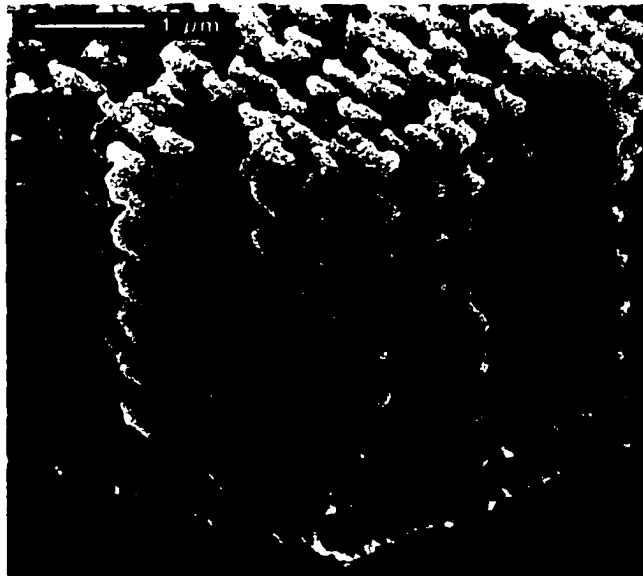


Figure 3-6: SEM of a LH helical GLAD film  $\text{SiO}_2$ , 8.4 turns, pitch  $p = 410$  nm.

Fig. 3-7(a) below shows the transmission spectra for LCP and RCP incident normal to the film (parallel to the helical axis). The difference spectra of right minus left is plotted in Fig. 3-7(b)<sup>9</sup>. For this sample, the transmission of RCP is higher, suggesting the preferential reflection or scattering of LCP. This result is consistent with earlier predictions of preferential reflection/scattering of the circular polarisation which matches the handedness of the

9. The jagged nature of the transmission difference spectrum is likely due to stepper motor jitter in the monochromator of the spectrophotometer used (Unicam 8700 series).

film. The peak transmission difference is approximately 6% at  $\lambda \sim 570$  nm. The overall transmission can be seen to be low, especially at the lower wavelengths, indicating substantial diffuse scattering in the film. (To the naked eye, porous, optical GLAD films have a cloudy, translucent look.)

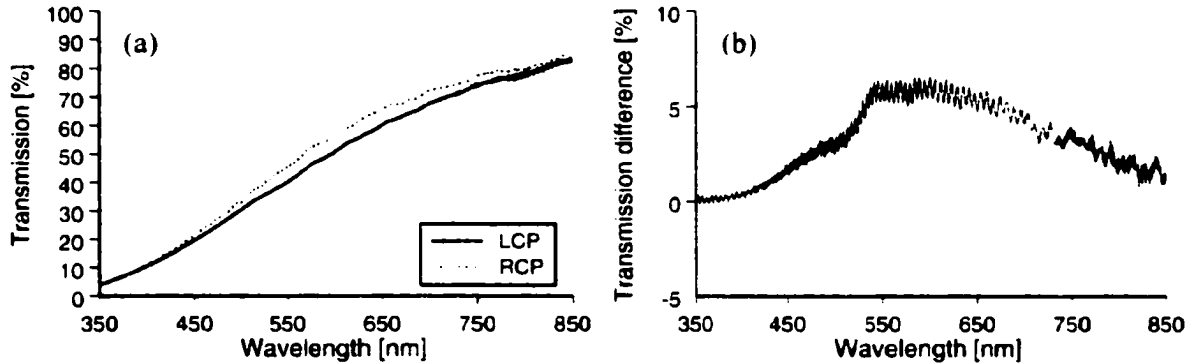


Figure 3-7: LCP/RCP transmission measurements  
Measurements are for sample shown in Fig. 3-6. (a) Transmission of LCP and RCP components. (b) Difference spectra  $\%T_{RCP} - \%T_{LCP}$

Optical measurements performed on a second sample, shown in Fig. 3-8, are also presented here. This sample, also made of  $\text{SiO}_2$ , has RH helical structure with approximately 13.3 turns and  $p = 290$  nm. LCP/RCP transmission measurements for this film are shown in Fig. 3-9(a). For this film, the transmission of LCP is greater than that of RCP, which is the opposite case to what was observed in the measurements for the LH film above. This result is consistent with predictions that the coupled circular polarisation is preferentially scattered/reflected by the film and thus exhibits lower transmission. Since LCP transmission is higher than RCP transmission, the transmission difference in Fig. 3-9(b) is calculated in this case as  $(\%T_{LCP} - \%T_{RCP})$ . For this sample, the peak transmission difference was approximately 2% at  $\lambda \sim 670$  nm. The optical rotatory dispersion for this same film was also measured and is shown below in Fig. 3-9(c)<sup>10</sup>. The film exhibits a peak rotation of about  $-4.5^\circ$  at  $\lambda \sim 450$  nm. The negative sign on the peak rotation indicates that the film is levro-rotatory, and this result is consistent with the film being a RH sample.

10. Limitations in the instrument and measurement process for optical rotatory dispersion restrict the wavelength range.



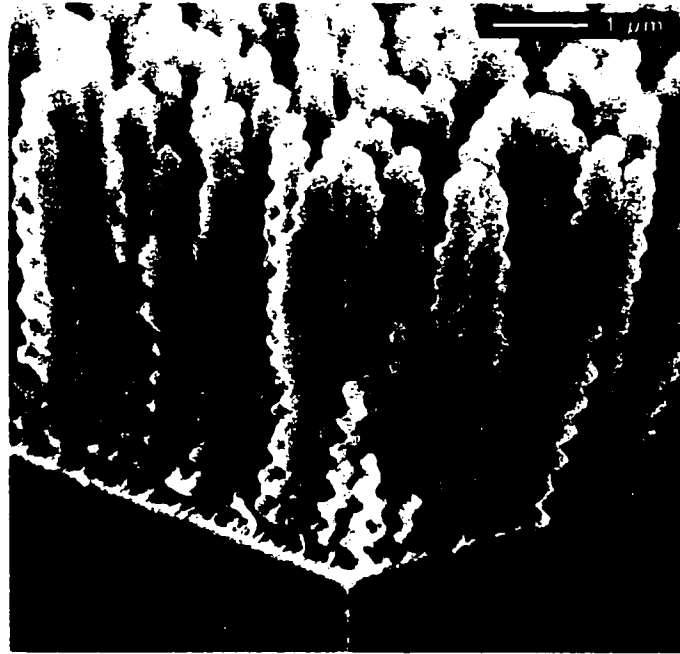


Figure 3-8: SEM of a helical film used in optical rotation measurements. Film has RH helical structure, with 13.3 turns at pitch  $p = 290$  nm (total thickness  $3.8 \mu\text{m}$ ). This GLAD film was deposited by e-beam evaporation of a  $\text{SiO}_2$  source.

A careful observer will immediately notice the mismatch between the wavelength for peak transmission difference and the wavelength for peak optical rotation. (The same effect is seen in other measurements performed.) As of yet, no explanation can be offered to explain this discrepancy. The presentation of more extensive results and further discussion is deferred until Chapter 4, where the effects on CD/ORD spectra of various structural parameters of the GLAD film are discussed in the context of control of the GLAD structure leading to control over the orientation of LC in GLAD-LC composite films.

### 3.4.3 Discussion

For the purposes of elucidating the chiral optical response in optically active media such as GLAD films with chiral microstructures, several simplifying assumptions were made earlier. Most of these assumptions were made for the ideal case and must be revisited to account for the realistic case. First, it was assumed that the chiral medium was perfectly discriminating between the coupled and uncoupled polarisations. In reality, the coupling of circular polarisation which matches the handedness of the film will be less than 100%. Meanwhile, coupling of the opposite polarisation will be greater than 0%. From a different

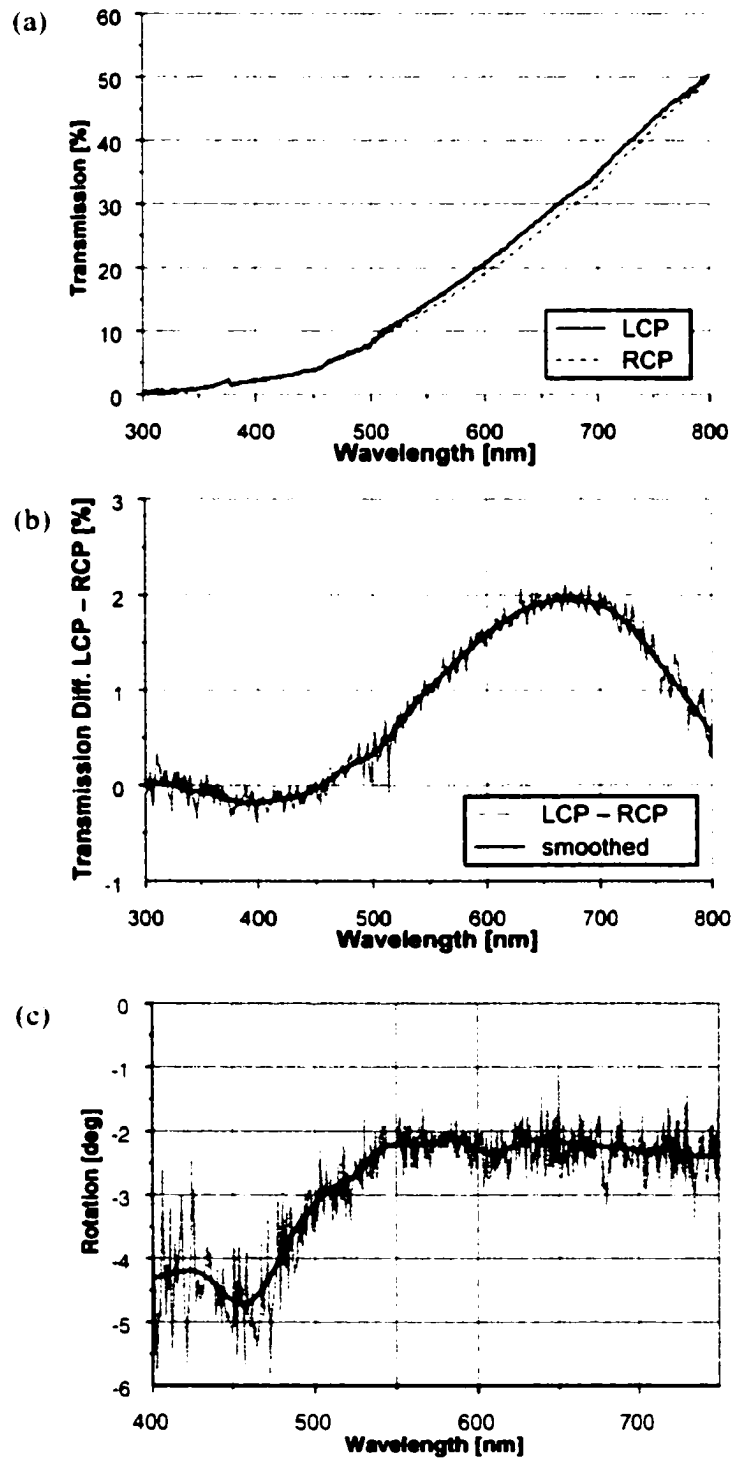


Figure 3-9: Chiral optical measurements for RH helical GLAD film. Measurements are for sample shown in Fig. 3-8. (a) Transmission of LCP and RCP, taken individually. (b) Transmission difference spectra,  $\%T_{LCP} - \%T_{RCP}$  (c) Optical rotatory dispersion.

perspective, this statement implies that the coupled polarisation “sees” an effective refractive index of less than that of the film material while the uncoupled polarisation “sees” an effective refractive index of greater than that of the void material. Continuing the example of a LH GLAD film, in terms of the circular birefringence, the following relation can still be expected to hold:

$$n_{\text{void}} < n_{\text{RCP}} < n_{\text{LCP}} < n_{\text{film}} \text{ (for a LH medium)} \quad (3-13)$$

Another assumption that was made was that the voids in GLAD films contained only air (i.e. that  $n_{\text{void}} = n_{\text{air}} = 1.0$ ). Voiding in optical thin films has always been a problem because of environmental effects. Humidity (i.e. water) can penetrate into defects and voids in films and cause the optical properties to change (especially with respect to refractive index). The slow drift in optical properties over time due to these environmental effects is in general detrimental to the performance of the optical device. For a multilayer optical filter, only a small percentage drift in properties of one layer may be sufficient to completely foul up the overall response of the device. Thus, in conventional thin film deposition, one would like to achieve dense, and ideally, highly crystalline films which would be more impervious to infiltration by water. With the GLAD technique, however, the films are deliberately made highly porous (especially when depositing at more oblique angles  $\alpha$ ) which only serves to exacerbate their environmental sensitivity. The high surface area and accessible nature of the voids allows water to be easily adsorbed. High surface area in GLAD films can be deliberately exploited for sensor applications [34] including humidity sensors of course!

The simplified model of coupling in chiral media presented earlier in this chapter, while straightforward in describing the chiral optical effects qualitatively, is clearly insufficient to explain the observed phenomena fully. More robust models which look at the problem from the electromagnetic point of view are required. Lakhtakia (e.g. Refs 69-72) has looked at interactions of electromagnetic waves with “helical bianisotropic media”. Pierce [81] describes slow wave propagation along a helical wire in travelling-wave tube amplifiers. Travelling-wave tubes have been used for amplification of microwave frequen-

cy signals (GHz range). Another useful model is to consider chiral films as helical antennae [82]. The electromagnetic approach is expected to provide a substantially better model to explain the chiral optical effects seen.

One other effect which has not been discussed is that of scattering [83, 84]. The high porosity and surface area in GLAD films contributes to a substantial amount of diffuse scattering in the films. SEM micrographs of GLAD films show that the surfaces of the columns tend to have a rough or fuzzy texture. The high porosity, micro-scale roughness, and index mismatch between film and void materials all contribute to the scattering. To the naked eye, GLAD films, especially those with more porous microstructures, appear cloudy. When deposited on glass substrates, GLAD films resemble frosted glass.

### **3.5 Liquid crystals**

At this juncture, discussion switches to introduce liquid crystalline materials. As these materials possess unique optical properties such as linear birefringence and the chiral optical response presented earlier, there will be an inevitable comparison between chiral GLAD films and LCs. This sets the stage for the central work of this thesis, wherein GLAD films are combined with LCs.

#### **3.5.1 Introduction**

Liquid crystals (LC) [85, 86, 87] are a class of materials which exhibit one or more intermediate states called mesophases between their crystalline solid and isotropic liquid states (Fig. 3-10). LC materials are often referred to as a "fourth state of matter". The name "liquid crystal" arises because LCs exhibit both partial molecular ordering (solid-like behaviour) and fluidity (like liquids). Liquid crystalline materials, which generally are organic compounds or mixtures, typically possess one of two anisotropic molecular shapes: long and rod-like (calamitic) or flat and disc-shaped (discotic). In this work, though, only calamitic LCs were used. (The rod-like molecular shape is also by far the more common.) The LC mesophases are defined by the way in which the molecules are arranged. The degree of molecular ordering depends on the temperature and with molecular ordering decreasing with increasing temperature.

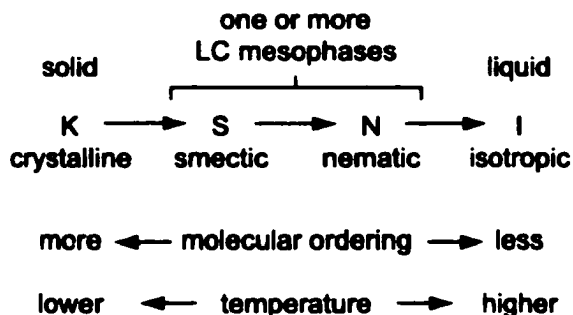


Figure 3-10: Liquid crystal mesophases  
 LC materials exhibit one or more intermediate states (mesophases) between their crystalline solid and isotropic liquid phases. The mesophases are classified according to the way in which the molecules are ordered.

The molecular orientation of LCs may comprise translational (positional) order, rotational (orientational) order, or a combination of the two. In the simplest LC mesophase, the nematic phase (Fig. 3-11(a)), the LC molecules possess long range orientational order, but no positional order. For LCs composed of rod-like molecules, orientational order implies that the long axes of the molecules are more or less aligned in the same direction. The nematic director (denoted  $\hat{n}$ ) is defined as a unit vector which represents the average orientation of the LC molecules.

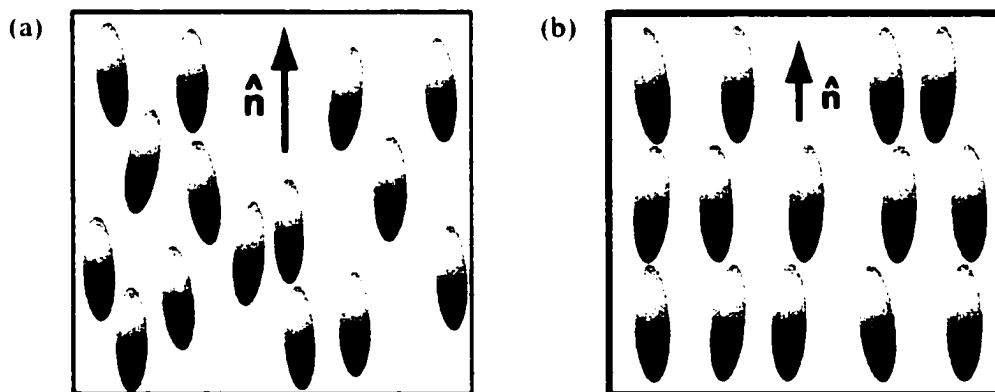


Figure 3-11: Nematic and smectic liquid crystal phases  
 (a) In the nematic mesophase, the LC molecules exhibit orientational order, but no positional order. The director  $\hat{n}$  indicates the average orientation of the molecules.  
 (b) In the smectic phase, the LCs have both orientational order and positional order. In this example of a smectic phase the LC molecules are aligned in layers.

A second class of mesophases, called the smectic phases, contains a degree of both orientational and positional molecular ordering. There is a plethora of further subclassifications (smectic A, smectic C, *etc.*) based on the type of ordering of the molecules. Apart from being oriented in the same average direction as with a nematic phase (orientational or rotational ordering), the LC molecules in a smectic phase are arranged in lines, layers, or sheets (translational or positional ordering). At this point in time, LCs that form smectic phases have not been studied in combination with GLAD films. Work thus far has concentrated on nematic, and to a limited degree, chiral nematic (described below) LC types.

A third type of molecular ordering is the cholesteric<sup>11</sup>, or chiral nematic, phase (Fig. 3-12). The chiral nematic phase can be thought of literally as a “nematic phase with a twist”. This structure consists of a stack of achiral nematic sheets where the nematic director, which is in the plane of the sheet, is rotated slightly between each sheet (Fig. 3-12(b)). The endpoint of the director traces out a helix, with the helical axis normal to the nematic sheets. The thickness for a full  $2\pi$  rotation of the director defines the pitch  $p$  of the helix. The non-chiral nematic phase may be thought of as a chiral nematic phase where  $p \rightarrow \infty$ .

Chiral nematic phases may arise from LCs with chiral molecules, or alternately, from non-chiral LCs which have had a quantity of chiral material added to them — chiral dopants [88, 89]. For chiral nematic phases based on chiral LCs, the “twisting power” is intrinsic to the molecules themselves, whereas the properties of chiral nematic phases based on chiral dopants depend on the “twisting power” bestowed by the chiral dopant. The concentration of the chiral dopant controls the pitch of the chiral nematic phase. A higher concentration of chiral dopant gives more “twist” to the helix and hence a tighter (smaller) pitch; a lower concentration likewise gives less twist and a longer pitch. Without getting into too much detail, there are many possibilities to experiment with chiral dopants and/or chiral LCs. A mixture of chiral and non-chiral nematic LCs will produce a chiral nematic phase and the pitch can subsequently be controlled by varying the relative concentration of the two components. And to hint at the discussion later in this thesis: given the similarities be-

---

11. The cholesteric phase is named as such because this type of molecular orientation was first observed in LC materials based on cholesterol-type molecules.

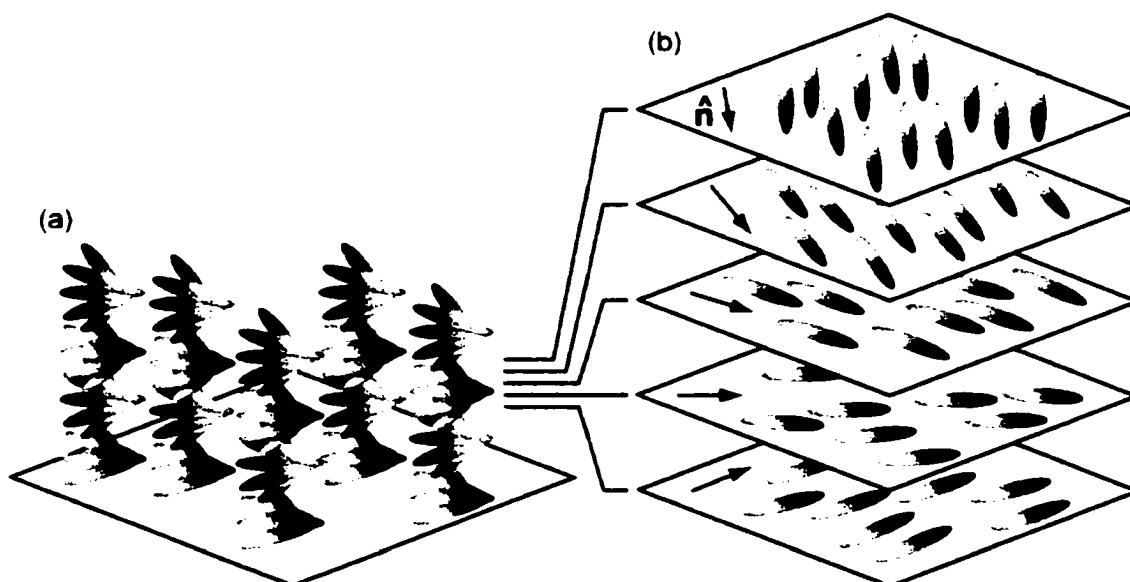


Figure 3-12: Chiral nematic liquid crystal phase  
 (a) The chiral nematic phase consists of (b) a stack of achiral nematic sheets where the nematic director is rotated slightly between each successive sheet.

tween the optical response of chiral GLAD films and of CLCs, does a chiral GLAD film structure function similarly to a chiral dopant?

### 3.5.2 Properties

It was mentioned earlier that LC molecules possess an anisotropic molecular shape. The molecular structure and inter-molecular forces not only lead to the existence of LC mesophases, but also give LCs leads to many unique properties. The chemical structure of the LC molecules determines many of the properties. A typical rodlike LC molecule such as that shown in Fig. 3-13 might consist of two rings joined by a linking group and side chain or terminal groups attached to either end of the structure. The rings may be phenyl/benzene (unsaturated) or cyclohexane (saturated). The linking group A may be as simple as a single bond between the two rings (biphenyl LCs) or may be a third ring or other functional group. The side chain X can be any number of variants including: alkyl chain ( $C_2H_{2n+1}-$ ), alkoxy chain ( $C_2H_{2n+1}O-$ ), or alkenyl chain with a double bond. Terminal group Y, which influences the dielectric constant  $\epsilon$  and dielectric anisotropy  $\Delta\epsilon$  of the LC, may be for example a cyano group ( $-CN$ ), an alkyl chain ( $-C_2H_{2n+1}$ ), or a halide ( $-F$ ,  $-Cl$ ).

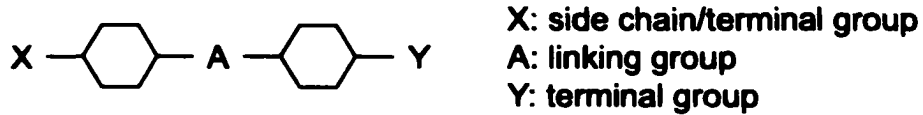


Figure 3-13: Structure of a typical rod-like LC molecule  
 Substitution of different functional groups for linking group A and for terminal groups X and Y yields different properties for the LC.

The elongated molecular shape leads to anisotropic properties. For LCs, perhaps the two most important anisotropic properties are those of refractive index and dielectric constant (Fig. 3-14). Anisotropic refractive index is of course better known as the linear birefringence of the material with:

$$\Delta n = n_e - n_o \quad (3-14)$$

where  $n_e$  is the extraordinary index and  $n_o$ , the ordinary index. LCs in general show fairly strong birefringence. The dielectric anisotropy,

$$\Delta \epsilon = \epsilon_{\parallel} - \epsilon_{\perp} \quad (3-15)$$

means that LCs are sensitive to electric fields and because of their fluid characteristics, the LC molecules will align with their long axes either parallel or perpendicular to an applied electric field (depending on whether  $\Delta \epsilon$  is positive or negative, respectively). LCs can thus be switched by an electric field, perhaps their most important attribute of all. (Upon removal of the electric field, the LC molecules relax back to their original orientation.)

### 3.5.3 Alignment techniques

In Chapter 1, it was emphasized that the structure of a thin film greatly affects the properties of the film and hence, to control the properties, one requires control over the structure. The same tenet applies to liquid crystals: to control the optical properties, one must achieve control over the structure, that is, the molecular alignment of the LC.

A variety of techniques are used to produce molecular alignment in LC devices such as displays. Probably the most well known is rubbing of the substrates<sup>12</sup> to cause nematic LCs



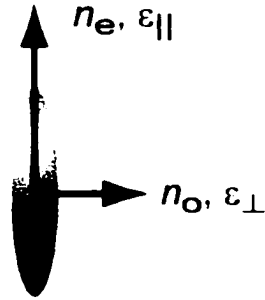


Figure 3-14: Anisotropic properties in LCs  
The properties of LCs depend on whether one is looking parallel to the long axis ( $n_e, \epsilon_{||}$ ) or perpendicular to the axis ( $n_o, \epsilon_{\perp}$ ).

near the substrate to orient parallel to the direction of rubbing [90]. Rubbing results in a planar (parallel) orientation of the LC. (Calamitic LCs will align parallel to the rubbed substrate and parallel to the direction of rubbing.) A second technique for controlling LC orientation is the use of obliquely deposited thin films as “tilt” alignment layers at the substrate [91, 92]. In this case the LC molecules take on a small tilt angle to the substrate. Yet another technique is to treat the substrate surface with certain types of polyimides which generate a homeotropic (perpendicular) LC alignment. Here, the surfactant (polyimide) is used to modify the interaction between substrate and LC.

Because they influence LC orientation at and near the substrate surfaces only, an inherent limitation with these substrate surface treatment techniques is the inability to attain and/or maintain the desired LC orientation under one or more of the following conditions:

- when a thicker cell is required
- when more complex LC geometries such as chiral nematic/cholesteric LCs are used
- when reversible switching is desired

Loss of molecular orientation after electro-optic addressing (that is, irreversible switching) is a particular problem when CLCs are used [93]. For better control over LC alignment, a technique which induces LC alignment throughout the cell is required, rather than influenc-

12. Usually, the substrate would be treated with a polyimide which is then rubbed or polished to produce the alignment surface.

ing the LC orientation near the substrate surfaces only. Polymer- and gel-dispersed liquid crystals (PDLC, GDLC) [94] are guest-host composite media with a polymer or gel network (host) embedded with droplets of LC (guest) dispersed throughout the network. They represent one method of controlling LC orientation, but are generally limited to small spherical inclusions of LC rather than having a fully controllable porous structure like that possible with GLAD.

### 3.5.4 Application in displays

The largest application of LC optics is undoubtedly in information displays [87, 95]. The twisted nematic liquid crystal display (TN-LCD), shown in Fig. 3-15, is a common configuration used in LCDs today. The TN-LCD cell has two glass substrates which are treated to induce planar alignment. Linear polarisers are attached to the glass plates, with the transmission axis parallel to the rubbing direction. The glass plates are aligned such that the polarisers are crossed. A nematic LC is used and a small amount of chiral dopant is added to induce a preferential LH or RH twist, so that the LC aligns in the unaddressed state with a  $90^\circ$  twist as shown in Fig. 3-15(a). In the unaddressed or “off” state, the twisted nematic causes a  $90^\circ$  rotation of the plane of polarisation so the light is able to pass through both polarisers. (The rotation is actually a waveguiding effect as in this case  $\lambda \ll p$ , rather than the Bragg regime where  $\lambda \sim p$ .) Because of this, the “off” state is also called the transparent state or white state. In the addressed or “on” state, a voltage is applied across the cell and causes the LC to align parallel to the field (LC takes on a homeotropic orientation). The polarisation rotation vanishes and the light which is admitted by the first polariser is now blocked by the second polariser. The addressed state is thus also called the “black” state.<sup>13</sup>

In terms of light efficiency (the percentage of light produced by the backlight actually seen by the user), the TN-LCD is terribly inefficient. To calculate the overall light efficiency of an LCD, the light efficiencies of each component must be multiplied together. Given that each component will by definition have an efficiency less than 100%, the overall light efficiency ends up quite low (generally on the order of only 5%) because there are many com-

---

13. The TN-LCD display described here is called the “normally white” type because the cell is transmitting when unaddressed. There are also “normally black” variants.

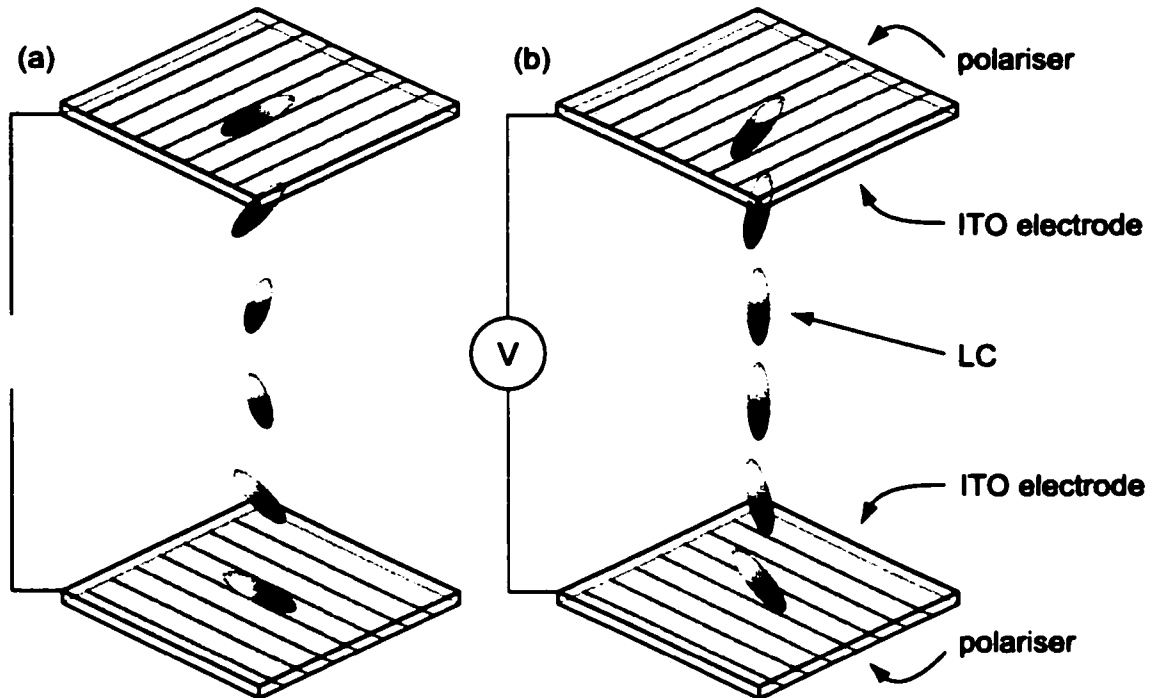


Figure 3-15: Twisted nematic liquid crystal display cell

The LC is planar aligned at the two substrates. (a) In the unaddressed state, the twisted nematic rotates the plane of polarisation from being aligned with the first polariser to being aligned with the second polariser, which allows light to be transmitted through the cell. (b) In the addressed state, the LC is aligned parallel to the electric field and there is no rotation of the plane of polarisation, so the light is blocked by the second polariser.

ponents in an LCD. A further implication of this calculation is that the overall light efficiency will be lower than that of the component with the lowest efficiency. This analysis is exactly like that encountered in an engineering reliability problem where devices are in series and one is required to determine the overall reliability of the system given the reliability of each device.

For the TN-LCD, the components which contribute the most inefficiency (in other words, the biggest “light bottlenecks” in the system) are the back polariser, colour filters, and effective area for colour sub-pixels. Table 3-3 below lists the light efficiencies of these three elements along with the overall efficiency of the three taken together. Because absorptive polarisers are used, the back polariser (at the bottom of the LCD structure shown in Fig. 3-15) has a maximum theoretical light efficiency of 50% (half the light is thrown away). In

practise, the efficiency is closer to 40% for this component. To achieve full-colour, a display system uses red, green, and blue (RGB) sub-pixels. In an LCD, a broadband white light backlight is used in conjunction with RGB colour filters to produce the primary colours. As the colour filters are absorbing films (they are usually placed on the front glass), their maximum efficiency would be on the order of one-third as they transmit one of the primary colours and absorb the other two. In practise, a typical efficiency value of the colour filters is 28%. One further consideration of having RGB elements is that the sub-pixels for each primary colour occupy only one-third of the display area, as two-thirds of the area are obviously taken up by the other two primary colour sub-pixels.

Table 3-3: Light efficiency of several key TN-LCD elements

Element	Light efficiency [%]	
	Maximum theoretical	Typical value
Back polariser	50	40
Colour filter	~33	28
Area for colour sub-pixel (R, G, B)	33	33
Overall efficiency	$0.50 \times 0.33 \times 0.33 = 5.4$	$0.40 \times 0.28 \times 0.33 = 3.6$

Taken together, the light efficiency of these three elements taken together is a paltry 3.6% (a typical value). Even the theoretical maximum, assuming perfect polarisers and colour filters, is only 5.4%, leaving little room for improvement. When the efficiencies of the other elements of the LCD not discussed here (backlight waveguide, light diffuser, etc.) are also taken into account, the overall efficiency of the display is on the order of only 1%.

### 3.5.5 Reflective displays and chiral LCs

The preceding discussion of TN-LCDs clearly shows that the design of this type of display has fundamental and inescapable inefficiencies due to the absorptive polarisers and colour filters. To overcome the light efficiency limitations, new types of LCDs are sought. One of the more promising technologies being studied is the reflective display which can dispense with the absorptive polarisers and colour filters. As the name suggests, this type of

display works on the basis of reflection of ambient light rather than transmission of the backlight. One method of implementation for a reflective display is to use chiral nematic LCs. CLCs display a strong reflection band in the wavelength range  $pn_o < \lambda < pn_e$  ( $p$  is the pitch and  $n_o$  and  $n_e$  are the ordinary and extraordinary refractive indices, respectively). Controlling the pitch in CLCs gives one control over the spectral properties. The concept of the reflective display is central to the discussion of GLAD/LC hybrid materials and will be revisited in the following chapter.

### 3.6 Discussion

Given the similarities between the optical response seen in chiral GLAD films and that seen in chiral nematic LCs, a comparison between the two technologies is in order. In this section, “traditionally” deposited thin films, GLAD thin films, and LCs are compared as optical technologies. A comparison of these three technologies is presented below in Table 3-4.

Table 3-4: Comparison of conventional thin film, GLAD thin film, and LC optics

Technology base	Conventional thin film ( $\alpha < 70^\circ$ )	GLAD thin film ( $\alpha > 70^\circ$ )	LC
Structural control	inherent to deposition process	inherent to deposition process, high degree of control over column structure	external means of control (alignment layers) or additives
Optical response strength	moderate to strong	generally weak, due to high scattering	stronger!
Environmental stability	average	poor	good
Switchability	no	no	yes
Allows for addition of a second material	no	yes	N/A

In both conventional thin film and GLAD thin film techniques, structural control is inherent in the deposition process whereas for LC optics, control over the LC orientation is generally

achieved either through external means such as alignment layers or through chemical additives such as chiral dopants. GLAD technology enables high degree of control over the columnar structure in deposited films. Structures such as pitch gradients or stacked layers with different pitch and/or handedness are very easy to implement with GLAD, but very difficult with LC techniques.

As stated earlier, voiding in optical films leads to vulnerability to environmental and humidity effects. High birefringence may be achieved by utilising oblique angle deposition and taking advantage of anisotropic column shape. At the same time, however, oblique deposition causes voids (gaps) in the film where humidity (water) or other substances can penetrate easily. GLAD, which uses highly oblique angles, pushes film porosity even further, making GLAD films even more sensitive to environmental effects. While it is certainly possible to seal thin film optics, it may not always be practical. On the other hand, LC optics are contained in sealed devices which one expects would provide better protection against changes due to environmental effects.

Two of the main strengths of LC technologies are that LCs have strong optical response and that they are switchable. These are two significant advantages over thin film technologies. Because of the strong market in information displays (flat panel displays for notebook computers, projectors, smaller displays for handheld computers, etc.) LC technology has become a very mature field.

It will be shown, in the subsequent discussion, that GLAD/LC hybrid materials combine many of the strengths of LCs, including strong optical response and switchability, with the structural control offered by GLAD.

## Chapter 4

# Liquid crystal hybrid optics

---

Whereas Chapter 3 laid out the groundwork and fundamentals of GLAD and LC chiral optics, this chapter presents the central work of this thesis: the combination of porous GLAD films and liquid crystals. Discussion opens with the rationale for studying the combination of the two technologies. Previous experiments are described briefly.

The second section of this chapter describes the experimental setup, including film deposition, cell fabrication and filling, and the optical measurements. The results of optical measurements on GLAD and GLAD/LC films are presented. This section illustrates the first significant effect of using GLAD/LC hybrids, the enhancement of the chiral optical properties.

The topic of electro-optic switching is then discussed and presented with results of optical measurements for switching cells. Switching is the second significant aspect of GLAD/LC hybrid optics and is the key to applications in dynamic devices such as displays.

### 4.1 Introduction

It was mentioned in the introductory section of this thesis that control over the structure in thin films is the key to optimisation of their properties. Similarly, for liquid crystal devices, control over the long-range orientation of the LC molecules is critical to the optimisation of the optical properties. Several techniques for controlling LC orientation were mentioned previously. These include rubbing of the substrates and “pre-tilt” thin film alignment layers. The drawback with these conventional techniques is that they work at the substrate surfaces and their influence falls off as distance from the substrate. Thus their ability to influence LC alignment throughout the entire cell is limited.

For improved control over LC alignment, a technique which can induce LC alignment throughout the entire span of the cell would be desired. In the previous chapter, chiral do-

pants added to LCs were mentioned as one method of inducing or controlling a chiral nematic orientation in LCs. Naturally, the question of utilising GLAD films as a “chiral dopant” arises. It has already been shown that the structure of these films may be easily controlled via the deposition process and control software. GLAD films with chiral microstructure were also shown to exhibit unique chiral optical properties and their optical response has been compared to that seen in CLCs. Finally, the highly porous nature of GLAD films permits infiltration by fluids very easily. Adsorption of water, for instance, is well known to influence the properties of the GLAD film strongly. This is much to the delight of the experimenter designing a sensor application, but much to the chagrin of the experimenter trying to study the optical properties free of the influence of environmental effects. The key question is, then, what happens when liquid crystalline materials are introduced into a GLAD film?

The first experiments with GLAD/LC composite materials were conducted by Robbie, Broer, and Brett [96]. They embedded helical GLAD films with several compounds including isotropic liquids, polymers, and reactive and non-reactive LC materials. Measuring circular dichroism<sup>1</sup> as the difference in transmission between LCP and RCP, they found that filling with an isotropic liquid such as water or some types of polymers caused the loss of the transmission difference as these fluids were approximate index matches for the film material. More importantly, however, filling GLAD films with birefringent materials such as nematic LCs was found to enhance the transmission difference. Here, it was suggested that the helical GLAD film acted as an alignment structure for the LC and imposed a chiral nematic-like ordering of the LC molecules. This was a significant and exciting result. These initial experiments have led to a continued collaboration with Dr D. J. Broer, a research fellow in the Polymers and Organic Chemistry Group of Philips Research Laboratories (Eindhoven, The Netherlands).

The ability to switch the liquid crystal component is critical to the development of active

---

1. Recalling discussion from the previous chapter, calling the measurement “circular dichroism” may be a bit of a misnomer as it does not reflect how the various chiral optical effects described are intertwined in the measurements.



optical devices based on GLAD thin films and is the logical progression from initial studies based on embedding LCs into GLAD films. Thus the current pursuits are twofold: first, to investigate further the effects of embedding LCs into GLAD films and better understand the interaction between GLAD structures and the LC; and second, to demonstrate the electro-optic switching of the LC component in devices based on GLAD/LC hybrid materials. The ultimate aim is to understand and hence be able to control the optical properties of the hybrid system. The work presented here first presents new data showing how the chiral GLAD film structure influences the LC alignment including effects of pitch, handedness, and film material. The fabrication and demonstration of a switchable device based on GLAD/LC composite materials is also presented.

## **4.2 Experimental setup**

### **4.2.1 Film deposition**

Chiral GLAD thin films with various structures were grown by thermal or electron-beam evaporation of suitable optical materials<sup>2</sup>. Over the course of study of this project, a large sample space has been mapped out including different materials, substrates, GLAD film microstructure type, pitch, and handedness. A list of the parameters of this sample space is shown in Table 4-1 below. Optical materials used to fabricate the films include alumina ( $\text{Al}_2\text{O}_3$ ,  $n = 1.66$ ), magnesium fluoride ( $\text{MgF}_2$ ,  $n = 1.38$ ), silicon dioxide ( $\text{SiO}_2$ ,  $n = 1.47$ ), and titania ( $\text{TiO}_2$ ,  $n = 2.2$ ). Other optical materials such as  $\text{ZrO}_2$ ,  $\text{CeO}_2$ ,  $\text{HfO}_2$ , and  $\text{Nb}_2\text{O}_5$  could also be considered for future experiments. As the GLAD process is able to produce high porosity, engineered microstructures from virtually any material, the choice of film material depends on desired optical properties and other considerations such as cost of the material and ease of deposition<sup>3</sup>.

The films were grown on glass substrates, some of which had a coating of indium-tin oxide (ITO, a transparent conductor) to serve as an electrode. Witness samples were grown on pieces of silicon wafer. (One practical reason is that Si substrates are easier to cleave to

- 
2. GLAD by sputter deposition (Chapter 2) is also a viable technique but was not used for the materials used in experiments described here.
  3. Toxicity of the material may also be a consideration!

Table 4-1: Optical GLAD film sample space parameters

Materials used	Al <sub>2</sub> O <sub>3</sub> , MgF <sub>2</sub> , SiO <sub>2</sub> , TiO <sub>2</sub>
Substrates	Si wafer, Si wafer with Al electrode, glass, glass with ITO electrode
GLAD structures	helical, twisted ribbon, others
Pitch	250-800 nm, some films with pitch gradients
Handedness	LH and RH, some films with stacked layers of opposite handedness

obtain samples for viewing in a scanning electron microscope.) Some films were also grown on Si wafers which had a layer of aluminum on them to serve as an electrode. Si/Al substrates would serve as reflective substrate for a reflective type GLAD/LC cell, although in the work presented here does not include characterisation of the reflective type cells. The samples prepared for device fabrication were 25 mm (1-inch) square pieces. To facilitate electrical contact to the underlying electrode layer, a strip approximately 2 to 3 mm wide along one edge of the front surface of the substrate was masked from deposition using wafer saw dicing tape which, after deposition could be peeled away, leaving a clean edge with no sticky residue. Because of the relatively small size of the substrates used in these experiments, several substrates could be mounted on the substrate holder for each deposition. The substrate holder used was 125 mm (5 inches) in diameter and as such could accommodate several (five to six, typically) of the small square glass/ITO pieces along with a Si wafer for a witness/SEM sample. Having several samples of the same film facilitates investigation of the effects of different LC types or surface treatment of the counter electrode, for instance.

While most of the films grown for these experiments possessed helical chiral microstructure, some films were grown also with other chiral microstructures such as the twisted ribbon (Fig. 2-8 (p. 35)) and also the “square staircase” helical (grown like a regular helical film but with stepped rotation ( $\varphi$ ) of the substrate, rather than continuous rotation). The pitch of the films, which controls spectral properties of the optical response, was generally in the range of 250 to 800 nm such that the “active range” of the film’s spectral response would usually fall in the visible wavelength regime (400-700 nm). A mixture of LH and RH samples was prepared. A few films with more “exotic” microstructures such as a pitch

gradient or stacked layers of LH and RH helices were also grown.

With these sample space parameters, an extensive set of chiral GLAD films was fabricated for these experiments. Table 4-2 below lists a selection of the films fabricated and details

Table 4-2: A selection of GLAD optical thin film samples used

Sample <sup>a</sup>	Material	Film structure	Turns	×	Pitch (nm) <sup>b</sup>	=	Thickness (μm)
A	SiO <sub>2</sub>	RH helical	11.1	×	350 (375)	=	3.88 (4.17)
B	SiO <sub>2</sub>	LH helical	11.1	×	390 (375)	=	4.35 (4.17)
C	SiO <sub>2</sub>	RH helical	13.3	×	290 (375)	=	3.80 (5.00)
D	SiO <sub>2</sub>	RH helical	5.0	×	424 (450)	=	2.12 (2.25)
E	SiO <sub>2</sub>	RH helical	7.0	×	417 (450)	=	2.92 (3.15)
F	SiO <sub>2</sub>	RH helical	9.0	×	424 (450)	=	3.82 (4.05)
G	SiO <sub>2</sub>	RH helical	11.1	×	450 (450)	=	5.00 (5.00)
H	SiO <sub>2</sub>	LH helical	11.1	×	434 (450)	=	4.82 (5.00)
J	SiO <sub>2</sub>	RH helical	9.5	×	533 (525)	=	5.08 (5.00)
K	SiO <sub>2</sub>	RH helical	11.1	×	527 (525)	=	5.85 (5.83)
L	MgF <sub>2</sub>	LH helical	7.0	×	880	=	6.15
M	MgF <sub>2</sub>	LH helical	14.0	×	450	=	6.30
N	MgF <sub>2</sub>	LH helical	21.0	×	350	=	7.35
P	MgF <sub>2</sub>	LH helical	5.0	×	480	=	2.40
Q	MgF <sub>2</sub>	LH helical	8.0	×	480	=	3.80
R	MgF <sub>2</sub>	LH helical	11.7	×	480	=	6.00
S	SiO <sub>2</sub>	LH helical	10	×	350~500 (gradient)	=	4.25
T	MgF <sub>2</sub>	LH helical	9	×	400	=	3.60
U	Al <sub>2</sub> O <sub>3</sub>	RH square helical	15	×	410 (400)	=	6.18 (6.00)
V	Al <sub>2</sub> O <sub>3</sub>	LH twisted ribbon	10	×	400	=	4.00

a. Sample L through Q were grown by S. R. Kennedy.

b. Brackets denote original design values.

their relevant structural parameters. In general, the sample parameters were designed such that sets of films map out cross-sections of the structural parameter space. For instance, samples D, E, F, and G (Fig. 4-1) form a set where the pitch and handedness are kept constant, but the number of turns is the experimental variable. Samples G and H are nearly identical except for being of opposite handedness, so they form an enantiomeric pair. Samples A, G, and K form a set with identical number of turns, but varied pitch. These sets with varied number of turns, varied handedness, and varied pitch help to illustrate the effects of these structural parameters on the optical response. The study of the effect of different film materials and GLAD structures is also possible with the set of films produced.

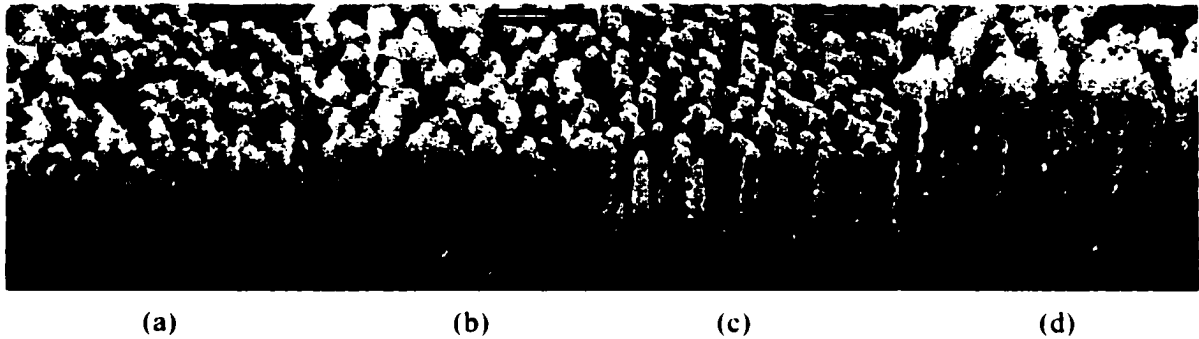


Figure 4-1: Films with fixed pitch/handedness and variable number of turns  
 A set of RH helical  $\text{SiO}_2$  GLAD films with pitch and handedness kept constant and a variable number of turns: (a) sample D, 5.0 turns; (b) sample E, 7.0 turns; (c) sample F, 9.0 turns; (d) sample G, 11.1 turns.

### 4.2.2 LC cell fabrication

In initial experiments performed by Robbie *et al.* on embedding materials such as LCs into GLAD films, the material to be embedded was introduced into the film by using an eyedropper and adding a few drops to the film surface. The material to be impregnated into the film would then wet into the film and fill it by diffusion and capillary effects. One problem with adding the material by drops onto the surface of the film is that this technique often results in a layer of the filling material remaining on the surface of the film. For anisotropic materials such as LCs, it would then become difficult to decouple the optical effects of the LC-embedded film and those arising from the LC-only layer resting above the film. Furthermore, as capillary filling may be impeded by variations in density and thickness of the medium (these are caused by defects and masking), non-uniformity of filling could

present a problem. Following discussions between the author and D. J. Broer, it was decided that, for the experimental work presented in this thesis, a more robust switching cell construction would be used to study GLAD films embedded with LC materials.

For this work, LC switching cells were constructed from the GLAD films deposited on glass substrates with a bottom ITO electrode (transparent, transmission type cells) and on Si substrates with a bottom Al electrode (reflective cells). A glass substrate with ITO (which may have been treated as described later) is used as the counter-electrode. A liquid epoxy dispensing system (line plotter) was programmed to dispense UV curing epoxy on the counter-electrode in a set pattern which seals all the edges of the cell except for a small fill port. The two glass pieces are then brought together to form the cell structure shown in Fig. 4-2, with the GLAD film “sandwiched” in between the glass plates. Normally when fabricating LC cells, spacers such as microspheres are used to control the cell gap. For GLAD/LC cells, spacers are not necessary as the GLAD film itself serves to regulate the cell gap. The two substrates which form the cell are offset slightly to facilitate contact to the ITO electrodes. This was the reason that the one edge of the film sample was masked during film deposition. After filling, the fill port is sealed with UV curing epoxy.

### 4.2.3 Cell filling

The main two types of liquid crystals used were the (non-chiral) nematics E7 and ZLI4792 (Merck<sup>4</sup>). Some key properties of these LCs are given in Table 4-3 below. To fill the film with LC, the cell is suspended with the fill port facing down in a vacuum oven which is heated above the isotropic clearing temperature of the LC<sup>5</sup>. Temperatures of approximately 70°C when filling with E7, and 100°C when filling with ZLI4792 are used. The oven is evacuated with a small rotary vacuum pump. The cell is then dipped into a small pool of the LC which fills the cell by capillary action. The filling process takes between 10 and 30 minutes on average, depending on the sample. After the cell is filled, it is removed from the vacuum oven and its fill port is sealed off with UV-cure epoxy.

---

4. Merck KGaA (Darmstadt, Germany).

5. Exposure of the LCs to high temperature for extended periods of time was minimised as high temperatures tend to drive off the more volatile (generally, lower molar mass) components of the LCs (both LC types used here are mixtures).

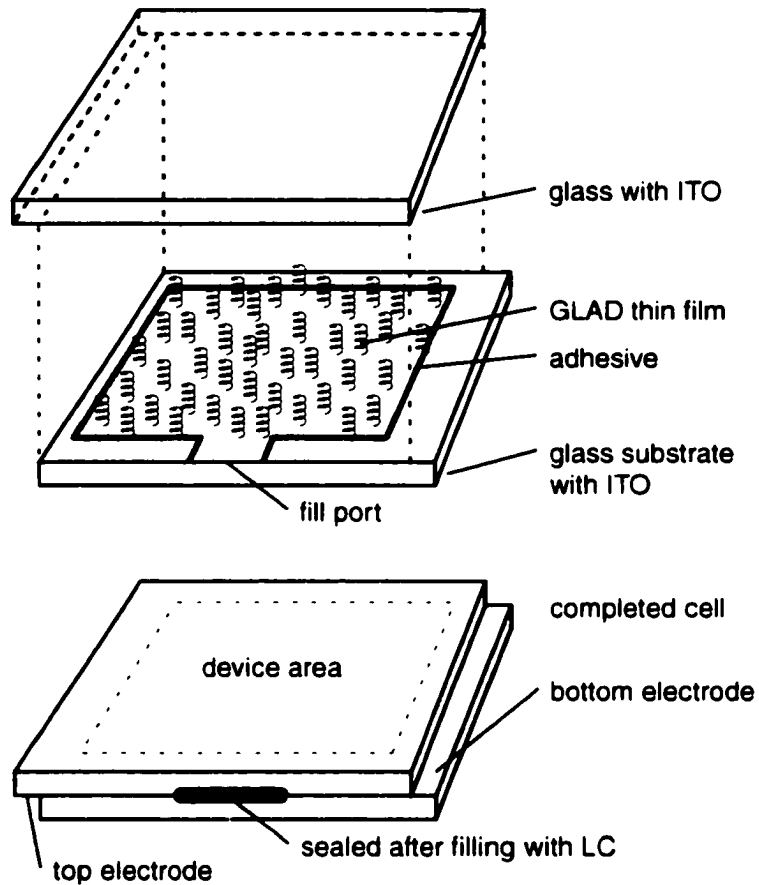


Figure 4-2: LC switching cell fabrication

A GLAD film is deposited on an ITO-coated glass substrate. A second ITO/glass substrate is used to “sandwich” the GLAD film. UV-cure epoxy is used to seal the edges of the structure, leaving a small port for LC filling. The glass substrates are offset slightly to facilitate electrical contact to the ITO electrodes

Table 4-3: Properties of liquid crystals used

Property / LC type	E7	ZLI4792
Ordinary index, $n_o^a$	1.5216	1.4794
Extraordinary index, $n_e$	1.7462	1.5763
Birefringence, $\Delta n$	+0.2246	+0.0969
Dielectric anisotropy, $\Delta\epsilon/\epsilon_0$ (at 1 kHz)	+14.5	+5.2
Clearing point, $T_{N-I}$ [ $^{\circ}\text{C}$ ]	60.5	92

a. Refractive indices given at  $\lambda = 577$  nm and  $20^{\circ}\text{C}$  (room temperature) for E7;  $\lambda = 589$  nm and  $20^{\circ}\text{C}$  for ZLI4792.

#### **4.2.4 Inspection**

After filling the cells with LC, they are inspected visually. As mentioned earlier, unfilled GLAD films exhibit substantial diffuse scattering resulting in low transmission. These films, especially thicker samples, would be described as translucent more than transparent. Filling the film with either an isotropic index matching fluid (described later) or LC significantly reduces the scattering and results in a clear cell. This is due to the reduced index mismatch between the film (typically  $n \sim 1.4$ ) and void (typically  $n \sim 1.0$ , i.e. air) materials. The visible change in scattering can be used to track the progress of LC filling.

Cell samples can be inspected by viewing them between crossed polarisers or under a polarising microscope. A polarising microscope is an optical microscope fitted with polarisation optics. Generally the sample will be placed between crossed polarisers on a rotating stage. The polarisers and stage can all be rotated and devices such as a tilting compensator can be inserted and used to estimate birefringence of a sample. With the polarisers crossed and no sample present, all that is seen is a dark field. Depending on the orientation of the LC molecules, LC cells can exhibit some stunningly beautiful colour patterns. The polarising microscope also makes defects arising from problems with cell fabrication stand out clearly.

#### **4.2.5 Surface treatment of substrates**

Two problems were observed in the first generation of switching cells fabricated. These were the presence of a multi-domain LC texture and the presence of flow patterns. In many of the first-generation cells fabricated, a multi-domain LC texture can be observed through the polarising microscope. This appears as a speckled, multi-colour texture. Domain boundaries in LC form because of discontinuities in the LC alignment between adjacent regions. Domain formation in LCs is similar to that observed in magnetic materials. One might also describe this multi-domain LC texture seen in GLAD/LC cells as being somewhat analogous to “amorphous” in materials crystallography definitions. A multi-domain texture is in general undesirable as it indicates orientation disorder in the LC. Ideally, a single domain, or “single crystal” would be desired.

A second problem was the presence of flow patterns. Flow patterns resulting from the LC filling process, described in the foregoing sections, were also sometimes observed in the cells after filling. These patterns, which resemble a rippled surface of lines or tracks, suggest the LC is inhomogeneous across the cell. The flow patterns were also found to persist even after electro-optic switching of the LC (cycling the cell between unaddressed and addressed modes by applying and removing a driving voltage) or heating the cell to above the isotropic clearing point and allowing it to cool back down to room temperature.

To combat these problems, one technique used was pre-treatment of counter-electrode using polyimides or other surfactants. These may be used to induce either a planar or homeotropic alignment of the LC at the counter-electrode surface. Optimer AL1051 Display Material was used for planar alignment, while Nissan Sunever 7511L polyimide varnish was used for homeotropic alignment. The use of lecithine (3-sn-phosphatidylcholine), a natural homeotropic surfactant found in egg yolk, was also briefly investigated.

While the primary objective of the cell construction described earlier is to fabricate a structure which permits application of an electric field across the film for switching the LC, the switching cell brings several other benefits as well. In conjunction with the substrate surface treatments here, a known LC orientation can be produced at the surface of the counter-electrode, thereby minimising difficulties in having to separate optical effects of the GLAD/LC hybrid proper and a layer of LC resting on the surface of the film. Additionally, the cell structure also provides mechanical and environmental protection for the composite film.

The motivation for surface treatment of the counter-electrode is that it produces a known orientation of the LC. Surface treatment is not limited to the counter-electrode, however, and could be applied to the GLAD film to modify the surface properties of the film which in turn may have an effect on LC-to-film surface anchoring. In this case, polyimides might be applied by using a dilute solution and then driving off the solvent. Another possibility is to apply a gaseous phase surfactant such as silane.



While some experiments were conducted to study the effects of various substrate and film surface treatment, there was not sufficient data to provide conclusive results or comparisons between different surface treatment methodologies. For the majority of cases, the counter electrodes were treated with homeotropic polyimide surfactants as this tended to result in the fewest occurrences of LC flow patterns. Treatment with surfactants (including treatment of the GLAD film) is under further investigation.

#### **4.2.6 Optical measurements**

Optical measurements were performed on the films without LC and on cells made from the films after filling with LC. Measurements of the relative transmission ( $%T$ ) for LCP and RCP and measurements of optical rotation dispersion were performed and the spectral data analysed. The experimental setup for measurement of LCP/RCP transmission and of ORD were described in the previous chapter. (See “Measurements of GLAD films” on p. 49.)

### **4.3 Results – Enhancement of optical properties**

#### **4.3.1 Effect of addition of an isotropic index matching fluid**

CD/ORD measurements on unfilled GLAD films were presented in Chapter 3 and show that the chiral GLAD film on its own exhibits measureable chiral optical activity. A peak transmission difference between LCP and RCP on the order of a few percent was observed. The measurements verify the current understanding that the chiral optical activity in GLAD films arises from the structural chirality and index difference between the film material and void material (assumed to be air for unfilled films). It follows that a reduction of the index difference would diminish the chiral optical properties, and further, that a perfect index match would fully extinguish the chiral optical properties.

To test this hypothesis, a small piece of the film shown in Fig. 3-8 (measured earlier in Chapter 3—see Fig. 3-9) was filled with an index matching impregnate and the measurements repeated. The film, made from  $\text{SiO}_2$ , was assumed to have a refractive index of  $n = 1.458 \approx 1.46$ . Carbon tetrachloride ( $\text{CCl}_4$ ,  $n = 1.459$ ) was used at first as it would have been a nearly perfect index match. Unfortunately, the  $\text{CCl}_4$  was found to be too volatile and

evaporated very quickly. A second attempt at determining the effect of the addition of an index matching fluid was more successful. A mixture of toluene ( $C_7H_8$ ,  $n = 1.496$ ) and ethanol ( $n = 1.361$ ) was prepared with the proportions such that the refractive index of the mixture would be close to that of the film. A refractometer was used to measure the index of the mixture. While not as volatile as the carbon tetrachloride, the toluene/ethanol mixture also tended to evaporate easily, but sufficed for this experiment.

Addition of the index matching fluid to the film was found to reduce the transmission difference between LCP and RCP, verifying the prediction of suppression of the chiral optical properties upon filling the voids of the GLAD film with an index matching medium. The residual transmission difference indicates that the index match was not perfect. This experiment also supports the postulate that the magnitude of the index difference (circular birefringence) controls the strength of the optical response.

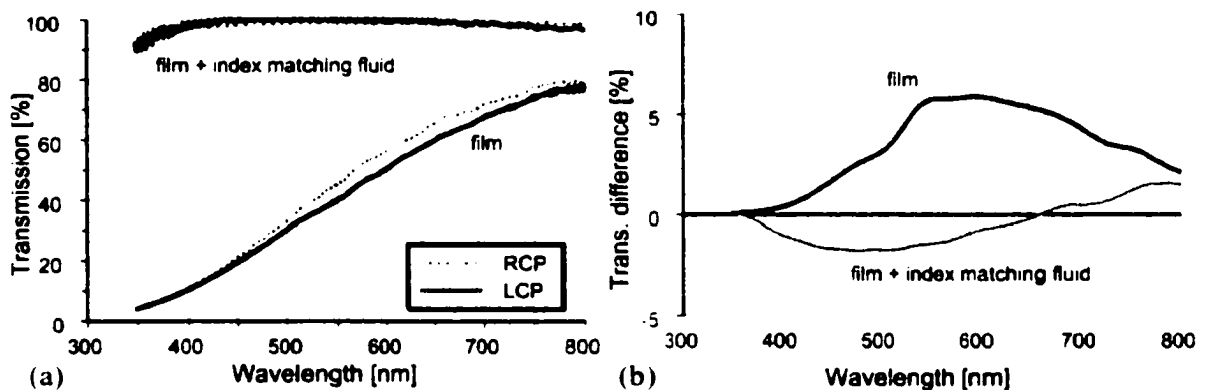


Figure 4-3: LCP/RCP transmission measurements for a  $SiO_2$  helical film. Measurements were taken on the film alone and when the film was filled with an approximate index matching fluid. (a) % $T$  measurements for LCP and RCP. (b) Transmission difference spectra (RCP – LCP).

### 4.3.2 Effect of addition of LC

LCP and RCP transmission was measured for a chiral GLAD film before and after filling (Fig. 4-4). The film, sample C, without embedded LC (“film alone”) exhibits low transmission due to the diffuse scattering of the porous GLAD film. After filling the film with ZLI 4792 LC, the overall transmission is higher, with peak transmission increasing from 40% to 55%. This improvement in transmission is consistent with visual observations of

reduced scattering.

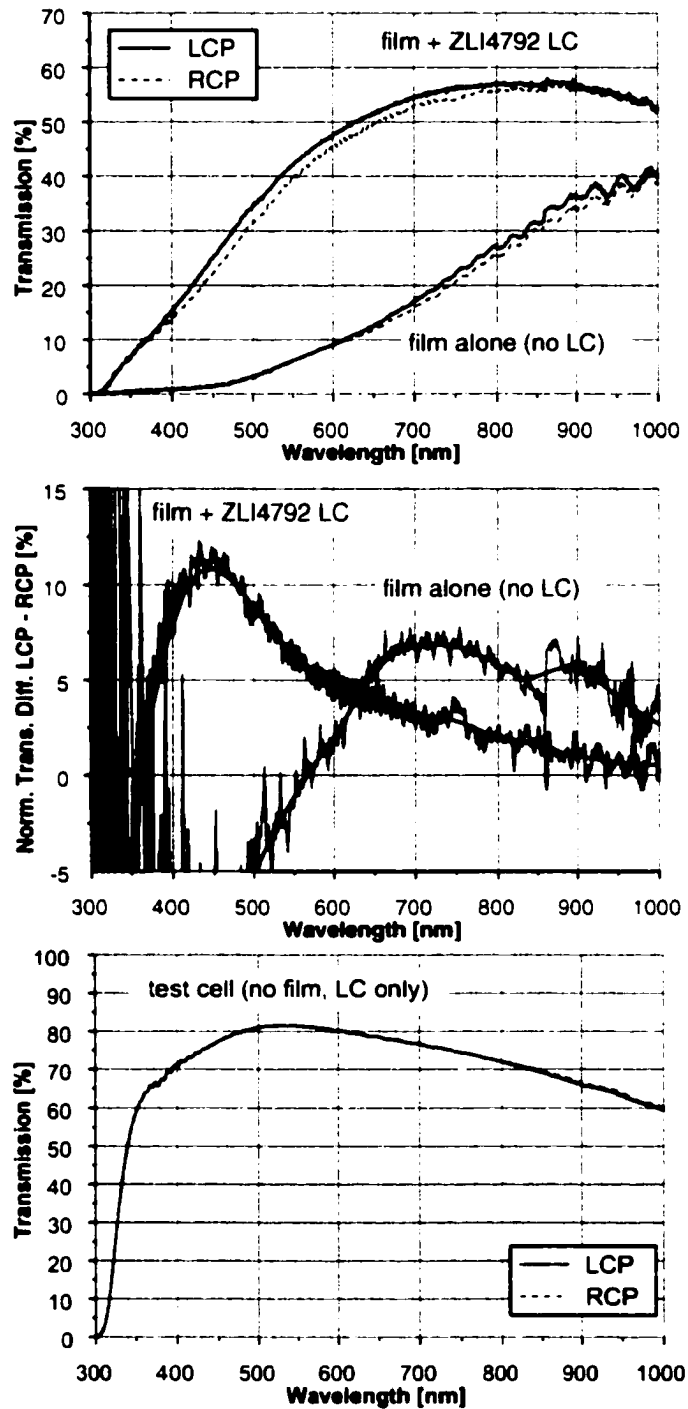


Figure 4-4: Effect of addition of LC  
 (a) Measurements of LCP and RCP transmission. (b) Difference spectra normalised to the uncoupled polarization. (c) Measurements on a test cell with LC only.

Also shown is the difference spectra ( $\%T_{\text{LCP}} - \%T_{\text{RCP}}$ ) normalised to the transmission of the uncoupled polarisation (LCP in this case). As the film is right-handed, LCP (the non-coupled polarisation) is expected to have higher transmission than RCP. Before filling, the film exhibits a peak difference of 7% at 710 nm; after filling, this peak difference increases to 11% but the peak shifts to 450 nm. Addition of the LC ("film + ZLI 4792") yields both higher overall transmission and an enhancement in the transmission difference. The enhancement of the chiral optic response indicates that the film acts as an alignment structure for the LC and induces an alignment similar to a chiral nematic phase.

For comparison, a test cell containing ZLI 4792 LC only (no GLAD film) was constructed and LCP/RCP measurements of this cell were taken and are shown in Fig. 4-4(c). The substrate surfaces for this cell were coated with a surfactant which produces homeotropic (perpendicular) alignment of the LC molecules at the substrates. The cell spacing was controlled through the use of 4.2  $\mu\text{m}$  diameter microsphere spacers (the same technique is used for standard LCD cell fabrication). The transmission data shows a high peak transmission (>80%), however, because the test cell structure is fundamentally different than that of cells based on sample C (the measurements shown in Fig. 4-4(a) and (b)), a direct comparison between the raw transmission values is not necessarily valid (hence they were graphed separately). Of particular significance, however, is the lack of transmission difference between LCP and RCP. While it produces what seems like a simple result, this measurement is nonetheless important in showing that the LC alone, in the absence of the chiral GLAD structure, does not produce a transmission difference between left- and right-handed circular polarisations.

The same LCP/RCP measurements were also performed on sample T, a  $\text{MgF}_2$  LH helical film first without LC and then with ZLI4792 and E7 LCs. Fig. 4-5(a) shows the  $\%T$  spectra for LCP/RCP while Fig. 4-5(b) shows the transmission difference spectra. As consistent with the sample being LH, the LCP transmission exhibits a "dip" in the active wavelength range of the film. For this film, addition of ZLI4792 produced almost no noticeable enhancement of the transmission difference. Addition of E7, on the other hand, produced an approximate three-fold increase in the transmission difference and a shift of the peak trans-

mission difference toward the red end of the spectrum (a “red-shift”). Even more interesting, however, is the presence of a second peak at the blue end of the spectrum (near 360 nm). No explanation can be given at this time, and clearly further study needs to be done to explain some of the behaviour observed.

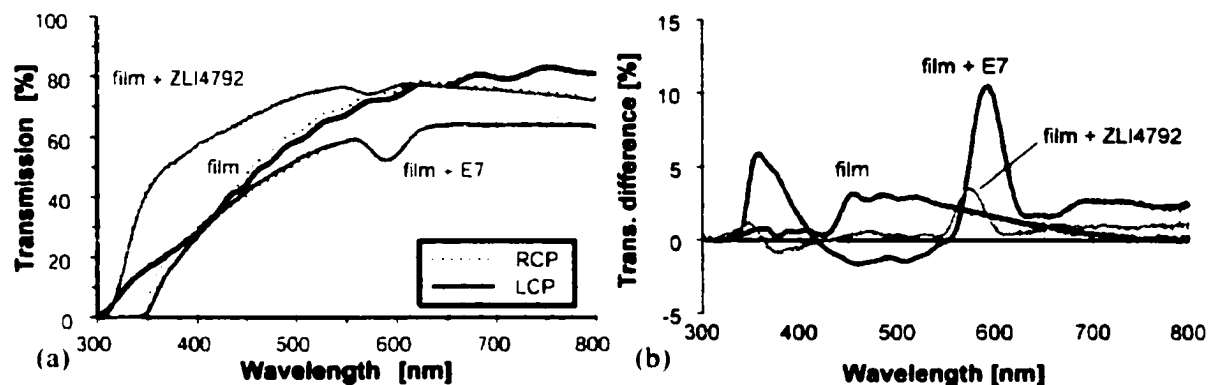


Figure 4-5: LCP/RCP transmission measurements for a  $\text{MgF}_2$  helical film (a) % $T$  measurements for LCP and RCP. (b) Transmission difference spectra (RCP – LCP).

The enhanced circular dichroism (i.e. the larger transmission difference between the uncoupled and coupled polarisations) suggests that a quasi-chiral nematic phase is induced in the LC by the presence of the chiral GLAD “backbone” [96]. The LC molecules tend to align into a phase which minimizes potential energy. The effect of the chiral GLAD film is similar to that produced by the addition of chiral dopants to achiral nematic LCs.

### 4.3.3 Effect of film handedness

As a simple demonstration, LCP and RCP transmission was measured for the enantiomeric (opposite handedness) pair of samples, G and H (Fig. 4-6), after filling the cells with ZLI 4792 LC. The films each had 11.1 turns and pitch  $p \sim 450$  nm (within 5% error). The RH film, sample G, was expected to show higher LCP than RCP transmission, whereas the opposite was expected from the LH film, sample H. Fig. 4-7 below shows the difference spectra (LCP – RCP) for the two cells. The spectra were normalized to the uncoupled polarization (LCP for sample G and RCP for sample H). The maximum normalized circular polarized transmission difference for sample G was 8% at 560 nm, while that of sample H

was -6% at 480 nm. The small discrepancies in the wavelength at which the peak response is seen and in the magnitude of the peak response are most likely because the two samples are not a perfect enantiomeric pair.

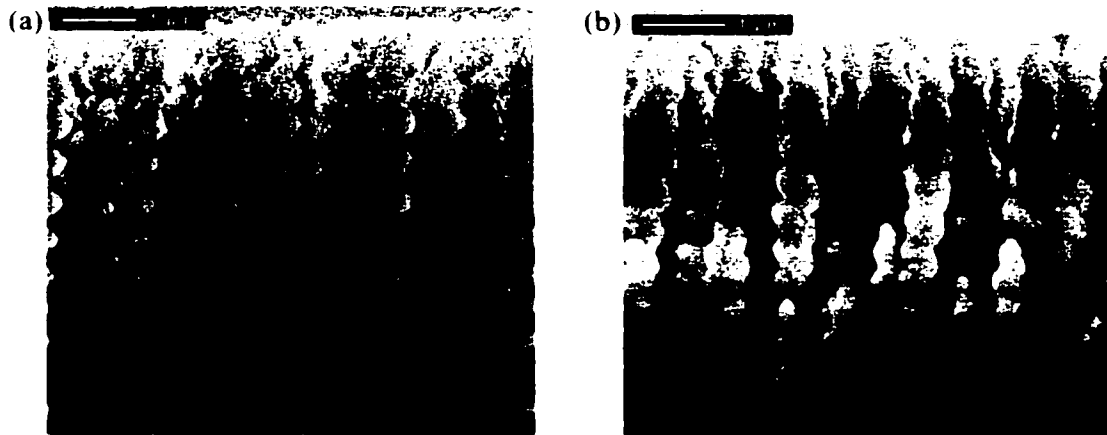


Figure 4-6: Enantiomeric pair of GLAD thin films  
(a) Right-handed (sample G) and (b) left-handed (sample H) versions of  $\text{SiO}_2$  films with 11.1 turns and pitch  $p \sim 450$  nm.

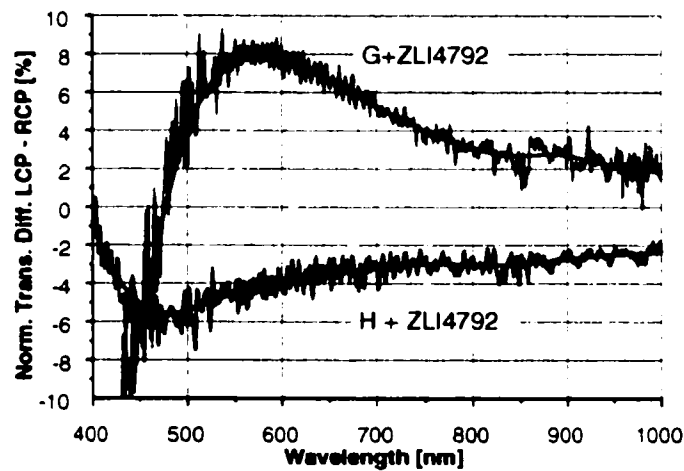


Figure 4-7: Effects of handedness  
Difference spectra for circularly polarized transmission measurements on a pair of samples with similar geometries, but opposite handedness.

#### 4.3.4 Effect of film pitch

LCP and RCP transmission difference measurements were performed on a set of  $\text{SiO}_2$  films before and after filling with ZLI4792. The wavelength at which peak (normalized) transmission difference occurred was determined from the measured spectra and the results are

summarized in Table 4-4 below.

Table 4-4: Peak LCP/RCP transmission difference wavelength for SiO<sub>2</sub> films

Sample	Pitch (nm)	$\lambda_{\text{peak}}$ (nm)	
		(without LC)	(with LC)
C	290	710	440
G	450	720	620
K	527	1000	730

The peak wavelength plotted as a function of helical pitch is shown in Fig. 4-8. Best fit lines were determined by linear regression to determine the slope. In keeping with the relation  $\lambda_{\text{peak}} = n_{\text{eff}}p$ , the best fit line was forced through the origin. The slope would then represent, according to this relation, the effective index of refraction. For the unfilled films, the best fit line has equation  $\lambda_{\text{peak}} = 1.87p$ ; while for the filled films, the best fit line is given by  $\lambda_{\text{peak}} = 1.40p$ . The data for the LC-films is inconclusive but suggests that the effective index of refraction increases after filling the films with LC.

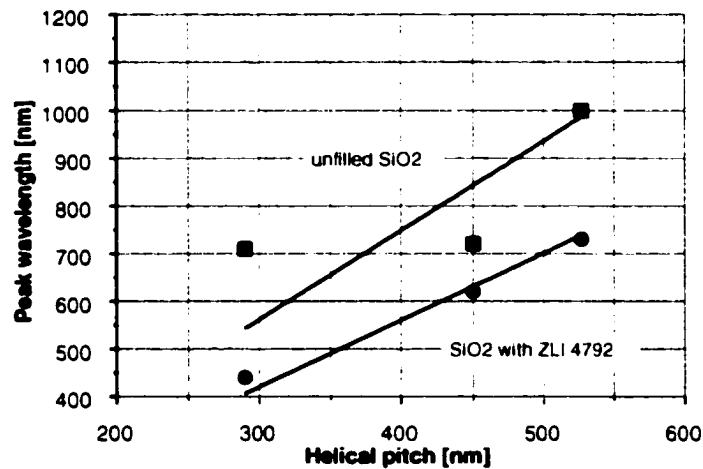


Figure 4-8: Effect of helical pitch  
Wavelength at which peak circularly polarised transmission difference occurs versus helical pitch for a set of SiO<sub>2</sub> GLAD films before and after filling with ZLI4792 LC.

Measurements of optical rotation were also performed on the films. The rotatory dispersion (see also “Optical activity” on p. 45) of sample C is shown below in Fig. 4-9 before and after filling with ZLI 4792 liquid crystal. The unfilled film exhibits a peak of  $-4^\circ$  rotation at  $\lambda \sim 450$  nm.

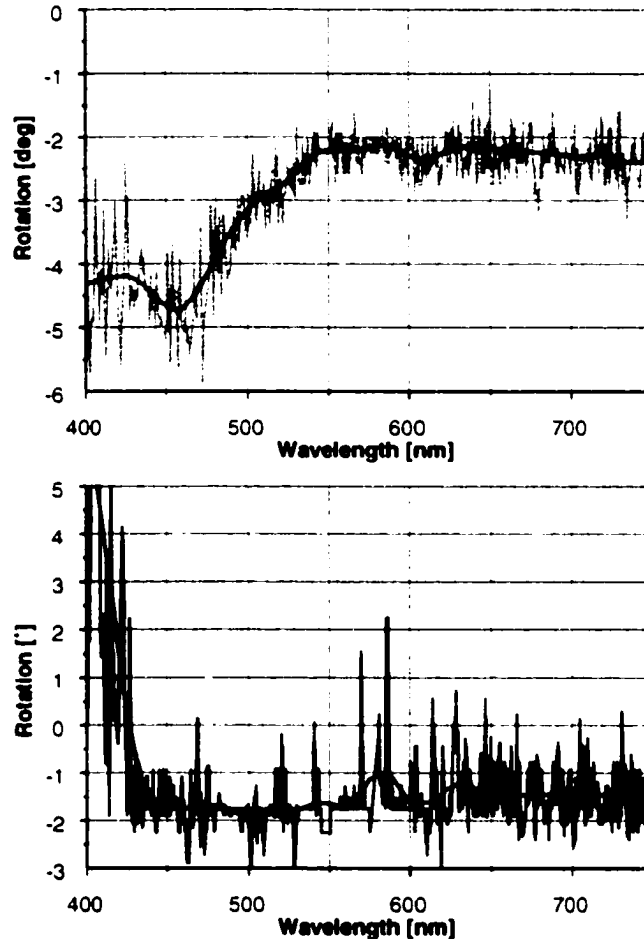


Figure 4-9: Rotatory dispersion ORD for a  $\text{SiO}_2$  film (a) before filling with LC; (b) after filling with ZLI4792.

### 4.3.5 Optical rotatory dispersion measurements

Rotation measurements were also performed in collaboration with colleague S. R. Kennedy on sets of  $\text{MgF}_2$ ,  $\text{SiO}_2$ , and  $\text{Al}_2\text{O}_3$  films. These sets of films were all deposited at  $\alpha = 85^\circ$  with pitch  $p \sim 450$  nm. The number of turns was the experimental variable. The results for measurements on the films without LC and after filling with ZLI4792 are summarised below. Table 4-5 outlines the rotation versus number of turns for the films of each material.



Table 4-6 lists the rotation per unit length ( $^{\circ}/\mu\text{m}$ ) for the films in each set.

Table 4-5: Maximum rotation versus number of turns

Material	Sample	Number of turns	Maximum rotation ( $^{\circ}$ )	
			without LC	with ZLI4792
SiO <sub>2</sub>	D	5.0	1.5	3.0
	E	7.0	2.0	7.5
	F	9.0	2.2	8.0
	H	11.1	4.0	
MgF <sub>2</sub>	P	5.0	0.25	-0.25
	Q	8.0	0.75	-1.50
	R	11.7	1.00	-14.00
Al <sub>2</sub> O <sub>3</sub>		6.0	2.0	-5.0
		8.2	3.0	-5.5
		10.0	3.5	-6.0
		12.0	4.5	-10.0

Normally, the sign convention used for optical rotation is determined by the absolute direction of rotation with a clockwise rotation (looking back at the light source) taken as positive and called dextrorotatory; counter-clockwise is negative rotation or levorotatory. (See also "Optical activity" on p. 45.) In general, a LH chiral medium is dextrorotatory and a RH medium, levorotatory. For the analysis in this section, a different sign convention was used to accommodate the mixture of LH and RH samples in the sets of films. Optical rotation in the "expected" direction (i.e. CW rotation for a LH medium, CCW for a RH medium) was taken as positive in this sign convention. Rotation in the opposite sense to what is expected was taken as negative.

The rotation data in Table 4-5 is also plotted in Fig. 4-10 below. For the three sets of films, the rotation was generally found to be, as expected, an increasing direct linear function of the number of turns. The slope of the linear best fit lines are what appear in Table 4-6. (The

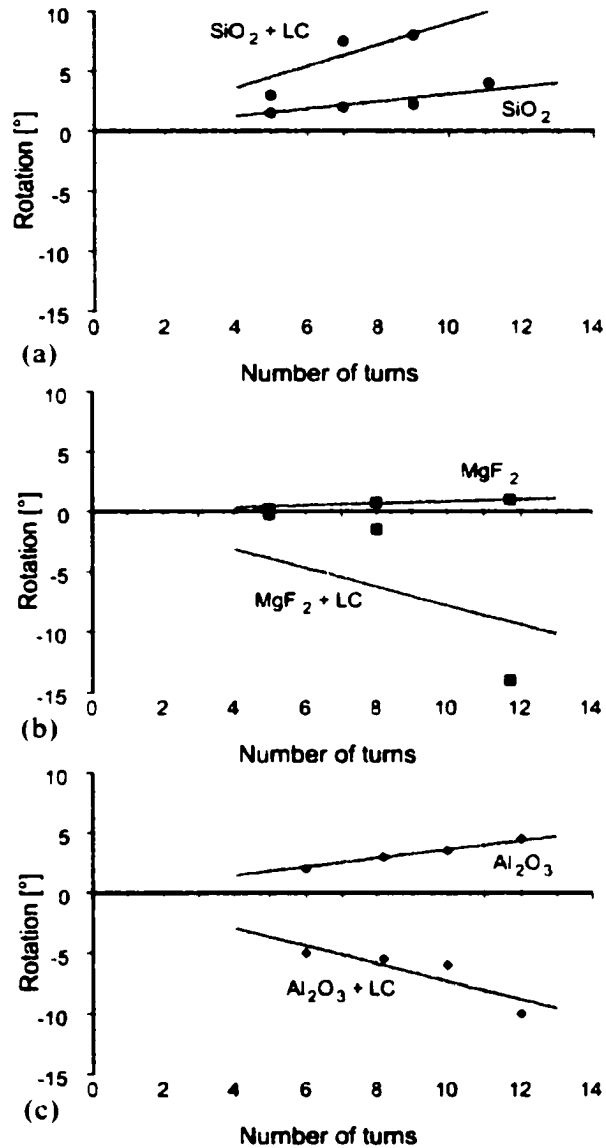


Figure 4-10: Maximum optical rotation for films before and after adding LC. For clarity, the data is plotted on separate sets of axes but is plotted at the same scale to facilitate comparison. (a) SiO<sub>2</sub> films (b) MgF<sub>2</sub> films (c) Al<sub>2</sub>O<sub>3</sub> films.

intercept was set to zero since a film of zero turns is equivalent to having no film present which results in zero rotation). For the unfilled films, there is also an increasing relationship between the maximum rotation per  $\mu\text{m}$  and the bulk index of the material. This result is also expected and is consistent with the theory presented in Chapter 3.

After the addition of the ZLI4792 LC to the films, several important observations were made. First the, the magnitude of optical activity increased for all cases which again lends

Table 4-6: Maximum rotation per  $\mu\text{m}$  before and after adding LC

Material <sup>a</sup>	Maximum rotation ( $^{\circ}/\mu\text{m}$ )	
	without LC	with ZLI4792
MgF <sub>2</sub> ( $n = 1.38$ )	0.16	-0.96
SiO <sub>2</sub> ( $n = 1.47$ )	0.67	1.34
Al <sub>2</sub> O <sub>3</sub> ( $n = 1.66$ )	1.05	-2.30

a. This data from S. R. Kennedy *et al.* [100]

support to the notion that the presence of the chiral GLAD film induces some sort of chiral nematic-like alignment in the LC. The increase in chiral optical response in the form of optical rotation is consistent with the earlier results for LCP/RCP transmission difference increasing after addition of LCs.

Interestingly, though, MgF<sub>2</sub> and Al<sub>2</sub>O<sub>3</sub> films with embedded LCs exhibited a reversal of sign for the polarisation rotation, meaning that the plane of polarisation rotates in the opposite sense for the GLAD/LC composite film compared to rotation exhibited by the GLAD film alone. Furthermore, this very unexpected phenomenon was not observed for SiO<sub>2</sub>. In initial experiments, only MgF<sub>2</sub> and SiO<sub>2</sub> films had been studied, and given that MgF<sub>2</sub> exhibited this rotation reversal while SiO<sub>2</sub> did not, led to a preliminary hypothesis that perhaps some sort of “inverse optics” effect was occurring because MgF<sub>2</sub> has a lower index than the LCs involved whereas the index of SiO<sub>2</sub> is about the same as the indices of the LCs used. However, since Al<sub>2</sub>O<sub>3</sub> has an even higher index and like MgF<sub>2</sub> exhibits this rotation reversal effect, it means that there is some other explanation still. A trend of decreasing rotation with wavelength was seen which implies that the spectral range investigated lies to the right of the resonance point and hence the change in direction could not have been simply a wavelength shift to the opposite side of the resonance/critical wavelength point. Further study is required to determine the origin of this phenomenon.

#### 4.3.6 Effects of GLAD film structure

Up until this point, the optical measurements presented have all been for chiral GLAD films with helical microstructure. Here, optical measurements for GLAD/LC cells with other

chiral structures are presented.

A square “staircase” helical film is fabricated similarly to the usual standard smoothly bent helix, but instead of using a continuous substrate rotation in  $\varphi$ , a stepped rotation is used. RCP/LCP transmission measurements were performed for sample U, a  $\text{Al}_2\text{O}_3$  square helical film shown in Fig. 4-11 below. The film measured was right-handed, with 15 turns at pitch  $p = 410$  nm.

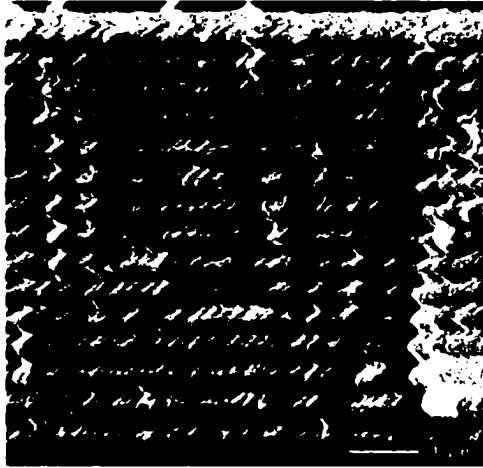


Figure 4-11: SEM of a square spiral helical GLAD film  
This RH chiral film was grown by e-beam evaporation of  $\text{Al}_2\text{O}_3$  and has 15 turns at pitch  $p = 410$  nm.

Measurements were performed on the film without LCs and for a cell constructed from this film after addition of ZLI 4792. Fig. 4-12(a) shows the  $\%T$  spectra for LCP and RCP for the film before (“film”) and after addition of ZLI 4792 (“film + ZLI4792”); Fig. 4-12(b) shows the difference spectra ( $\%T_{\text{LCP}} - \%T_{\text{RCP}}$ ). The film alone has a peak transmission difference of about 3% at 525 nm. Addition of ZLI 4792 increases the peak transmission difference five-fold, to 15%, and causes a red-shift of the peak to 655 nm. One interesting feature to note is the presence of what appear to be sidelobes on either side of the peak in the difference spectra for the square spiral helical film. While it is surmised that a chiral nematic-like phase is induced in the LCs for helical GLAD films, one might venture that this square spiral structure induces some sort of chiral, smectic phase, in keeping with the segmented structure of the columns.

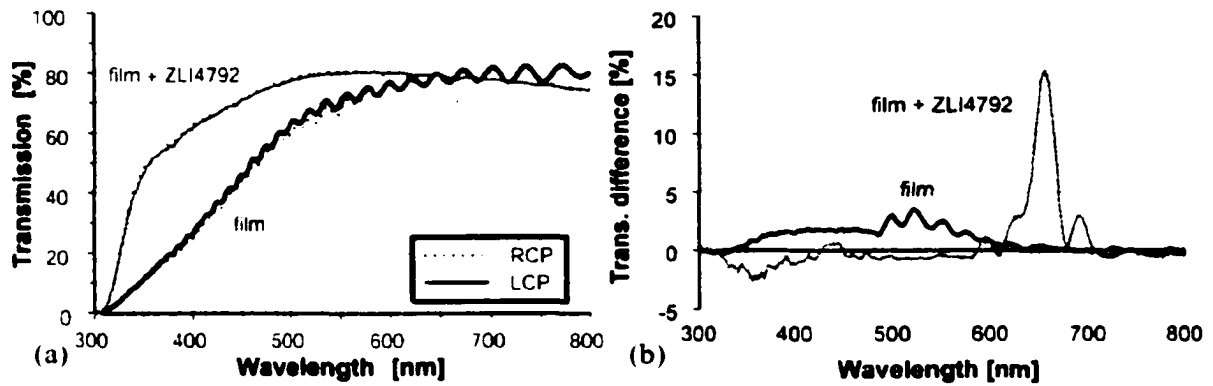


Figure 4-12: LCP/RCP transmission measurements for square helical film. Measurements were performed for a cell constructed from film in Fig. 4-11. (a) % $T$  measurements for film without LC and after addition of ZLI 4792. (b) Transmission difference spectra shows a five-fold increase after addition of LC.

Measurements performed on the twisted ribbon chiral film shown in Fig. 2-9 (p. 36) unfortunately gave inconclusive results and thus are not included here. One feasible explanation is: first, that the film structure itself is not yet optimised and thus shows very little chiral optical response on its own; and second, that the film is also too dense to allow for adequate infiltration by LCs. Further work on optimising the twisted ribbon microstructure is required.

#### 4.4 Electro-optical switching

At this point, it has been established that the chiral GLAD film exhibits chiral optical activity including polarisation rotation and circular dichroism. When (achiral) nematic liquid crystals are introduced into the film, the chiral optical activity is enhanced due to a reduction in scattering and, more importantly, that the nematic LC is aligned by the GLAD film in some sort of chiral nematic-like texture. The results so far show that the GLAD film controls the pitch and handedness of the chiral nematic phase induced in the LC. These results in themselves are significant and useful, but to develop an active device, one needs to be able to switch or actuate it. The LC component fits the bill perfectly. Moreover, the switching behaviour in a GLAD/LC device must be designed to do something “useful”. That development is detailed here.

What happens, then, when an electric field is applied across the cell? Because of the (positive) dielectric anisotropy of the LCs used, in the addressed state, the LCs will align parallel to the  $E$ -field, which is parallel to the helical axis of the GLAD film and perpendicular to the cell plates (homeotropic alignment). An illustration of unaddressed and addressed states in a GLAD/LC switching cell is shown in Fig. 4-13.

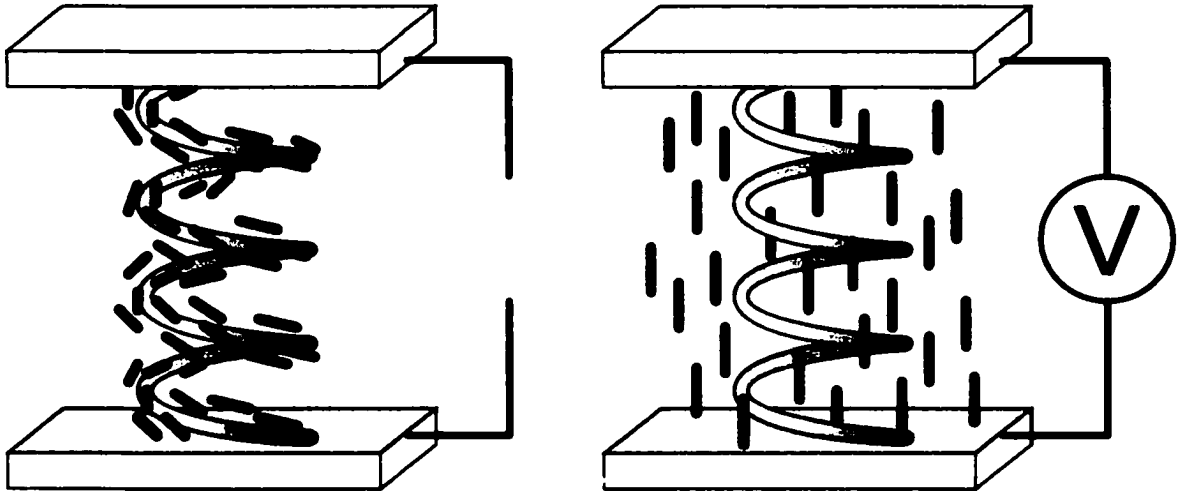


Figure 4-13: Electro-optic switching of LC component in GLAD/LC devices  
 When the cell is unaddressed (left), the LC is aligned by the presence of the chiral GLAD medium in an orientation similar to that seen in a chiral nematic phase.  
 When the cell is addressed by application of an electric field (right), the LC molecules align parallel to the electric field.

In the addressed mode, light transmitted through the cell along the helical axis (and now parallel to the LC) will “see” the ordinary refractive index  $n_o$  of the LC. If  $n_o$  is chosen to index match with that of the GLAD film, then in addressed mode, the GLAD/LC cell appears to be a homogeneous medium of index  $n = n_o = n_{\text{film}}$ . Consequently, the chiral optical response is expected to vanish in addressed mode.

LCP/RCP transmission measurements were performed on a switching cell fabricated from sample S. This film, which is shown in Fig. 4-14(a), is left-handed with 10 turns and has a deliberately introduced gradient in the pitch from 500 nm at the substrate to 350 nm at the top of the film. Pitch gradation is one technique used to broaden the reflection band with CLCs [97]. The GLAD/LC switching cell fabricated from this film was embedded with E7

LC. Circular polarised transmission measurements were performed on this cell in addressed and unaddressed modes (Fig. 4-14(b)). In the unaddressed state (no voltage applied), enhanced circular dichroism as compared to the unfilled film is observed (“unaddressed” versus “unfilled film”). When the cell was addressed by the application of a 200 V (peak-to-peak), 1 kHz signal, all transmission difference between LCP and RCP vanished (“addressed”). As described above, in addressed mode, the electric field causes the LC molecules to change their alignment from the quasi-chiral nematic phase to orient parallel to the field. Transmitted light through the cell thus “sees” the ordinary index of the LC,  $n_o$  (1.52 for E7), which is an approximate index match for the GLAD film material (in this case  $\text{SiO}_2$ ,  $n = 1.47$ ), causing the chiral nature of the film to be effectively cancelled and resulting in the loss of circular polarization transmission difference. When the electric field was removed, the cell reverted to its unaddressed state [98, 99].

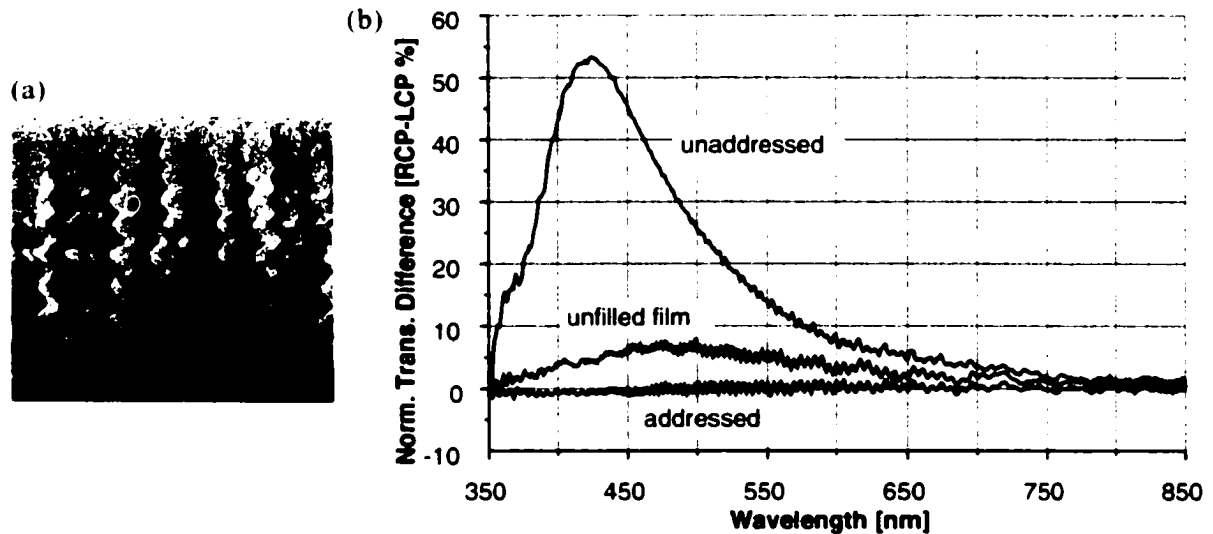


Figure 4-14: Measurement of electro-optic switching in a GLAD/LC cell (a) Switching cell was fabricated from this LH,  $\text{SiO}_2$  film. (b) Measurement of transmission difference in unaddressed and addressed modes. In the unaddressed mode, the cell exhibits enhanced chiral optical response compared to the film alone without LC. In addressed state, the transmission difference vanishes. This figure is from Sit *et al.* [98].

#### 4.4.1 Switching characteristic

An Autronic display measurement system<sup>6</sup> at Philips Research Laboratories was used to

6. Autronic-MELCHERS GmbH, Germany. Website: [www.autronic-melchers.de](http://www.autronic-melchers.de)

perform a few additional tests to characterise the switching characteristics of the cell. The Autronic system is highly flexible and well suited for characterisation of flat panel displays. The device under test is placed on a translating ( $x, y$ ) and rotating ( $\varphi$ ) stage above which is mounted the photodetector on a tilting arm which permits measurements from any polar angle ( $\theta$ ) (for characterisation of viewing angle in LCDs). The sample can be illuminated from above or below the stage, thus permitting reflection and transmission measurements. Using the computer interface, the system also allows for spectrometric (wavelength) and electro-optic (for example, intensity versus driving voltage).

Using the Autronic system, the switching characteristic was measured for a cell constructed from the  $\text{SiO}_2$  film shown in Fig. 3-6 (p. 53). For these measurements the cell was placed between crossed polarisers and illuminated from below. In the unaddressed mode, optical activity and scattering produces transmission of light. However, addressing the cell eliminates the chiral optical activity as described in the previous section and the crossed polarisers block all light transmission.

The transmission for this sample was measured at various values for the driving voltage applied to the cell. The transmission spectra are shown below in Fig. 4-15. As the voltage is increased, the LC begins to align to the applied  $E$ -field, extinguishing the chiral optic activity, and the light becomes blocked by the polarisers.

The overall luminance as a function of driving voltage is shown in Fig. 4-16. Again, the cell was placed between crossed polarisers and the transmission as a function of driving voltage was measured. This graph corresponds approximately to taking a vertical slice of the graph shown in Fig. 4-15. The switching characteristic shown in Fig. 4-16 shows a smooth transition from “off” to “on” states rather than any sort of “threshold” effect.

#### **4.4.2 Switching speed**

The Autronic system was also used to characterise the time-domain switching characteristics of a GLAD-LC cell. The initial results obtained were not remarkable and hence are not included here, but did show a response time in the tens of microseconds which is similar to



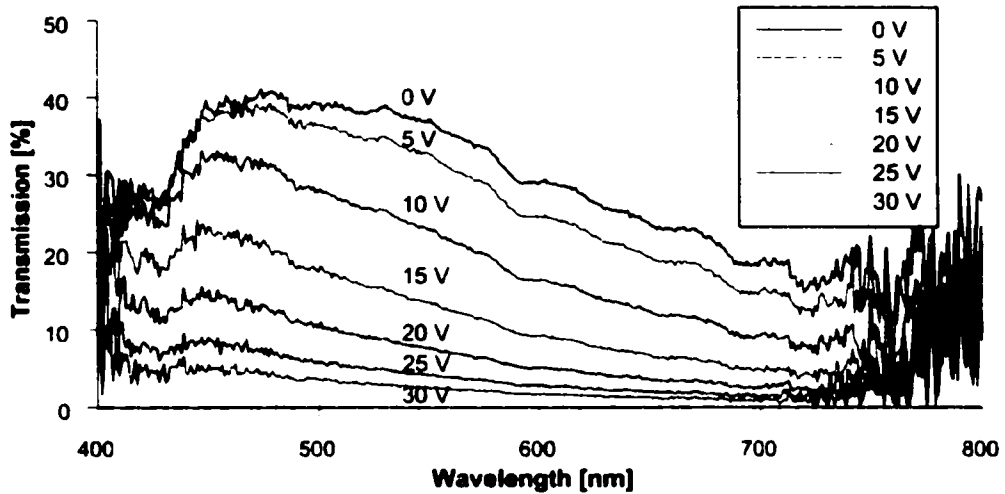


Figure 4-15: Transmission spectra for a GLAD/LC cell versus driving voltage. The cell was fabricated from the film shown in Fig. 3-6 (p. 53). Transmission was measured for the cell placed between crossed polarisers.

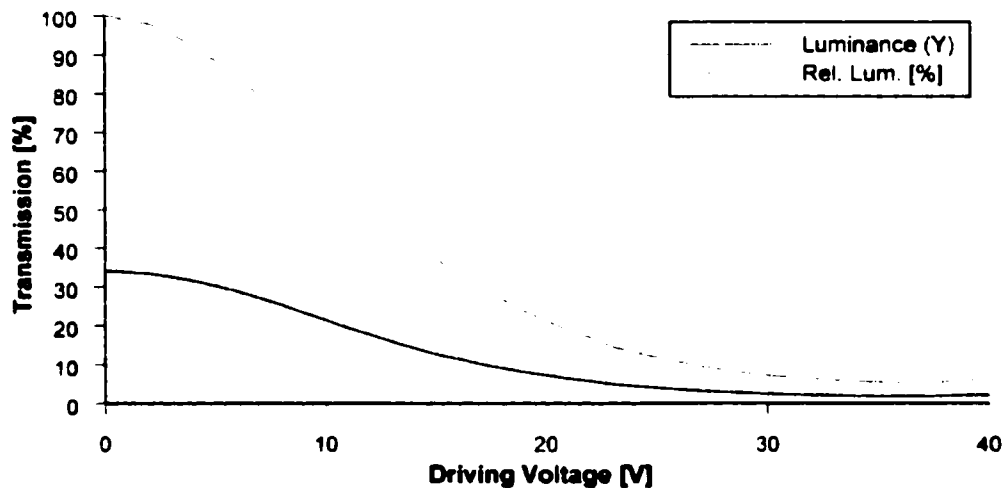


Figure 4-16: Luminance versus cell driving voltage. This measurement was made in the same configuration as above. The luminance (overall transmission) was measured as a function of driving voltage. No "threshold" is present in this switching characteristic. "Relative luminance" is a simple scaling of the luminance curve to 100%.

that seen in standard LC cells, and are therefore neither significantly better nor worse than regular LCDs. Further switching speed tests are required for more conclusive data.

## 4.5 Discussion

### 4.5.1 Summary of results

The addition of LCs to chiral GLAD films was generally found to enhance the chiral optical response compared to that exhibited by the film on its own. Pitch and handedness of the induced LC orientation, and hence the spectral properties of the optical response, were shown to be largely controlled by the microstructure of the GLAD film which is in turn determined by substrate motion during the deposition process.

The effects on optical rotation were also studied for three different materials and resulted in several important observations. The magnitude of the rotation was found to increase after addition of LCs, as compared to that observed in GLAD films without LC. However, for  $\text{MgF}_2$  and  $\text{Al}_2\text{O}_3$ , the sign of the rotation also reversed. This behaviour was unexpected and was not seen, in contrast, in films made of  $\text{SiO}_2$ .

Measurements of the chiral optical response on non-helical chiral GLAD films such as the square spiral structure demonstrates the flexibility of GLAD in its ability to fabricate these microstructures and lends emphasis to the basic principle underlying GLAD/LC hybrid materials—the GLAD film structure controls the orientation of the LC.

One parameter of GLAD films that has not been investigated directly by the author for its effect on the optical properties is that of deposition angle  $\alpha$ . (Recall that all other conditions being equal,  $\alpha$  is the primary determinant of the porosity of a GLAD film.) Studies led by colleague S. R. Kennedy on the effect of varying  $\alpha$  in the range of  $83$  to  $86^\circ$  [100] have shown that the more open, porous structure produced by higher flux incidence angles is conducive to stronger optical rotation in the unfilled films. Additionally, it was found that the higher porosity is even more important for LC-filled films. The explanation for this observation is that the increased porosity allows for larger amounts of LC to be incorporated into the film (per unit volume).

Switching of the LC component in GLAD/LC composite optical devices has been demon-

strated. Through proper design of index matching between  $n_o$  of the LC and  $n_{\text{film}}$ , the chiral optical response in a GLAD/LC may be “turned off” by addressing the cell. Preliminary characterisation of switching behaviour reveals that GLAD/LC switching characteristics are reasonably similar to those of standard LC technology.

#### 4.5.2 Evaluation of GLAD/LC technology

The marriage of LC and GLAD chiral optics to produce composite optical materials and devices has so far yielded encouraging results. A brief comparison of the three technologies, LC optics, GLAD optics (sans LC), and GLAD/LC hybrid optics is presented in Table 4-7.

Table 4-7: Comparison of LC, GLAD, and hybrid GLAD/LC technologies

	Liquid crystals	GLAD film	GLAD/LC hybrid
Spectral properties controlled by:	Helical pitch/handedness in chiral nematic phase. May be influenced by chiral dopants. Possibility for dynamic control.	Pitch/handedness of film structure. Determined during deposition. “Exotic” structures possible.	Pitch/handedness of GLAD film “backbone”. Dynamic control possible?
Optical performance	Strong	Weak, scattering	Strong
Device stability	Generally sealed into cell structures.	Porous films delicate and subject to environmental effects.	Uses cell structure.
Switchability	Yes, inherent to LCs.	No.	Yes, because of LC.

Taken individually, it would seem that chiral optics based on LC technology would better than based on GLAD in almost every aspect of comparison. LCs have a known, strong optical response and are inherently switchable. GLAD is an unproven technology in comparison and its optical response tends to be stifled by substantial diffuse scattering. However, one key advantage in favour of GLAD is its ability to control the columnar microstructure of the films precisely. While describing GLAD as allowing “completely arbitrary control”

over column shape may seem a bit crude, it is an accurate description of just how much control one has over film microstructure. Stacked layers of different pitch and/or handedness and pitch gradients are all easily accomplished with GLAD but very difficult to do with LC technology. The promise of GLAD/LC technology thus lies with the ability of the GLAD “backbone” structure to control the LC orientation.

At present, GLAD/LC technology has been demonstrated with very encouraging initial results. By themselves, porous chiral GLAD films exhibit low overall transmission due to scattering. Their intrinsic chiral optical activity is likewise fairly weak, with peak optical rotation on the order of  $0.2$  to  $1.0^\circ/\mu\text{m}$  and peak transmission difference typically between 2 to 5%. Addition of liquid crystalline materials to the GLAD films results in improvement in all these areas. Overall transmission increases due to decreased light scattering while peak optical rotation and peak transmission difference (between LCP and RCP) were shown to improve two- to five-fold as compared to the performance of the GLAD films without LC. Given that a test cell containing only the LC exhibited no chiral optical activity, the data from optical characterisation of GLAD/LC hybrids supports the hypothesis that there is an interaction between the GLAD film and LC components wherein the chiral film induces chiral orientation of the LC molecules to result in accentuated chiral optical activity.

LC technology currently in use and in development still has significantly stronger performance characteristics than GLAD/LC hybrids at this juncture. Peak optical rotation and RCP/LCP transmission difference in LC cells is typically on the order of 5 to 10 times better than the initial results for GLAD/LC seen here. Although much further work is required to improve the performance of GLAD/LC materials, the initial demonstration of this technology is very promising.

## Chapter 5

# Summary and conclusions

---

### 5.1 Summary of this thesis

This thesis presents the work concerning the union of porous, engineered thin films and liquid crystalline materials. Using the specialised glancing angle deposition (GLAD) technique for thin film fabrication, porous thin films consisting of an easily controllable columnar structure can be grown. The key to controlling properties in thin films is to control the structure of the film and this in turn is controlled by the deposition process. Using GLAD, the columnar microstructure may be made nearly any conceivable shape through careful control of substrate motion during deposition. A wide range of materials including metals, oxides, fluorides, and semiconductors have been demonstrated with GLAD. Recently, other researchers have even demonstrated GLAD-like techniques with the deposition of amorphous solid water [101].

Using some of the techniques presented in Chapter 2, the GLAD “toolbox” can be expanded to extend the capabilities of this deposition technology. Sputter deposition widens the range of materials accessible to GLAD. Advanced microstructural control techniques build on the basics of GLAD substrate motion to permit a higher degree of control over the structural parameters of GLAD films. Decoupling of structural parameters allowing for near-independent control gives another degree of freedom for GLAD and leads to new structures such as the periodically bent nematic and twisted ribbon chiral.

GLAD optics were presented in Chapter 3. Certain classes of GLAD films, those with chiral microstructures, exhibit unique optical properties including polarisation rotation and circular Bragg reflection. A simplified electromagnetic model is used to explain these effects. Measurements show that the optical response is similar to that seen in chiral nematic (cholesteric) liquid crystals (CLCs). However, the high porosity of GLAD films leads to potential problems with environmental stability and furthermore contributes to a substantial amount of scattering. While the initial simplified model facilitates a qualitative descrip-

tion of the observed optical phenomena, more robust models (slow wave propagation and helical antenna models were highlighted briefly) are required for a fuller understanding of the optical response. Discussion of liquid crystals and LC displays sets the stage for the central section of this thesis, the embedding of LC materials into GLAD films and the investigation of the resultant composite optical material.

When GLAD films are embedded with LC materials as described in Chapter 4, the LC molecules take on an orientation governed by the presence and shape of the GLAD film structure. Achiral nematic LCs embedded into chiral GLAD films become oriented in a chiral nematic-like mesophase. Most importantly the GLAD/LC composites exhibit enhanced optical properties (typically two- to five-fold enhancement) compared to those of the film alone. Measurements presented show that the pitch and handedness of the film control the spectral properties of the optical response of the GLAD/LC hybrid. Some surprising results are also presented, including reversal of the sign of the chiral optical activity which was observed after filling films with LC. These anomalous results, not explained by the current theory and understanding, warrant further study.

Because of their electro-optic characteristics, the LC component in GLAD/LC composite films may be switched by an electric field, yielding active devices based on these hybrid materials. The construction of switching cells for GLAD/LC is described and experimental considerations are discussed. In the unaddressed mode (with no voltage applied), GLAD/LC cells exhibit the enhanced chiral optical properties mentioned earlier. In the addressed mode, however, the LCs are oriented parallel to the electric field, and, for sufficiently matched refractive indices of the LC ordinary index ( $n_o$ ) and of the film ( $n_{\text{film}}$ ), the addressed GLAD/LC cell appears as a homogenous medium and thus extinguishes all chiral optical activity.

To conclude this thesis, this chapter presents some ideas for future experiments that could be undertaken with the twofold goals of improving the performance of GLAD/LC films and of aiding scientific understanding of this composite material.

## **5.2 Future experiments**

This research project, studying GLAD thin film/liquid crystal composite materials has certainly generated no shortage of ideas for experiments. By bringing together GLAD and LC technologies to produce a new composite material based on embedding LC materials into GLAD films, the number of parameters in the sample space is essentially doubled. One can investigate the effect of manipulation of not only the many structural parameters of the GLAD film backbone (such as density, pitch, or thickness), but also the many parameters of the LC material (such as LC type, additives, or surface treatment). While having more parameter “knobs” to turn gives the researcher more degrees of freedom, the situation is at the same time far more challenging for the very same reason. One must map out the wide range of possibilities and decide on what investigations to undertake. Doing so while maintaining sight of the goal of the research is key to continued success. Some ideas for future research directions are presented here.

### **5.2.1 GLAD films**

Looking first at only the GLAD film component in GLAD/LC hybrids, reveals many opportunities for investigation. These possible future research directions include new structures, improvement on the deposition process, and seeded substrates (described briefly later in this chapter).

One of the key features of the glancing angle deposition technique is that any arbitrary structure can be created by the appropriate permutation of stacked layers of the four fundamental microstructure types as introduced in Chapter 1 (see “Basic forms” on p. 15). Structures possible but not yet fully investigated include: films with stacked layers of different pitch and/or handedness, pitch gradients, and other structures such as the periodically bent nematic (PBN) and the twisted ribbon. A film consisting of layers of two different pitches might conceivably exhibit two reflection bands at different wavelengths. Pitch gradients are known to broaden the reflection band in CLCs [97] and would be expected to do the same for GLAD/LC hybrids. The results of optical characterisation on GLAD/LC films based on different types of chiral GLAD microstructure types (helical, square staircase, twisted ribbon) begs further investigation to determine if there is an optimum microstruc-

ture type.

The PBN structure [38] (see “Column angle control: paused growth versus spinning growth” on p. 26) consists of smoothly bent two-dimensional “S”-shaped columns. PBNs are two-dimensional analogues of the three-dimensional helix. Helical GLAD films are chiral and hence have an optical response which depends on the circular polarisation of the incoming light. That is, they can be described as sensitive to the circular polarisation of incoming light. Helical GLAD films exhibit circular Bragg reflection when the wavelength and pitch are comparable (scaled by the effective index of refraction). PBNs, in contrast, can be described as linearly polarisation sensitive and are expected to exhibit Bragg reflection, but only for the polarisation parallel to the plane of the “S”-shaped columns. (Theoretical analysis shows that the zig-zag microstructure will not exhibit Bragg phenomena [102].) To test this hypothesis, PBN films should be grown and characterised. Further experimental steps can be taken, including embedding LC materials into PBN films and looking for any enhancement of the Bragg reflection.

The twisted ribbon structure (first described in “Column cross-section shape control” on p. 32) shows promise as a second type of chiral structure. In terms of LC alignment, the twisted ribbon microstructure may actually resemble a chiral nematic phase more closely than helical GLAD films which have a “wire spring” type of structure. Successive cross-sectional slices of a twisted ribbon GLAD film look very similar to the stack of achiral nematic sheets which make up the chiral nematic mesophase. (Recall the small rotation of the nematic director between successive sheets.) At this point, there has been insufficient characterisation of twisted ribbon films to draw any conclusions. The similarity in structure between twisted ribbon films and the chiral nematic mesophase suggests that further investigation is in order.

One of the challenges with GLAD is to produce “clean” looking microstructures minimising film defects and achieving consistent film structures. Improved procedures and the increased experience that comes with the natural maturation of GLAD technology will eventually solve many of these issues. Optimisation of the deposition process would also be



desired. GLAD, by its very nature, is not a highly efficient deposition process and a compromise must be struck between porosity and deposition rate. Increasing interest in manufacturing aspects of GLAD would eventually address this issue.

### **5.2.2 Surface treatments**

Several possibilities for surface treatments of the counter-electrode and film were outlined in Chapter 4 (see "Surface treatment of substrates" on p. 77). Preliminary investigations into the effect of silane treatment of the GLAD films have been undertaken but the results so far are inconclusive due to the limited number of trials performed. (Gaseous phase silane treatment of SiO<sub>2</sub> GLAD films was performed and the cells filled with LC at Philips Research Laboratories, while optical measurements were performed at the University of Alberta.) The logical experiment to try is to take several samples of the same film and perform optical characterisation on them after subjecting each to a different surface treatment. Modification of the surface properties in GLAD films is a broad topic and warrants extensive study to aid in understanding the interaction between LC materials and the GLAD film structures into which they are embedded.

### **5.2.3 Cell fabrication**

Once improved optical performance is achieved in GLAD/LC cells, the fabrication of larger cells with pixel arrays is the next step on the road toward the development of a new display technology. A pixel array could help with reliability and device yield. In these initial experimental stages, one's efforts to fabricate switchable devices may be frustrated by the presence of defects which could render the entire cell inoperable. This problem is compounded because samples are not made in large quantities. At this point in the experiments, the goal is instead to map out as wide a sample space as possible. A pixel array increases the number of independent devices per cell/sample.

One method of creating GLAD/LC films with stacked layers of different microstructures, handedness, and/or pitch is to use two GLAD films each grown on ITO-coated glass substrates to construct the cell instead of using a single film with stacked layers.

### 5.2.4 LC experiments

Given the wide variety of liquid crystals available, there are nearly endless possibilities for experiments with different LCs or LC blends. LCs which exhibit negative dielectric permittivity ( $\Delta\epsilon < 0$ ) such as BL109 will switch in the opposite “sense” to the LCs used in this work. Negative  $\Delta\epsilon$  LCs will align with their molecular axes perpendicular to an applied electric field (planar orientation), rather than parallel to the field (homeotropic orientation) as with LCs such as E7 or ZLI4792 as shown in Fig. 4-13 (p. 92). Of course, if one is to use this property for a device, one must have a goal in mind and have devised a type of device that requires this property.

As stated in the introduction to liquid crystals, they form a very diverse class of materials. Two classes of LCs not even considered so far are those which form smectic phases (containing both orientational and positional order) and ferroelectric LCs which have great importance for very fast electro-optic switching [103]. Chiral nematic LCs have likewise not been investigated for use in GLAD/LC hybrids.

The use of chiral dopants for GLAD/LC experiments is also worth investigating. Chiral dopants are chemicals which can be added in low concentrations to achiral nematic LCs to induce chiral nematic mesophases. The pair of C15 and CB15 chiral dopants can be added to LCs such as E7. The addition of C15 induces a LH twist, while the addition of CB15 induces a RH twist. One experiment that could be tried to is to mix a small amount of CB15 into E7 to create a “bias” RH twist before adding this mixture to a RH GLAD film. The “pre-bias” may help to reduce domain formation in the LC. On the other hand, one could add C15 to create a bias LH twist before adding this mixture to a RH GLAD film. The results of this experiment could be very interesting. Perhaps the LH chiral nematic LC would counteract the RH GLAD film backbone, resulting in a “titration” of sorts for the chiral optical properties.

### 5.2.5 Display ideas

For a full colour display, red, green, blue (RGB) primary colour subpixels are required. For a display based on GLAD/LC composite materials, this would mean then that structures

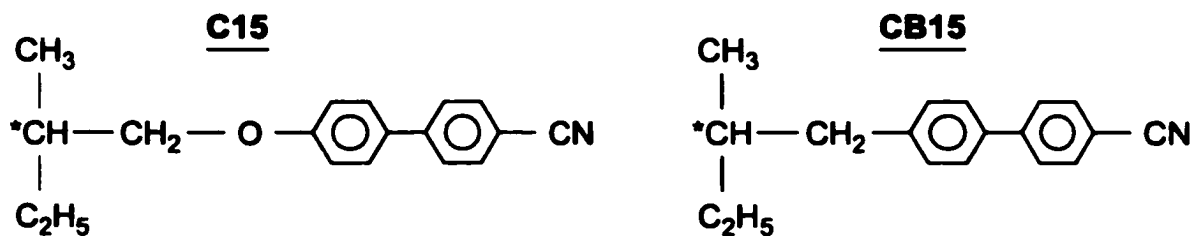


Figure 5-1: Chiral dopants C15 and CB15

These chiral dopants can be mixed in low concentrations with achiral LCs such as E7 to create chiral nematic mesophases.

with three different pitches are required on the same substrate. This is obviously a difficult problem to solve. A different approach would be to aim for a true colour reflective display. However again there is the difficulty of having to vary the pitch dynamically. A scheme based on varying  $E$ -fields might be one possibility, wherein the voltage applied to the cell is chosen such that partial, rather than complete, switching of the LC occurs.

While the idea of achieving a full or true colour display is no doubt appealing, solving the technological problems will be very challenging. One goal that is likely more in reach is that of breaking the 50% reflectivity barrier. With CLCs, the maximum theoretical reflectivity is one-half or 50% assuming that all of the circular polarisation which matches the handedness of the CLC is reflected. Unfortunately, as the opposite circular polarisation passes through the CLC unperturbed, that part of the light is lost. What would be desirable is a structure that reflects both LCP and RCP yet is reversibly switchable. One interesting possibility, which relates to the more exotic GLAD structures mentioned earlier, would be to use a GLAD film with a LH layer and a RH layer stacked together. For a structure such as substrate/LH layer/RH layer/air, incoming light from the air side will be incident on the RH layer. This layer would reflect RCP while LCP passes through unperturbed. The LCP component which passes through the RH layer, then encounters a LH medium which reflects the LCP. The reflected LCP light then passes through the RH layer (unperturbed again). Thus both RCP and LCP can be reflected with the possibility of achieving better than 50% reflectivity. If this LH-RH stacked layer concept is combined with pitch gradation, then a broadband, full reflector might be possible. The key though is that the LC component is still switchable.

## **5.3 Related projects**

A few related projects under investigation by colleagues of the author are worth mentioning and are reviewed briefly in context of possible tie-ins with future GLAD/LC research and experiments. Simulation of GLAD film growth and structure will be helpful in improving the quality and consistency of deposited films and may conceivably be of use for electromagnetic modelling. The use of periodically seeded substrates permits growth of GLAD in regular arrays. Work on photonic band gap (PBG) crystals inspires ideas for several GLAD/LC experiments. And finally, the ability to create “inverse” GLAD structures also leads to interesting optical properties.

### **5.3.1 Simulation of film deposition**

Another important item in the GLAD toolbox is the ability to use computer simulation to model the growth of GLAD films. The three dimensional simulator 3D-FILMS developed by Smy *et al.* [104] models processes including the growth of GLAD films through the use of algorithms which can emulate substrate motion. 3D-FILMS models growth by ballistic deposition of cubical particles. An example of a 3D-FILMS simulation of a helical GLAD film is shown below in Fig. 5-2. 3D-FILMS has been since extended with other simulation capabilities and was used by to model thermal properties of GLAD films designed as thermal barrier coatings [105, 31].

Computer modelling of GLAD film growth not only provides insight into growth mechanisms that influence GLAD, but may also be used to predict and engineer film properties. It is hoped that the structural simulation may be extended to modelling of the electromagnetic response in GLAD films, thereby aiding the understanding of the electromagnetic properties in GLAD films. As thin film properties are affected by film structure, an understanding of the growth of GLAD films is essential to achieving control over the structure, and hence properties, of the film.

### **5.3.2 Periodically seeded substrates**

Substrates with pre-structured surfaces may be used to influence the nucleation stage of GLAD film growth. In particular, the use of a periodic array of raised stripes or bumps

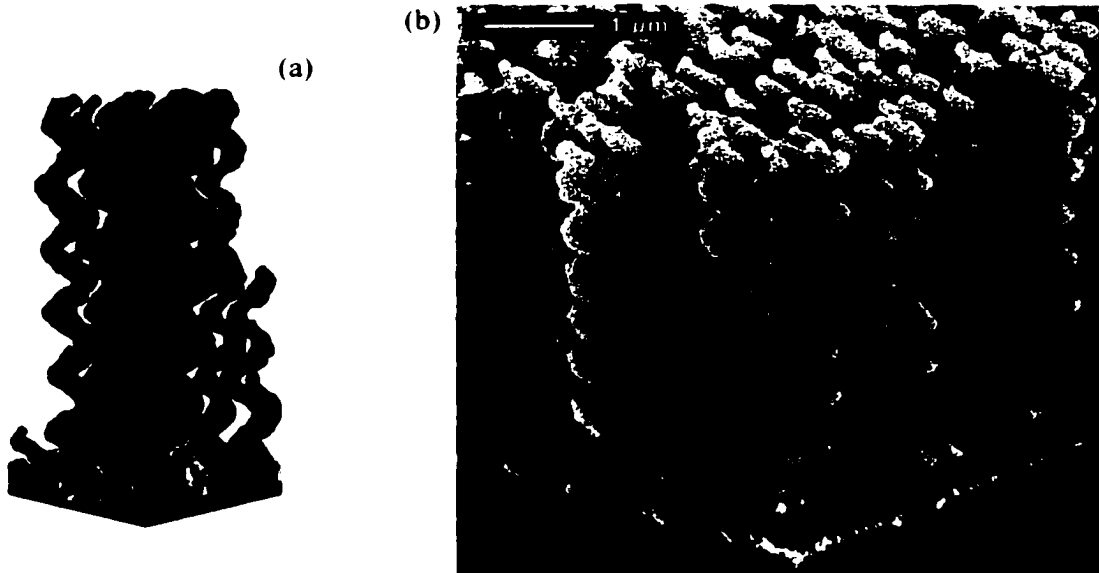


Figure 5-2: Helical GLAD film with 3D-FILMS simulation  
 (a) 3D-FILMS simulation of (b) a SiO<sub>2</sub> helical GLAD film.

yields one- or two-dimensional periodicity, respectively, in the spacing of columns in the GLAD film. For an appropriate geometry, including size scale and aspect ratio of peaks to valleys, the pre-structured substrate surface will be subject to the enhanced atomic shadowing conditions encountered in the GLAD deposition regime. At the deposition angle  $\alpha$ , each “bump” produces shadowing in the spaces between itself and its neighbours, behaving much like the nuclei do in GLAD deposition onto nonstructured substrates, but already arranged in a periodic array.

A detailed discussion of the GLAD growth mechanics [106] with periodically seeded substrates is beyond the scope of this thesis but the utility of pre-structured substrate surfaces extends to applications such as magnetics [107], where a regular arrays of magnetic “bits” may be used in next generation storage devices. Techniques used to produce periodically seeded substrates suitable for GLAD include standard photolithography, e-beam lithography [108], embossing of polymers [109], and laser interference lithography [110]

In terms of GLAD/LC hybrids, use of periodically structured substrates also presents an exciting opportunity. (So far, periodic GLAD structures has not been investigated with LC embedding.) Fundamental experimental problems to investigate include whether periodic

GLAD films would improve the LC alignment or reduce the problem with multi-domain formation.

### 5.3.3 Photonic band gap crystals

Photonic band gap (PBG) crystals are artificial, non-homogenous, periodic structures which exhibit the unique characteristic of a band gap wherein electromagnetic waves in that frequency range cannot propagate through the structure. Of particular interest are three-dimensional photonic band gap crystals with periodicity on the optical wavelength scale because their “stopband” falls in or near the visible wavelength spectrum [111-113]. Of note, Toader and John [114] recently reported a proposed square spiral microstructure which could be fabricated using GLAD and which would exhibit a large photonic band gap. Following the blueprint put forth by Toader and John, Kennedy and Brett [115] recently produced the first implementation of this structure using GLAD. S. W. Leonard *et al.* recently reported a tunable two-dimensional photonic crystal using LC infiltration [116]. From these recent reports, it appears that GLAD/LC technology is worthwhile of investigation for photonic band gap crystal applications. In fact, it was Kennedy’s work on the square spiral structure which motivated the investigation of that microstructure as an alternative to the helical chiral GLAD structures (see “Effects of GLAD film structure” on p. 89). The possibility to create tunable or switchable PBG materials based on GLAD/LC hybrids is also of interest and warrants further experimentation.

### 5.3.4 Inverse optics

It was postulated that the chiral optical response in GLAD films arises from the structural chirality and the index difference between film and void materials. Filling pores of the film with a material with index between that of air and the the film material was found to reduce the chiral optical response; while filling with an index matching material would be expected to extinguish the response altogether. According to the models presented in this thesis which describe the chiral optical activity, if one were to fill the voids of the film with a material with an index of refraction even higher than that of the film, the chiral optical response would remain, but the sign of the optical response would be expected to invert as now  $n_{\text{void}} > n_{\text{film}}$ .

Using techniques developed by Harris *et al.* [117], replamineform or “inverse GLAD” structures are possible. These techniques involve filling the voids of a GLAD film and then removing the original GLAD film (by etching). In terms of the chiral optical response, preliminary experiments performed by K. D. Harris [118] indicate that these “inverse GLAD” indeed exhibit optical response of the opposite sign. The natural question which arises is of what effect the addition of LC materials would have on inverse-GLAD/LC hybrids.

## **5.4 Closing remarks**

While much of the work presented in this thesis is clearly geared towards information display technology, it is definitely worth mentioning that GLAD/LC composite optical materials and devices may also be of utility in other optical switching and filtering applications such as telecommunications and adaptive optics.

This final chapter has presented some of the many ideas for future directions. In some cases, there are definite ideas for future experiments and a desire to try these ideas out as soon as possible. In other cases, however, there are simply many possibilities to try but perhaps without a concrete idea for an experiment. Those possibilities are left, at this point, to the imagination and curiosity of the experimenter. Certainly, there is no shortage of ideas to implement, questions to answer, and possibilities to explore.

*The ideas are plentiful, and the possibilities are nearly endless.*





## Appendix A

# Glancing angle deposition microstructural formulae

---

Each microstructure type is defined mathematically in terms of substrate tilt and rotation angles. Flux incidence angle<sup>1</sup>  $\alpha$  and substrate rotation angle<sup>2</sup>  $\varphi$  are specified as a pair of parameterized functions of thickness:

$$\begin{aligned}\alpha(z) &= f(z, \text{pitch, rise angle, other structural parameters}) \\ \varphi(z) &= f(z, \text{pitch, rise angle, other structural parameters})\end{aligned}\tag{A-1}$$

$\alpha(z)$  is given in degrees ( $^{\circ}$ ) while  $\varphi(z)$  is specified as the number of turns (revolutions, unitless). This appendix discusses the microstructural formulae for a selection of GLAD microstructure types.

### A.1 Tilted columnar film

The first of four fundamental GLAD film microstructures (Fig. 1-10(a)) is produced simply by deposition onto a stationary substrate held at an oblique or glancing angle  $\alpha$ :

$$\begin{aligned}\alpha(z) &= \alpha \text{ (constant)} \\ \varphi(z) &= 0 \text{ (arbitrary constant)}\end{aligned}\tag{A-2}$$

There are certainly no surprises with this definition!

### A.2 Zig-zag microstructure

Zig-zags, or chevron, type microstructure (Fig. 1-10(a)) is produced by depositing alternately from azimuthal angles  $0^{\circ}$  and  $180^{\circ}$ .

$$\begin{aligned}\alpha(z) &= \alpha \text{ (constant)} \\ \varphi(z) &= \frac{1}{2} \left\lfloor \frac{2z}{p} \right\rfloor\end{aligned}\tag{A-3}$$

---

1. Also referred to as tilt angle, or polar angle. See also Fig. 1-6 (p. 12).  
2. Also referred to as azimuthal angle.

The formula states that  $\varphi$  is increased by 0.5 for every half pitch (i.e. the thickness of a “zig” or a “zag” segment) deposited.

### A.3 Helical microstructure variants

#### A.3.1 Standard helical microstructure

This basic helical microstructure (Fig. 1-10(c)) is defined as:

$$\begin{aligned} \alpha(z) &= \alpha \\ \varphi(z) &= \pm z/p \end{aligned} \tag{A-4}$$

The  $\pm$  sign indicates that  $\varphi$  rotation may be taken either clockwise or counterclockwise, to make either left- (LH) or right-handed (RH) helices. One complete revolution in  $\varphi$  is made for each thickness  $p$  deposited.

#### A.3.2 Special case: pillar microstructure

The pillar or post microstructure control formula is identical to that of the standard helical microstructure. The only difference is in the value chosen for pitch  $p$ . For standard helical films,  $p$  is generally chosen in the range of 200 nm or greater. If however,  $p$  is made sufficiently small such that  $p$  is comparable to the thickness of the column, then individual turns of the helical structure are blurred and the helix degenerates into a vertical pillar or post. (See Fig. 1-10(d) and also “Basic forms” on p. 15 for further discussion.) A typical value for the post microstructure is  $p = 10$  nm.

#### A.3.3 Stepped (polygonal) helical microstructure

If instead of smooth rotation of  $\varphi$ , a stepped rotation of  $1/m^{\text{th}}$  of a revolution is applied for every  $1/m^{\text{th}}$  of the pitch deposited ( $p/m$ ), then a staircase-like structure results. (Assume for the moment  $m$  is a positive integer with  $m > 2$ .) This structure is similar to a helix, but is composed of  $m$  discrete segments for each complete revolution of the substrate. The profile of a helix, looking along the helical axis is a circle. The profile of this structure would then be an  $m$ -sided polygon.

$$\alpha(z) = \alpha \text{ (constant)}$$

$$\varphi(z) = \pm \frac{1}{m} \left[ \frac{mz}{p} \right] \quad (\text{A-5})$$

Comparing with Eqn. A-3 above, it is plain to see that the zig-zag structure is a special case of the stepped helical microstructure with  $m = 2$ , a two-dimensional degeneration of this structure. The standar helical structure can also be seen to be the limiting case when  $m$  is made large.

$m = 3$  would give a “triangular” helix, while a value of  $m = 4$  results in a “square staircase” helix. If one does not restrict  $m$  to an integer, then even more interesting structures would result.

### A.3.4 Graded pitch helical

For a helical GLAD film microstructure, the ratio of rotation rate ( $d\varphi/dt$ ) to deposition rate ( $dz/dt$ ) determines the pitch. For fixed pitch helical films, this ratio is kept constant. However, by dynamically varying this ratio, a pitch gradient can be produced. To implement this microstructure, a bit of algebra is required. First, the graded pitch helical microstructure is defined as having the pitch  $p$  of the helix varying linearly as number of turns  $n$  (in rotation  $\varphi$ ), thus the pitch as a function of number of turns deposited is defined by:

$$p(n) = p_1 + (p_2 - p_1)n/N \quad (\text{A-6})$$

where  $N$  is the total number of turns in the helix. The pitch evolves linearly from  $p_1$  to  $p_2$ . Pitch can be graded from large to small or from small to large.

The thickness of the film is given by the area under the graph of  $p(n)$  versus  $n$ . Integrating, the thickness as a function of number of turns deposited is:

$$z(n) = \int_0^n p(n)dn = p_1 n + \frac{p_2 - p_1}{2N} n^2 \quad (\text{A-7})$$

As  $\varphi(n) = n$ , to obtain  $\varphi(z)$ , Eqn. A-7 is solved for the inverse function  $n(z)$ . Using the quad-

ratic formula and noting that only the one solution is meaningful, one obtains the definition of the graded pitch helical algorithm:

$$\varphi(z) = \pm n = \pm \frac{-p_1 + \sqrt{p_1^2 + 2\frac{p_2 - p_1}{N}z}}{\frac{p_2 - p_1}{N}} \quad (\text{A-8})$$

and as usual,  $\alpha(z) = \alpha$ . Once again, the  $\pm$  sign indicates a chiral structure whose handedness can be chosen, depending on the sign. The total thickness of the film is found from Eqn. A-7, by calculating  $z(N) = N(p_1 + p_2)/2$ .

#### A.4 Twisted ribbon chiral

The twisted ribbon microstructure, described in Chapter 2 (see ‘‘Column cross-section shape control’’ on p. 32), can be thought of as a very small pitch zig-zag with the addition of a twist.

The small zig-zag segments have pitch  $p_2$ , while the overall ribbon structure has a pitch  $p_1$  (By necessity,  $p_2 \ll p_1$ ). For each thickness  $p_2$  deposited, the zig-zag ‘‘twists’’ by the fraction  $p_2/p_1$  of a turn, such that after each thickness  $p_1$  deposited, the ribbon has made two half-twists (a full  $360^\circ$  twist) which defines the pitch of this chiral structure.

$$\alpha(z) = \alpha$$

$$\varphi(z) = \frac{p_2}{p_1} \left\lfloor \frac{z}{p_2} \right\rfloor + \begin{cases} 0, & \text{for } \frac{z}{p_2} - \left\lfloor \frac{z}{p_2} \right\rfloor < \frac{1}{2} \\ \frac{1}{2}, & \text{for } \frac{z}{p_2} - \left\lfloor \frac{z}{p_2} \right\rfloor \geq \frac{1}{2} \end{cases} \quad (\text{A-9})$$

which can be rewritten as:

$$\varphi(z) = \frac{p_2}{p_1} \left\lfloor \frac{z}{p_2} \right\rfloor + \frac{1}{2} \left\lfloor \frac{2z}{p_2} \right\rfloor \quad (\text{A-10})$$

1. K. Robbie and M. J. Brett, "Sculptured thin films and glancing angle deposition: Growth mechanics and applications", *J. Vac. Sci. Technol. A* **15**, 1460-1465 (1997).
2. K. Robbie, "Glancing angle deposition", Ph.D. dissertation thesis, University of Alberta, Canada (1998).
3. K. Robbie and M. J. Brett, "Method of depositing shadow sculpted thin films", United States of America Patent 5,866,204 (02 February 1999).
4. R. Glang, in *Handbook of Thin Film Technology*, eds. L. I. Maissel and R. Glang, McGraw-Hill, New York (1970).
5. B. N. Chapman, *Glow Discharge Processes*, Wiley, New York (1980).
6. E. B. Graper, "Evaporation characteristics of materials from an electron-beam gun", *J. Vac. Sci. Technol.* **8**, 333-337 (1971).
7. E. B. Graper, "Evaporation characteristics of materials from an electron-beam gun II", *J. Vac. Sci. Technol. A* **5**, 2718-2723 (1987).
8. M. Ohring, *The Materials Science of Thin Films*, Academic Press, San Diego (1992).
9. H. König and G. Helwig, "Über die Struktur schräg aufgedampfter Schichten und ihr Einfluß auf die Entwicklung submikroskopischer Oberflächenrauigkeiten" [German], *Optik* **6**, 111 (1950).
10. D. O. Smith, M. S. Cohen, and G. P. Weiss, "Oblique-incidence anisotropy in evaporated permalloy films", *J. Appl. Phys.* **31**, 1755-1762 (1960).
11. A. Movchan and A. V. Demchishin, "Study of the structure and properties of thick vacuum condensates of nickel, titanium, tungsten, aluminium oxide and zirconium dioxide", *Phys. Met. Metallog.* **28**, 83-90 (1969).
12. J. A. Thornton, *Ann. Rev. Materials Science* **7**, 239 (1977).
13. R. Messier, A. P. Giri, and R. A. Roy, "Revised structure zone model for thin film physical structure", *J. Vac. Sci. Technol. A* **2**, 500-503 (1984).
14. R. Messier, "Toward quantification of thin film morphology", *J. Vac. Sci. Technol. A* **4**, 490-495 (1986).

15. H. van Kranenburg and J. C. Lodder, "Tailoring growth and local composition by oblique-incidence deposition: A review and new experimental data", *Mater. Sci. Eng. R. Rep.* **11**, 293-354 (1994).
16. L. Abelmann and C. Lodder, "Oblique evaporation and surface diffusion", *Thin Solid Films* **305**, 1-21 (1997).
17. M. W. Seto and M. J. Brett, "Play the angles to create exotic thin films", *Vacuum Solutions* **14**, 26-31 (March/April 2000).
18. K. Robbie, L. J. Friedrich, S. K. Dew, T. Smy, and M. J. Brett, "Fabrication of thin films with highly porous microstructures", *J. Vac. Sci. Technol. A* **13**, 1032-1035 (1995).
19. H. van Nieuwenhuizen and H. B. Haanstra, "Microfractography of thin films", *Philips Tech. Rev.* **27**, 87-91(1966).
20. R. N. Tait, T. Smy, and M. J. Brett, "Modelling and characterization of columnar growth in evaporated films", *Thin Solid Films* **226**, 196-201 (1993).
21. R. Messier, T. Gehrke, C. Frankel, V. C. Venugopal, W. Otaño, and A. Lakhtakia, "Engineered sculptured nematic thin films", *J. Vac. Sci. Technol. A* **15**, 2148-2152 (1997).
22. I. Hodgkinson, Q. H. Wu, A. McPhun, "Incremental-growth model for the deposition of spatially modulated thin film nanostructures", *J. Vac. Sci. Technol. B* **16**, 2811-2816 (1998).
23. T. Motohiro and Y. Taga, "Thin film retardation plate by oblique deposition", *Appl. Opt.* **28**, 2466-2482 (1989).
24. K. Robbie, M. J. Brett, and A. Lakhtakia, "First thin film realization of a helicoidal bianisotropic medium", *J. Vac. Sci. Technol. A* **13**, 2991-2993 (1995).
25. K. Robbie and M. J. Brett, "Shadow sculpted thin films", United States of America Patent 6,248,422 (19 June 2001).
26. K. Robbie, C. Shafai, and M. J. Brett, "Thin films with nanometre scale pillar microstructure", *J. Mater. Res.* **14**, 3158-3163 (1999).
27. M. W. Seto, K. Robbie, D. Vick, M. J. Brett, and L. Kuhn, "Mechanical actuation of thin films with helical microstructures", *J. Vac. Sci. Technol. B* **15**, 2172-2177 (1999).
28. M. W. Seto, B. Dick, and M. J. Brett, "Microsprings and microcantilevers: studies of mechanical response", *J. Micromechanics and Microengineering*, in press

(2001).

29. K. Robbie, A. J. P. Hnatiw, M. J. Brett, R. I. MacDonald, and J. N. McMullin, "Inhomogeneous thin film optical filter fabricated using glancing angle deposition", *Electron. Lett.* **33**, 1213-1214 (1997).
30. A. Y. Elezzabi, J. C. Sit, J. F. Holzman, K. Robbie, and M. J. Brett, "Thin film vertical diffraction gratings fabricated using glancing angle deposition", *Electron. Lett.* **35**, 491-493 (1999).
31. K. D. Harris, D. Vick, E. J. Gonzalez, T. Smy, K. Robbie, and M. J. Brett, "Porous thin films for thermal barrier coatings", *Surf. Coat. Technol.* **138**, 185-191 (2001).
32. M. J. Colgan and M. J. Brett, "Field emission from carbon and silicon films with pillar microstructure", *Thin Solid Films* **389**, 1-4 (2001).
33. B. Dick, M. J. Brett, T. J. Smy, M. R. Freeman, M. Malac, and R. F. Egerton, "Periodic magnetic microstructures by glancing angle deposition", *J. Vac. Sci. Technol. A* **18**, 1838-1844 (2000).
34. A. T. Wu, M. Seto, and M. J. Brett, "Capacitive SiO humidity sensors with novel microstructures", *Sens. Mater.* **11**, 493-505 (1999).
35. K. D. Harris, J. R. McBride, K. E. Nietering, and M. J. Brett, "Fabrication of porous platinum thin films for hydrocarbon sensor applications", *Sens. Mater.* **13**, 225-234, (2001).
36. K. D. Harris, M. J. Brett, T. Smy, C. Backhouse, "Microchannel surface area enhancement using porous thin films", *J. Electrochem. Soc.* **147**, 2002-2006 (2000).
37. J. C. Sit, D. Vick, K. Robbie, and M. J. Brett, "Thin film microstructure control using glancing angle deposition by sputtering", *J. Mater. Res.* **14**, 1197-1199 (1999).
38. K. Robbie, J. C. Sit, and M. J. Brett, "Advanced techniques for glancing angle deposition", *J. Vac. Sci. Technol. B* **16**, 1115-1122 (1998).
39. K. Robbie and M. J. Brett, "Glancing angle deposition of thin films", United States of America Patent 6,206,065 (27 March 2001).
40. R. N. Tait, S. K. Dew, W. Tsai, D. Hodul, T. Smy, and M. J. Brett, "Simulation of uniformity and lifetime effects in collimated sputtering", *J. Vac. Sci. Technol. B* **14**, 679-686 (1996).
41. S. M. Rossnagel, D. Mikalsen, H. Kinoshita, and J. J. Cuomo, "Collimated magnetron sputter deposition", *J. Vac. Sci. Technol. A* **9**, 261-265 (1991).

42. S. M. Rossnagel and J. Hopwood, "Magnetron sputter deposition with high levels of metal ionization", *Appl. Phys. Lett.* **63**, 3285-3287 (1993).
43. J. N. Broughton, M. J. Brett, S. K. Dew, and G. Este, "Titanium sputter deposition at low pressures and long throw distances", *IEEE Trans. Semicon. Manufact.* **9**, 122-127 (1996).
44. S. Dew, T. Smy, and M. J. Brett, "Step coverage, uniformity, and composition studies using integrated vapour transport and film-deposition models", *Jpn. J. Appl. Phys.* **33**, 1140-1145 (1994).
45. B. Dick, M. J. Brett, T. Smy, M. Belov, and M. R. Freeman, "Periodic submicrometer structures by sputtering", *J. Vac. Sci. Technol.* **B 19**, 1813-1819 (2001).
46. D. Vick, Y. Y. Tsui, M. J. Brett, and R. Fedosejevs, "Production of porous carbon thin films by pulsed laser deposition", *Thin Solid Films* **350**, 49-52 (1999).
47. R. B. Meyer, "Piezoelectric effects in liquid crystals", *Phys. Rev. Lett.* **22**, 918-921 (1969).
48. H. L. Ong and R. B. Meyer, "Electromagnetic wave propagation in a periodically bent nematic liquid crystal", *J. Opt. Soc. Am.* **73**, 167-176 (1983).
49. V. C. Venugopal and A. Lakhtakia, "Homogenization of cubically nonlinear, gyrotropic, composite media", *Proc. Bianisotropics 1997* (Glasgow, UK, 5-7 June 1997), 111-114 (1997).
50. R. N. Tait, T. Smy, and M. J. Brett, "Structural anisotropy in oblique incidence thin metal films", *J. Vac. Sci. Technol.* **A 10**, 1518-1521 (1992).
51. K. Kuwahara and S. Shinzato, "Resistivity anisotropy of nickel films induced by oblique incidence sputter deposition", *Thin Solid Films* **164**, 165-168 (1988).
52. K. Kurabayashi, M. Asheghi, M. Touzelbaev, and K. E. Goodson, "Measurement of Thermal Conductivity Anisotropy in Polyimide Films", *IEEE J. Micromech. Sys.* **8**, 180-191 (1989).
53. N. T. Kivaisi, "Optical properties of obliquely evaporated aluminum films", *Thin Solid Films* **97**, 153-163 (1982).
54. I. J. Hodgkinson, F. Horowitz, H. A. Macleod, M. Sikkens, and J. J. Wharton, "Measurement of the principal refractive indices of thin films deposited at oblique incidence", *J. Opt. Soc. Am.* **A 2**, 1693-1697 (1985).
55. I. J. Hodgkinson and P. W. Wilson, "Microstructural-induced anisotropy in thin films for optical applications", *CRC Crit. Rev. Solid State Mat. Sci.* **15**, 27-61



- (1988).
56. I. J. Hodgkinson, Q. H. Wu, M. J. Brett, and K. Robbie, "Vacuum deposition of biaxial films with surface-aligned principal axes and large birefringence  $\Delta n$ " in *Optical Interference Coatings*, OSA Technical Digest Series (Optical Society of America) **9**, 104-106 (1998).
  57. I. J. Hodgkinson and Q. H. Wu, "Serial bideposition of anisotropic thin films with enhanced linear birefringence", *Appl. Opt.* **38**, 3621-3625 (1999).
  58. B. E. A. Saleh and M. C. Teich, *Fundamentals of Photonics*, John Wiley & Sons, New York (1991).
  59. E. Hecht, *Optics*, 2<sup>nd</sup> ed., Addison-Wesley, Reading, MA, USA (1987).
  60. D. L. Jaggard, A. R. Mickelson, and C. H. Papas, "On electromagnetic waves in chiral media", *Appl. Phys.* **18**, 211-216 (1979).
  61. L. D. Barron, *Molecular Light Scattering and Optical Activity*, Cambridge University Press (1982).
  62. P. Crabbé, *An Introduction to the Chiroptical Methods in Chemistry*, Universidad Nacional Autonoma de Mexico/Universidad Iberoamericana (1971).
  63. K. Lindman, "Über die durch ein isotropes System von Spiralförmigen Resonatoren erzeugte Rotationspolarisation der elektromagnetischen Wellen", *Ann. Physik* **63**, 621 (1920).
  64. K. Lindman, "Über die durch ein aktives Raumgitter erzeugte Rotationspolarisation der elektromagnetischen Wellen", *Ann. Physik* **69**, 270 (1922).
  65. I. Tinoco, Jr., and M. P. Freeman, "The optical activity of oriented copper helices. I. Experimental", *J. Phys. Chem.* **61**, 1196 (1957).
  66. I. Tinoco, Jr., and R. W. Woody, "Optical rotation of oriented helices. II. Calculation of the rotatory dispersion of the alpha helix", *J. Chem. Phys.* **32**, 461 (1960).
  67. N. O. Young and J. Kowal, "Optically active fluorite films", *Nature* **183**, 104-105 (1959).
  68. R. M. A. Azzam, "Chiral thin solid films: Method of deposition and applications", *Appl. Phys. Lett.* **61**, 3118-3120 (1992).
  69. A. Lakhtakia and W. S. Weiglhofer, "Axial propagation in general helicoidal bianisotropic media", *Microwave Opt. Tech. Lett.* **6**, 804-806 (1993).

70. A. Lakhtakia and W. S. Weiglhofer, "On light propagation in helicoidal bianisotropic mediums", *Proc. R. Soc. Lond. A* **448**, 419-437 (1995).
71. A. Lakhtakia and W. S. Weiglhofer, "Perturbational solution for propagation in periodically bent neamtic liquid crystals and thin films", *Microwave Opt. Tech. Lett.* **11**, 320-323 (1996).
72. A. Lakhtakia and W. S. Weiglhofer, "Further results on light propagation in helicoidal bianisotropic mediums: oblique propagation", *Proc. R. Soc. Lond. A* **453**, 93-105 (1997).
73. K. Robbie, M. J. Brett, and A. Lakhtakia, "Chiral sculptured thin films", *Nature* **384**, 616 (1996).
74. K. Robbie and M. J. Brett, "Thin film HBMs and associated optical phenomena", *Proc. Bianisotropics '97*, Glasgow (June 1997).
75. P. I. Rovira, R. A. Yarussi, R. W. Collins, V. C. Venugopal, A. Lakhtakia, R. Messier, K. Robbie, and M. J. Brett, "Transmission ellipsometry of a thin-film helicoidal bianisotropic medium", *Thin Solid Films* 313-314, 373-378 (1998).
76. B. Fan, H. K. M. Vithana, J. C. Kralik, and S. M. Faris, "Optical circular dichroism of vacuum-deposited film stacks", *Opt. Comm.* **147**, 265-268 (1998).
77. I. Hodgkinson, Q. H. Wu, B. Knight, A. Lakhtakia, and K. Robbie, "Vacuum deposition of chiral sculptured thin films with high optical activity", *Appl. Opt.* **39**, 642-649 (2000).
78. C. Oldano, P. Allia, and L. Trossi, "Optical properties of anisotropic periodic helical structures", *J. Physique* **46**, 573-582 (1985).
79. A. Lakhtakia, V. K. Varadan, and V. V. Varadan, *Time-Harmonic Electromagnetic Fields in Chiral Media*, Lecture Notes in Physics **335**, Springer-Verlag, Berlin (1989).
80. I. V. Lindell, A. H. Sihvola, S. A. Tretyakov, and A. J. Viitanen, *Electromagnetic Waves in Chiral and Bi-Isotropic Media*, Artech House, Boston MA (1994).
81. J. R. Pierce, *Traveling-Wave Tubes*, D. van Nostrand Co., Princeton NJ (1950).
82. D. K. Cheng, *Field and Wave Electromagnetics*, 2nd ed., Addison-Wesley, Reading MA (1989).
83. I. J. Hodgkinson, P. I. Bowmar, and Q. H. Wu, "Scatter from tilted-columnar birefringent thin films: observation and measurement of anisotropic scatter distributions", *Appl. Opt.* **34**, 163-168 (1995).

84. I. J. Hodgkinson, S. Cloughly, Q. H. Wu, S. Kassam, "Anisotropic scatter patterns and anomalous birefringence of obliquely deposited cerium oxide films", *Appl. Opt.* **35**, 5563-5568 (1996).
85. S. Chandrasekhar, *Liquid Crystals*, 2nd ed., Cambridge University Press (1992).
86. E. B. Priestly, P. J. Wojtowicz, and Ping Sheng, eds., *Introduction to Liquid Crystals*, RCA Laboratories, Princeton, New Jersey (1975).
87. P. Yeh, C. Gu, *Optics of Liquid Crystal Displays*, John Wiley & Sons, New York (1999).
88. G. Friedel, *Ann. Physique* **18**, 273 (1922).
89. A. D. Buckingham, G. P. Ceasar, and M. B. Dunn, "The addition of optically active compounds to nematic liquid crystals", *Chem. Phys. Lett.* **3**, 540-541 (1969).
90. V. H. Zocher, *Naturwissenschaften* **13**, 1015-1021 (1925).
91. J. L. Janning, "Thin film surface orientation for liquid crystals", *Appl. Phys. Lett.* **21**, 173-174 (1972).
92. W. Urbach, M. Boix, and E. Guyon, "Alignment of nematics and smectics on evaporated films", *Appl. Phys. Lett.* **25**, 479-481 (1974).
93. R. A. M. Hikmet and H. Kemperman, "Electrically switchable mirrors and optical components made from liquid-crystal gels", *Nature* **392**, 476-479 (1998).
94. K. Kato, K. Tanaka, S. Tsuru, and S. Sakai, "Characteristics of right- and left-handed polymer-dispersed cholesteric liquid crystals", *Jpn. J. Appl. Phys.* **33**, 4946-4949 (1994).
95. W. C. O'Mara, *Liquid Crystal Flat Panel Displays: Manufacturing Science & Technology*, van Nostrand Reinhold, New York (1993).
96. K. Robbie, D. J. Broer, and M. J. Brett, "Chiral nematic order in liquid crystals imposed by an engineered inorganic nanostructure", *Nature* **399**, 764-766 (1999).
97. D. J. Broer, J. Lub, and G. N. Mol, "Wide-band reflective polarizers from cholesteric polymer networks with a pitch gradient", *Nature* **378**, 467-469 (1995).
98. J. C. Sit, D. J. Broer, and M. J. Brett, "Alignment and switching of nematic liquid crystals embedded in porous chiral thin films", *Liq. Cryst.* **27**, 387-391 (2000).
99. J. C. Sit, D. J. Broer, and M. J. Brett, "Liquid crystal alignment and switching in porous chiral thin films", *Adv. Mater.* **12**, 371-373 (2000).

100. S. R. Kennedy, J. C. Sit, D. J. Broer, and M. J. Brett, "Optical activity of chiral thin film and liquid crystal hybrids", *Liq. Cryst.*, in press (2001).
101. K. P. Stevenson, G. A. Kimmel, Z. Dohnálek, R. S. Smith, B. D. Kay, "Controlling the morphology of amorphous solid water", *Science* **283**, 1505-1507 (1999).
102. G. Y. Slepyan and A. S. Maksimenko, "Motohiro-Taga interface in sculptured thin films—absence of Bragg phenomena", *Opt. Eng.* **37**, 2843-2847 (1998).
103. N. A. Clark and S. T. Lagerwell, "Submicrosecond bistable electro-optic switching in liquid crystals", *Appl. Phys. Lett.* **36**, 899-901 (1980).
104. T. Smy, D. Vick, M. J. Brett, A. T. Wu, J. C. Sit, K. D. Harris, "Three dimensional simulation of film microstructure produced by glancing angle deposition", *J. Vac. Sci. Technol. A* **18**, 2507-2512 (2000).
105. T. Smy, D. Walkey, K. D. Harris, and M. J. Brett, "Thin film microstructure and thermal transport simulation using 3D-FILMS", *Thin Solid Films* **391**, 88-100 (2001).
106. D. Vick, T. Smy, B. Dick, S. Kennedy, and M. J. Brett, "Growth behaviour of engineered porous thin films: measurement and modeling", *Mat. Res. Soc. Symp. Proc.* **648**, ed. S. C. Moss, (2001).
107. B. Dick, M. J. Brett, T. J. Smy, M. R. Freeman, M. Malac, R. F. Egerton, "Periodic magnetic microstructures by glancing angle deposition", *J. Vac. Sci. Technol. A* **18**, 1838-1844 (2000).
108. M. Malac, R. F. Egerton, M. J. Brett, and B. Dick, "Fabrication of submicrometer regular arrays of pillars and helices", *J. Vac. Sci. Technol. B* **17**, 2671-2674 (1999).
109. B. Dick, J. C. Sit, M. J. Brett, I. M. N. Votte, and C. W. M. Bastiaansen, "Embossed polymeric relief structures as a template for the growth of inorganic microstructures", *Nano Lett.* **1**, 71-73 (2001).
110. J. P. Spallas, A. M. Hawryluk, and D. R. Kania, "Field emitter array mask patterning using laser interference lithography", *J. Vac. Sci. Technol. B* **13**, 1973-1978 (1995).
111. S. John, "Electromagnetic absorption in a disordered medium near a photon mobility edge", *Phys. Rev. Lett.* **53**, 2169-2172 (1984).
112. E. Yablonovitch, "Inhibited spontaneous emission in solid-state physics and electronics", *Phys. Rev. Lett.* **58**, 2059-2062 (1987).
113. S. John, "Strong localization of photons in certain disordered dielectric superlattices", *Phys. Rev. Lett.* **58**, 2486-2489 (1987).

114. O. Toader and S. John, "Proposed square spiral microfabrication architecture for large three-dimensional photonic band gap crystals", *Science* **292**, 1133-1135 (2001).
115. S. R. Kennedy, M. J. Brett, O. Toader, S. John, "Fabrication of square spiral photonic crystal structures", *IEEE Photonic Tech. Lett.*, in press (2001).
116. S. W. Leonard, J. P. Mondia, H. M. van Driel, O. Toader, S. John, K. Busch, A. Birner, U. Gösele, V. Lehmann, "Tunable two-dimensional photonic crystals using liquid-crystal infiltration", *Phys. Rev. B* **61**, R2389-R2392 (2000).
117. K. D. Harris, K. L. Westra, and M. J. Brett, "Fabrication of perforated thin films with helical and chevron microstructures", *Electrochem. Solid State Lett.* **4**, C39 (2001).
118. K. D. Harris, private communication.